NASA CONTRACTOR REPORT

NASA CR-2829

NASA CR-2829

DEVELOPMENT AND VALIDATION OF PURGED THERMAL PROTECTION SYSTEMS FOR LIQUID HYDROGEN FUEL TANKS OF HYPERSONIC VEHICLES

R. G. Helenbrook and J. Z. Colt

Prepared by
BELL AEROSPACE
Buffalo, N.Y. 14240
for Langley Research Center

NATIONAL AERONAUTICS AND SPACE ADMINISTRATION • WASHINGTON, D. C. • JUNE 1977

DISCLAIMER NOTICE

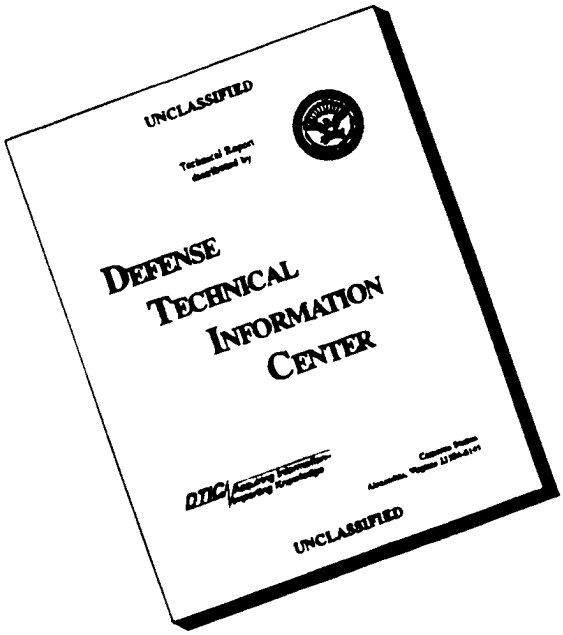

THIS DOCUMENT IS BEST QUALITY AVAILABLE. THE COPY FURNISHED TO DTIC CONTAINED A SIGNIFICANT NUMBER OF PAGES WHICH DO NOT REPRODUCE LEGIBLY.

1. Report No.	2. Government Accession No.	3. Recipient's Catalog No.
NASA CR-2829		

4. Title and Subtitle	5. Report Date
DEVELOPMENT AND VALIDATION OF PURGED THERMAL PROTECTION SYSTEMS FOR LIQUID HYDROGEN FUEL TANKS OF HYPERSONIC VEHICLES	June 1977
	6. Performing Organization Code
7. Author(s)	8. Performing Organization Report No.
R. G. Helenbrook and J. Z. Colt	8653-950001
	10. Work Unit No.
9. Performing Organization Name and Address	501-22-06-01
Bell Aerospace Division of Textron Inc. Post Office Box 1 Buffalo, NY 14240	11. Contract or Grant No.
	NAS1-10969
	13. Type of Report and Period Covered
12. Sponsoring Agency Name and Address	Contractor Report
National Aeronautics and Space Administration Washington, DC 20546	14. Sponsoring Agency Code

15. Supplementary Notes

Technical Monitor: Ellsworth L. Sharpe

Assistant: H. Neale Kelly Topical report

16. Abstract

An analytical and experimental investigation was conducted to develop and validate an economical, lightweight, safe, efficient, reliable and reusable insulation system for hypersonic cruise vehicle hydrogen fuel tanks. Results of the study indicate that a nitrogen purged, layered insulation system with nonpermeable closed-cell insulation next to the cryogenic tank and a high service temperature fibrous insulation surrounding it is potentially an attractive solution to the insulation problem. For the postulated hypersonic flight the average unit weight of the purged insulation system (including insulation, condensate and fuel boil off) is 6.31 kg/m^2 (1.29 psf). Limited cyclic tests of large specimens of closed cell polymethacrylimide foam indicate it will withstand the expected thermal cycle.

17. Key Words (Suggested by Author(s))	18. Distribution Statement
Cryogenic Insulation, Hypersonic Airplane, Cryopumping, Diffusion, Heat Transfer.	Unclassified - Unlimited Subject Category 34

19. Security Classif. (of this report)	20. Security Classif. (of this page)	21. No. of Pages	22. Price*
Unclassified	Unclassified	124	$5.50

*For sale by the National Technical Information Service, Springfield, Virginia 22161

FOREWORD

The work for this report was accomplished by Bell Aerospace Company and its subcontractor A. D. Little, Inc. John Z. Colt was the Bell Aerospace Program Manager. D. L. Richardson was the Principal Investigator at A. D. Little. Other Bell personnel contributing to the program were R. G. Helenbrook, A. Krivetsky, and J. D. Witsil, Jr. (Thermal Analysis), and J. Lajudice (Experimental Evaluation). The technical guidance of W. H. Dukes is gratefully acknowledged. R. Moore of A. D. Little designed the 76.2 cm (30 in.) diameter cryogenic insulation test apparatus.

CONTENTS

CONTENTS (CONTD)

ILLUSTRATIONS

ILLUSTRATIONS (CONT)

TABLES

SYMBOLS

A	-	area
B_o	-	permeability coefficient
c_p	-	specific heat of purge gas
c_{p_i}	-	specific heat of inner insulation
c_{p_o}	-	specific heat of outer insulation
c_{p_w}	-	specific heat of tank wall
C_1, C_2	-	integration constants
G	-	Volume flow rate
h	-	external heat transfer coefficient
h_{fg}	-	combined heat of fusion and evaporation of purge gas
k_f	-	thermal conductivity of frost
k_i	-	thermal conductivity of inner insulation
k_o	-	thermal conductivity of outer insulation
ℓ	-	thickness of thermal protection system
Q	-	heat flow
T	-	temperature
T_c	-	cryogenic fuel storage temperature
T_f	-	condensation temperature of frost
T_s	-	outer surface temperature
T_w	-	tank wall temperature
T_∞	-	ambient temperature
T	-	environment temperature
t_∞	-	thickness of permeability specimen
t_i	-	inner insulation thickness
t_w	-	tank wall thickness
U	-	overall thermal conductance of TPS
$\dot{w}$	-	purge gas flow rate
x	-	distance from outer surface
y	-	thickness of outer insulation
$\dot{z}$	-	frost thickness
z_m	-	mean frost thickness during flight
z_o	-	initial frost thickness
z_1	-	flight equilibrium frost thickness

Greek

Δp	-	pressure differential
ϵ	-	emissivity of vehicle outer surface
θ	-	time
θ_T	-	flight time
θ_1	-	time to reach equilibrium for a wet tank during flight
θ_2	-	time to evaporate all frost for a dry tank during flight
μ	-	purge gas viscosity
γ	-	void fraction of insulation
ρ_f	-	frost density
ρ_g	-	purge gas density
ρ_i	-	inner insulation density
ρ_o	-	outer insulation density
ρ_w	-	tank wall density
ρk	-	thermal efficiency parameter for insulations

SUMMARY

An analytical and experimental investigation was conducted to develop and validate an economical, lightweight, safe, efficient, reliable, and reusable insulation system for hypersonic cruise vehicle hydrogen fuel tanks. Results of the study indicate that a nitrogen purged, layered insulation system with nonpermeable closed-cell insulation next to the cryogenic tank and a high service temperature fibrous insulation surrounding it is potentially an attractive solution to the insulation problem.

The investigation concentrated on the innermost layer of insulation next to the cryogenic tank wall where cryodeposition of the purge gas is a problem. In the initial design concept, it was intended to permit some cryodeposition to occur in the innermost layer but to control and contain the cryodeposit within the insulation. It was determined analytically and verified experimentally, that the rate of cryodeposition is initially controlled by diffustion and then by heat transfer through the frost layer. To provide the low deposition rates desired, an insulation with relatively low permeability was required. Material screening tests determined that for materials with a high temperature capability only those with high densities provided the required low permeability. The system average unit weight (including insulation, condensate and fuel boil off) for the postulated hypersonic flight using these higher density insulations and a nitrogen purge was 18.0 kg/m^2 (3.69 psf). The feasibility of using available low service temperature, low density, closed cell plastic insulations with essentially zero permeability was also investigated. The average system unit weight with this type of insulation was 6.31 kg/m^2 (1.29 psf). Weight studies showed that N_2 purged systems were 10% lighter than CO_2 systems primarily because of the lower cryodeposition temperature of the former.

Although additional testing will be required to confirm the long-term suitability of the developed insulation system, limited cyclic tests of large (76.2 cm (30 in.)) diameter specimens of polymethacrylimide foam indicated that it would withstand the expected thermal cycle in which the temperature of the foam at the tank surface remained at 21K (-423°F) while the outer surface varied from 77K (-320°F) to 450K (350°F).

INTRODUCTION

Before hydrogen can be considered as the fuel for future hypersonic aircraft, several problems associated with the storage of liquid hydrogen must be solved. These problems include:

- Cryopumping of air because of the low temperature of hydrogen (21K (-423°F)). This continual condensation at the tank wall requires rejection of large quantities of heat which must be absorbed by evaporation of the fuel;

- Excessive fuel boil off as a result of the large temperature difference between the environment and the fuel tank. During cruise conditions this temperature difference can be as high as 1120K (2000°F) since the outer surface temperature of the vehicle can be 1144K (1600°F);

- The safety aspects of handling hydrogen which has both wide flammability limits and low energy requirements for ignition.

In addition to solving these problems, the thermal protection system must also be lightweight, retain its structural integrity under all environmental conditions, require minimum preflight preparation, and offer dependable reusability.

In an attempt to find solutions to these problems a variety of thermal protection systems including internal, sealed, and purged systems have previously been investigated. Internal insulation systems become inefficient because hydrogen gas permeates the insulation resulting in high thermal conductivity (Ref's. 1, 2, 3).

Lightweight sealed systems have proven to be unreliable because they are quite susceptible to leaks (Ref's. 4 and 5). Helium purge gas systems have been found to be relatively inefficient and expensive (Ref. 6). A CO_2 frost insulation system which relies on the sublimation of the frost to supply the purge gas (Ref's. 7, 8, 9, 10) offers weight advantages over the helium purge system but requires significant preflight servicing. In addition helium gas is used during frost deposition to control the frost density.

This report presents the results of an analytical and experimental investigation of a purged insulation system for liquid hydrogen tanks which does not require the use of helium or extensive preflight preparation. The system, which would use either nitrogen or carbon dioxide as a purge gas, would use the layer of insulation next to the tank wall to restrict or prevent the cryodeposition of purge gas and to contain any resulting cryodeposit. The analytical support of the investigation included a study of the environmental conditions to which the tankage is exposed, purge gas cryopumping analysis, and heat transfer analysis. The investigation consisted of screening candidate inner layer insulation materials for permeability, temperature capability, thermal conductivity, density, and strength; modifying candidate materials to improve their properties; and testing large diameter insulation specimens to verify their multicycle capability. Certain commercial materials are identified in this paper in order to specify adequately which materials were investigated in the research effort. In no case does such identification imply recommendation or endorsement of the product by NASA, nor does it imply that the materials are necessarily the only ones or the best ones available for the purpose. In many cases equivalent materials are available and would probably produce equivalent results.

STUDY GUIDELINES

Of primary concern for this study is the effective weight of the purged insulation system which is defined as the sum of the weight of the insulation, the average weight of cryodeposite present during flight, and the average weight of hydrogen boiled off during flight. The weight of a purge gas distribution system is not included on the premise that it is common to all insulation systems (excluding internal insulations). In reality the weight penalty may vary with purge gas flow rate. However, in order for the purge insulation system to be competitive with other systems (see Reference 11) the flow rate, as defined by cryodeposition during ground hold, must be limited to 4.86 kg/m^2 (1.0 lb/ft^2) for a three hour period.

For ground operation, the time between flights varied from 3 to 12 hours and the ambient air temperature was specified as 283K (50°F). The heat transfer coefficient at the external surface was varied between 2.84 and 28.4 J/m^2-sec-K (0.5 and 5.0 BTU/hr -ft^2-F) to account for conditions ranging from still air to relatively high wind velocity. At all times the external surface of the vehicle was to be maintained at temperatures above 273K (32°F). All fuel tanks were assumed to be full during ground operation with a corresponding tank wall temperature of 20K (-423°F).

During flight, heating of the external surface was defined by a specified vehicle shape and trajectory. The vehicle fuselage was approximated as a 20 degree cone/cylinder combination; the diameter of the cylinder was 7.6m (25 feet). The mission profile, shown in Figure 1, was used to compute heat transfer and temperature data. The method of Lee, Ref. 12, was used in laminar regions while the method of Spalding and Chi, Ref. 13, as modified by Neal and Bertram, Ref. 14, was used in turbulent regions. The heat transfer calculations were performed at a large number of locations.

Based on the heat transfer calculations a single station on the cylinder was selected as representative of the heating to be experienced by the vehicle and was used to determine the insulation requirements. Figure 2 presents the variation of the vehicle external surface temperature for three locations at the selected station for the specimen trajectory. During flight either wet or dry tank conditions were postulated depending upon whether liquid or gaseous hydrogen was in contact with the wall. For the thermal analysis the wet tank wall was treated as an isothermal surface at 20K (-423°F); the dry tank wall was treated as an adiabatic surface. Since an ullage volume exists during flight the top of the tank was always analyzed as a dry tank whereas both wet and dry conditions were considered at the bottom of the tank. To provide insight on the impact of thermal protection system (TPS) weight on an entire vehicle, tanks were sized to be representative of a Mach 8 vehicle; usage schedule similiar to that used in Ref. 15 was adopted; and the temperature data of Figure 2 were used in the section entitled Comparison of TPS Concepts.

As an initial guideline for this study, the fuel tank was to be capable of withstanding a maximum temperature of 811K (1000°F) with corresponding high temperature requirements placed on the insulation nearest the tank. Subsequent analysis indicated that a tank with an optimized thermal protection system would not attain this temperature, even when empty, therefore, the temperature restriction on the insulation was relaxed. The revised guideline was that the maximum service temperature of the selected insulation must not be exceeded under any operating conditions.

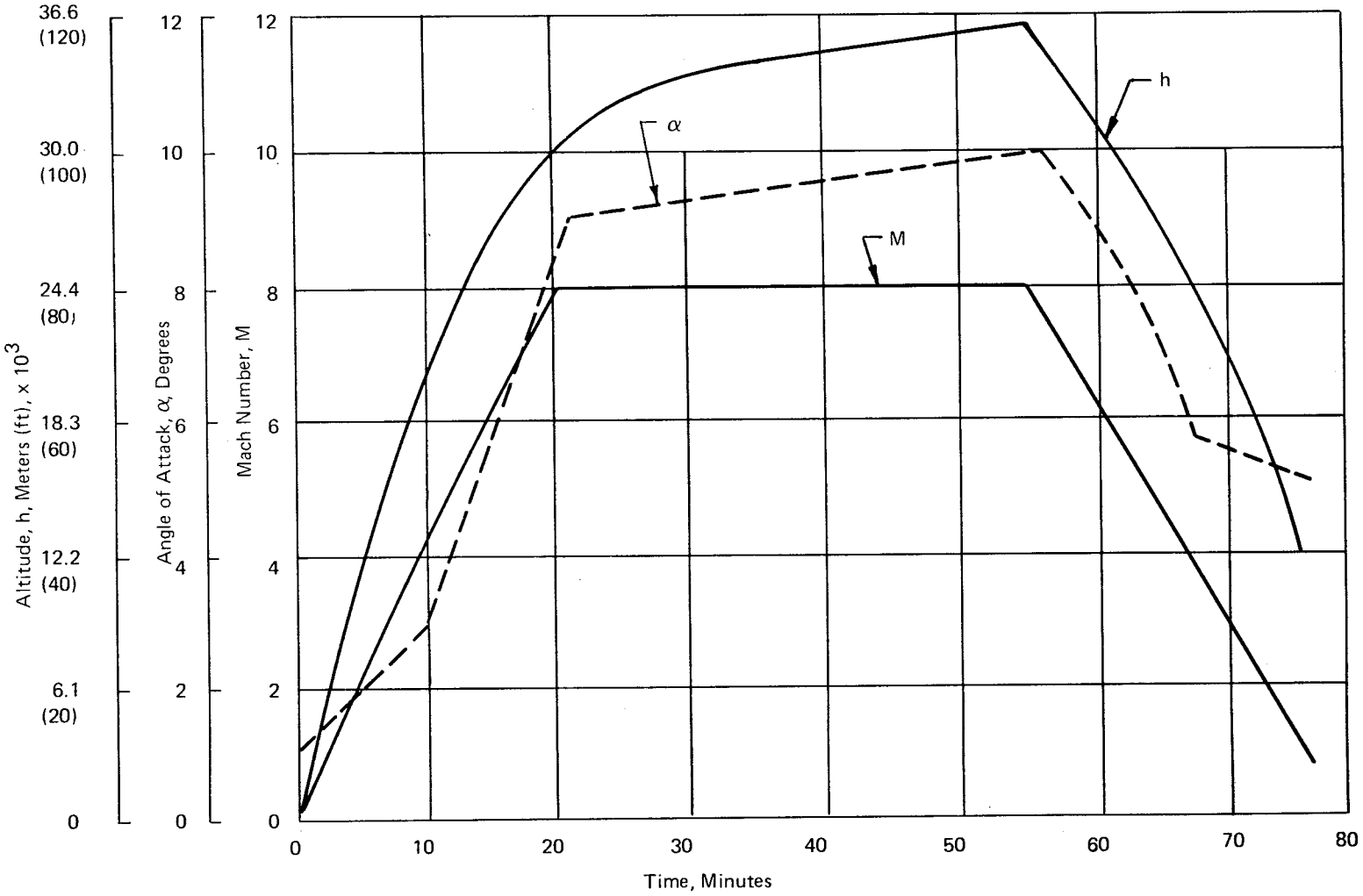

Figure 1. Hypersonic Transport Trajectory Data

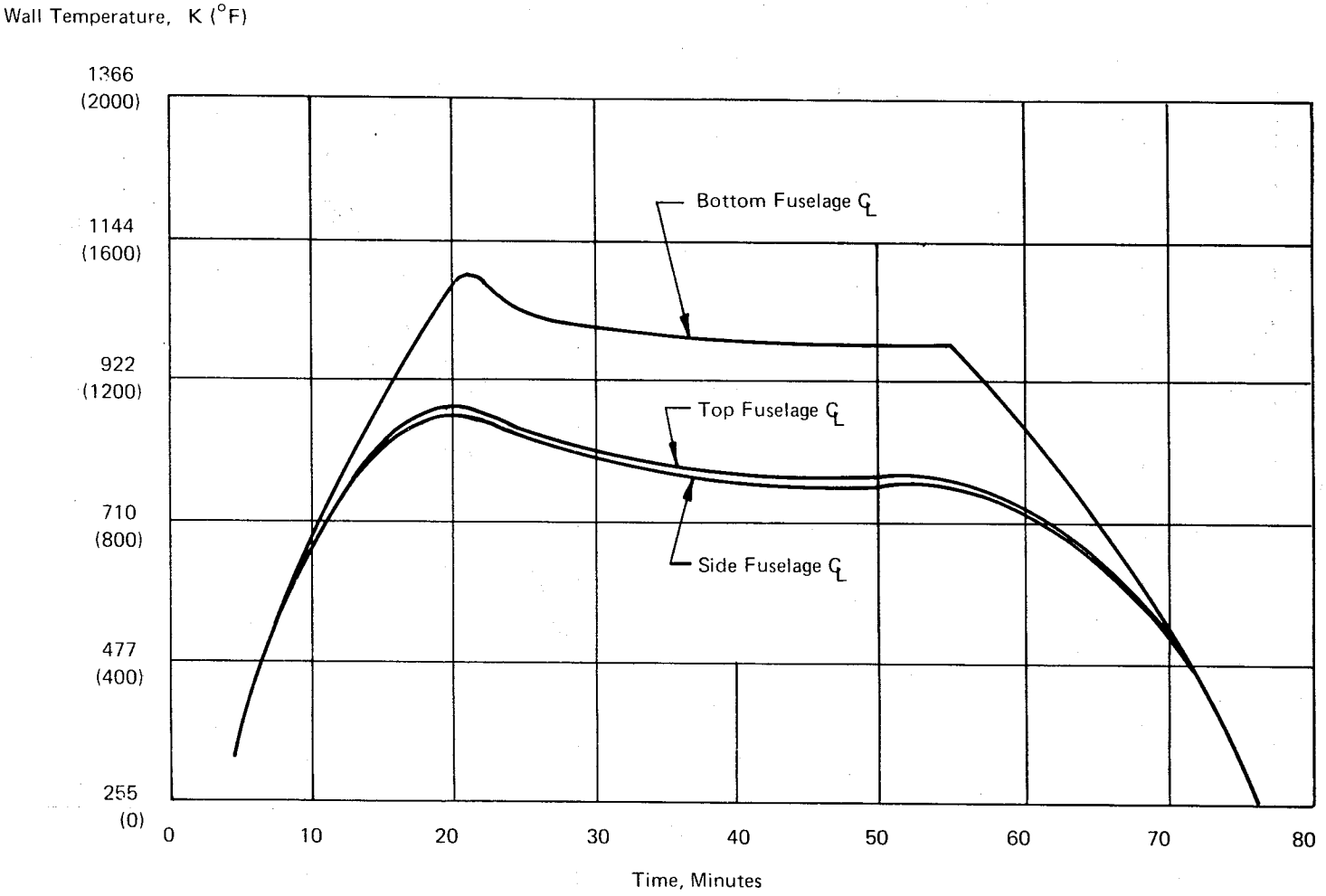

Figure 2. Radiation Equilibrium Temperature History for the Hypersonic Transport, $\epsilon = 0.8$, Station 27.4 M (90 ft)

THERMAL PROTECTION SYSTEM DESCRIPTION

As shown schematically in Figure 3, the thermal protection system concept studied consisted of an outer skin or heat shield, an inert purge gas, two layers of insulation and the hydrogen tank wall. The outer layer of insulation serves the sole purpose of reducing the heat flow to the tank and inner layer of insulation. As such, it is required to have a low ρK product and a high maximum service temperature, since it is exposed to heating from the outer surface which, for this application, reaches a maximum radiation temperature of almost 1144K (1600°F). Based on previous studies Dynaflex with a density of 96 kg/m^3 (6 pcf) was selected for this layer and used throughout the study.

The inner layer of insulation serves a more complex function. In addition to providing thermal insulation, it must restrict or prevent the flow of the condensible purge gas to the tank wall by cryopumping and contain any cryodeposit that may be formed. The selection of the material for this inner layer and validation of its performance are the primary objectives of the investigation.

Two inert purge gases were considered for the thermal protection system. Carbon dioxide was considered since it does not have a liquid phase at the pressures of interest which eliminates liquid run-off and potential cryopumping. However, its freezing temperature is 195K (-109°F) which is high in comparison to the liquid hydrogen tank temperature. This difference permits large thicknesses of CO_2 frost to deposit during ground hold. Nitrogen has a much lower freezing point of 77K (-320°F) which reduces the thickness of the frost layer. In addition, it is readily available at low cost; thus it was considered as a promising purge gas.

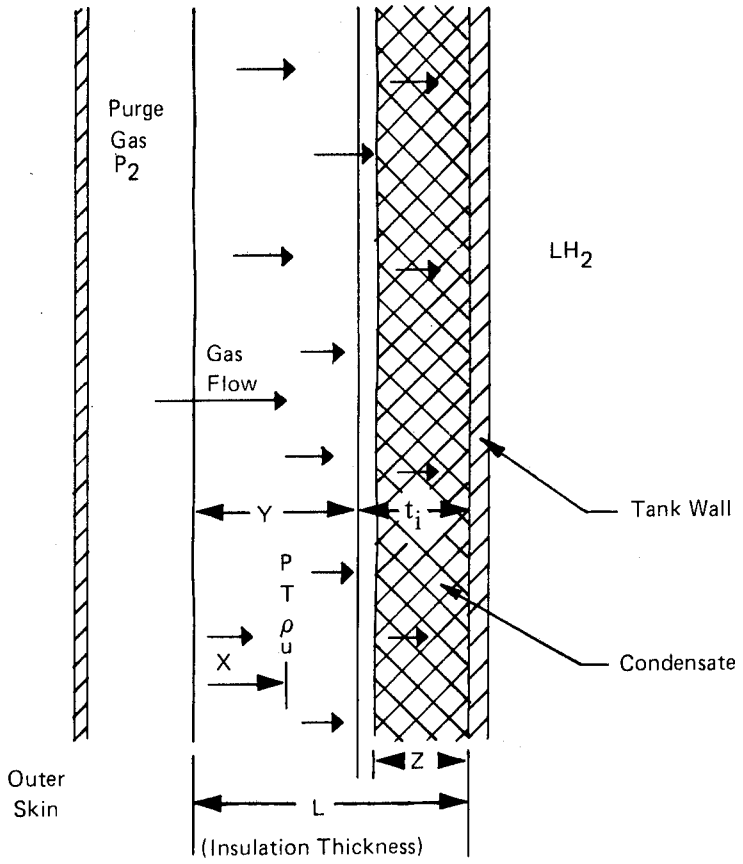

Figure 3. Schematic Drawing of Thermal Protection System for LH_2 Tankage

THERMAL PROTECTION SYSTEM ANALYSIS

Presented in this section are brief descriptions of the analysis methods and a summary of the results of application of the methods. Substantiative experimental results, although obtained concurrently, are in general, included in the following section. A more detailed description of the analytical model development and the analytical results are available in Appendix A.

Cryodeposition

Analysis of a permeable insulation system must consider the flow of heat and purge gas through the insulation. During ground hold, purge gas at the tank wall (see Figure 1) is condensed and a pressure gradient is induced through the insulation producing an inflow of purge gas which is condensed and deposited. As the cryodeposited layer grows, it begins to insulate the tank and it becomes progressively more difficult to remove heat from the purge gas. Thus, the physical process governing cryodeposition is a complex function involving the interaction of the insulation, purge gas, and cryodeposit on the mass and heat inflow.

For low permeability insulations, two limiting cases exist: One is limited by the rate the purge gas can diffuse through the insulation; the other is limited by the rate heat can flow through the insulation and cryodeposit layer. The equation for the deposition rate for the diffusion (permeability limited) process (developed more fully in Appendix A) is:

$$\dot{w} = \frac{\phi}{\sqrt{x^2 - 2\theta\psi}}$$

where:

$$\phi = \left[\frac{B_o \rho_g \Delta P}{\mu \nu \rho_f}\right] \text{ and } \psi = \left[\frac{B_o \rho_g \Delta P}{\mu}\right]$$

are positive quantities involving the purge gas properties and the permeability of the insulation (B_0). When diffusion dominates, both are essentially constant and it can be seen that the deposition rate of purge gas will increase with time since the distance the purge gas must diffuse as defined by the quantity $x^2 - 2\theta\psi$, will become progressively smaller.

Cryodeposition can continue to occur only as long as sufficient heat can be transferred through the insulation and cryodeposit to the tank wall where it can be absorbed by hydrogen boil off. Thus, in all cases, the cryodeposition rate eventually becomes heat transfer limited as the thickness of the cryodeposit increases (for highly permeable insulations, heat transfer very rapidly becomes the controlling factor). The following equation from Appendix A defines the deposition rate for the heat transfer limited case .

$$\dot{w} = \sqrt{\frac{\nu \rho_f k_f (T_f - T_w)}{2 h_{fg} \theta}}$$

As can be seen deposition for a heat transfer limited case continues at a continually decreasing rate approaching an equilibrium frost thickness. Although cryodeposition is actually controlled by an interaction of the two processes, the results of cryodeposition tests with small insulation samples, presented in Appendix C, indicates that these limiting cases are representative of the actual process.

Preliminary calculations using these equations with typical insulation and purge gas properties revealed that a diffusion controlled process was required to meet the cryodeposition limit of the study guideline i.e., 4.86 kg/m^2 (1 lb/ft^2) for a 3 hour period. Furthermore, Figure 4 shows that this deposition rate dictates an insulation with a permeability coefficient of less than 1 millidarcy for a carbon dixiode purge or .8 millidarcy for a nitrogen purge.

Parametric Weight Studies

By combining conventional heat transfer relationships for conduction through the insulation and the cryodeposition relationships including the properties and thickness of the frost build-up, it was possible to compute system weights for specified thicknesses of outer fibrous and inner permeable insulation materials. Because of the complexity of the equations, the minimum weight design had to be determined by an iterative technique. This involved initial analyses for several thicknesses of inner insulation with a single value for the outer insulation thickness. The weight data, ground surface temperature data, and the interface temperature data were each fitted by a least square polynomial with the inner insulation thickness as the independent variable. Utilizing these equations, with the differentiated form of the polynomial weight equation, permitted the determination of the inner insulation thickness that resulted in least weight while satisfying the ground surface temperature and interface temperature constraint. By repeating this procedure for several outer insulation thicknesses, it was possible to find the combination of insulation thicknesses that resulted in the least weight thermal protection system for any set of conditions based on a permeable inner insulation.

For the nonpermeable inner insulation the procedure was simplified because cryodeposition was avoided by requiring that the temperature of the interface between the high temperature insulation and the impermeable foam be slightly greater than the condensation point of the purge gas.

Permeable - Weight and thickness data were computed on a unit area basis for ground and flight conditions for 383 kg/m^3 (24 pcf) Microtherm insulation purged with nitrogen or with carbon dioxide. Microtherm insulation was selected since it was the only permeable insulation with an acceptable permeability that showed any promise during the small sample verification tests described in the next section. Lower and upper centerline locations were examined, the former for both wet and dry tank walls and the latter for only the dry wall case.

Parametric weight trends for the nitrogen purge are presented in Figure 5 as a function of the ground hold heat flux (air velocity) for a 6 hour ground hold. The break at about 350 W/m^2 (125 BTU/ft^{2}hr) represents a change from all Microtherm insulation to a combination of Dynaflex and Microtherm. At low heat fluxes the frost layer is thick and the use of only the Microtherm insulation is desirable.

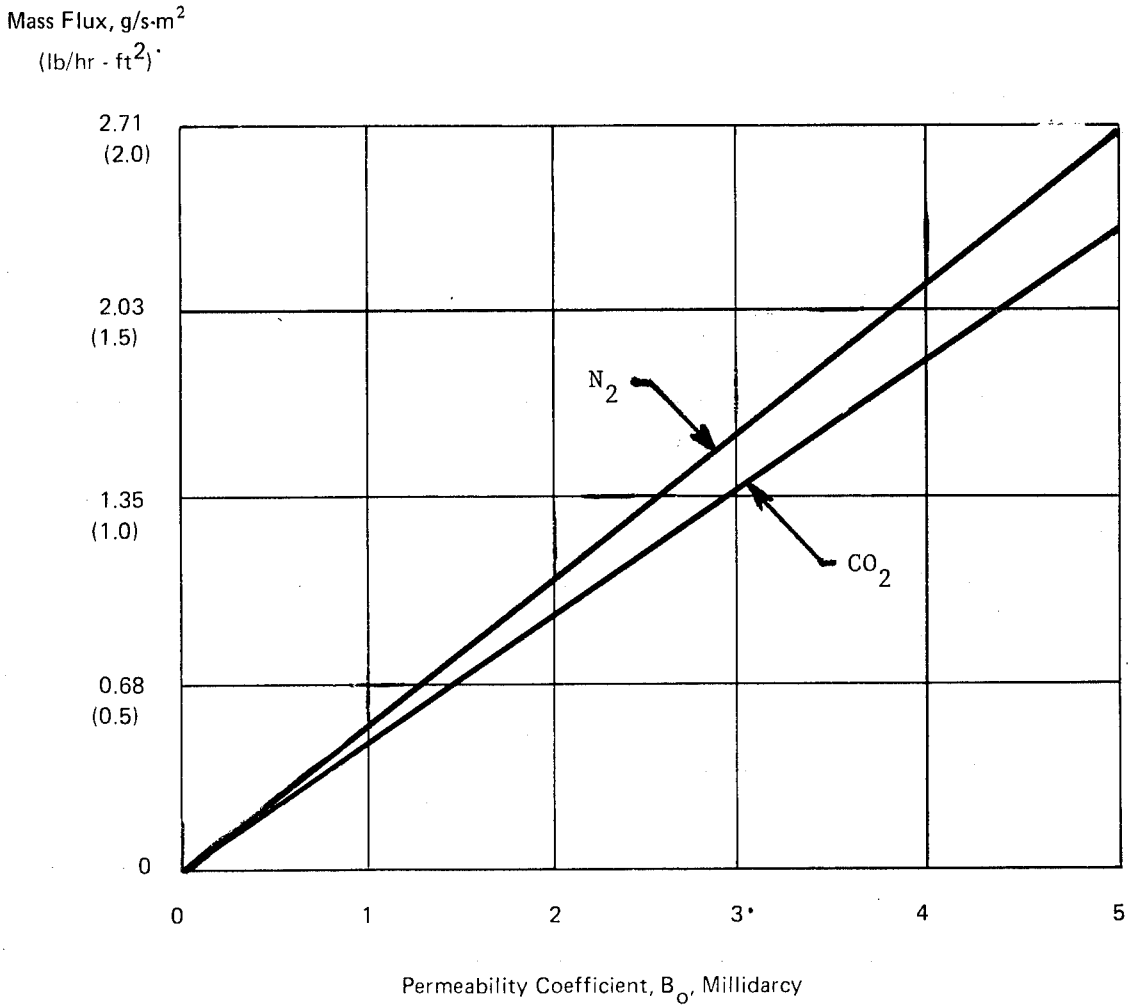

Figure 4. Permeability Effects on Mass Flux (for 2.54 cm (1.0 in.) thick insulation).

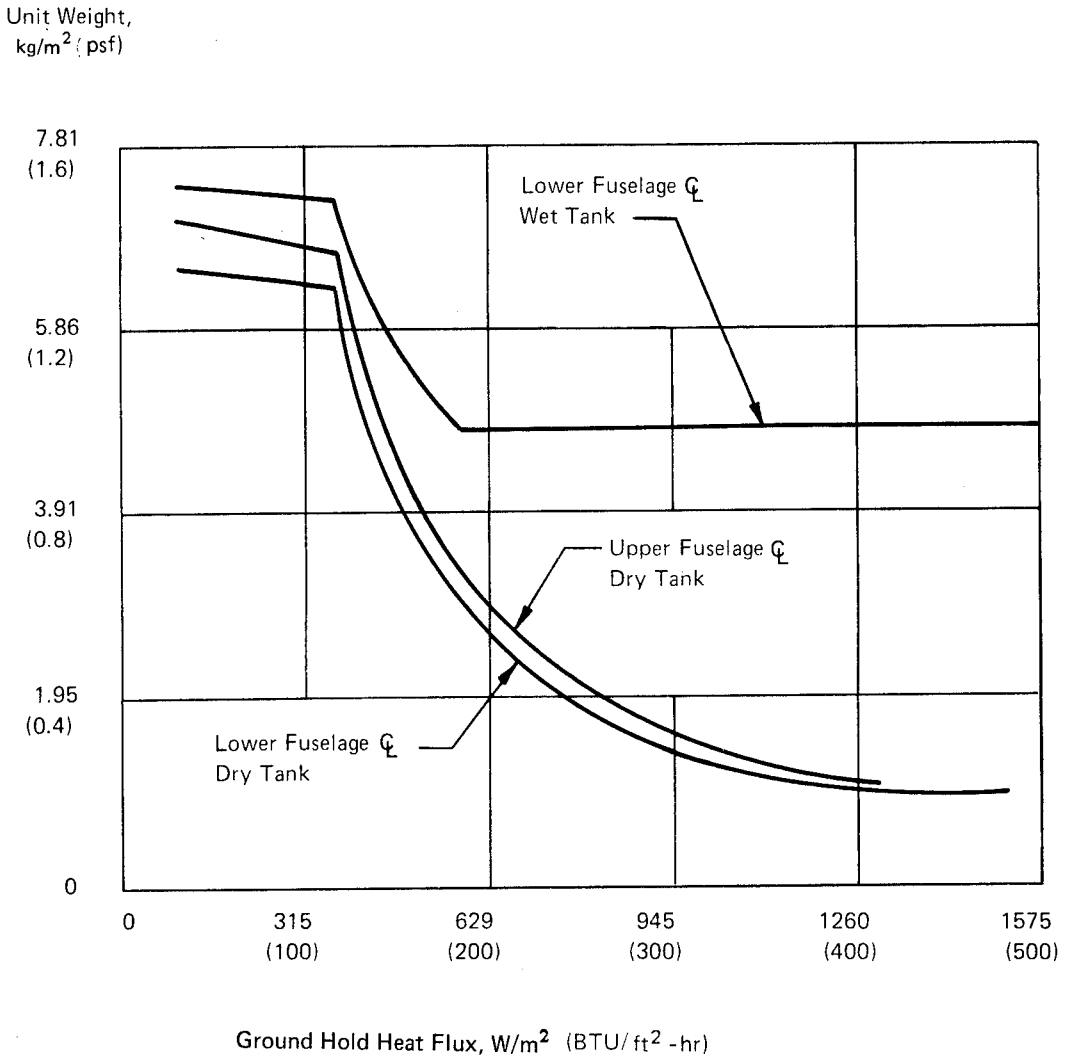

Figure 5. Effect of Ground Hold Heat Flux on TPS Weight, for the Hypersonic Transport Tankage, Nitrogen Purge Gas, 6 Hour Ground Hold

The second break in the wet tank case indicates where the insulation sizing is no longer influenced by the 6-hour ground hold condition but is dictated by flight conditions. The lighter weight of the lower centerline for the dry tank case is due to greater evaporation of the cryodeposit during flight. Trends for other hold times and for the carbon dioxide purge were similar. The most important conclusion to be drawn is that low ground heat flux conditions (still ambient air) dictate greater insulation thicknesses and TPS weights. Warm purge gas flowing at a moderate velocity during ground hold would reduce TPS weight by increasing the heat flux to the liquid hydrogen. However, this weight saving must be traded off against the added costs of heating the purge gas and replacing the hydrogen boil off.

The preceding results assumed a frost density of 640 kg/m^3 (40 pcf) and a frost conductivity of 0.115 W/m·K (0.8 BTU in./ft^{2}hr°F). Both parameters influence the sizing and weight of the permeable thermal protection system. This influence is illustrated in Figure 6 for the wet tank case with nitrogen purge. Results for the dry tank cases show similar trends with lower weights and somewhat less sensitivity to frost conductivity; weights with carbon dioxide were heavier. The break in the weight trend is caused by a change in the constraint that controls relative thicknesses of insulation. For the higher values of frost conductivity the heat flow to the hydrogen tankage is high and causes large weights of boil off. Least weight is achieved by minimizing frost thickness, eliminating Dynaflex and using Microtherm to minimize the rate of purge gas deposition. As the effective thermal conductivity of the frost layer is reduced the better thermal efficiency of the Dynaflex insulation dominates and it is desirable to minimize the thickness of Microtherm to the point where the frost line is just within the permeable insulation after the longest ground hold required.

Table I summarizes the results of the thermal analyses of the permeable insulation for carbon dioxide and nitrogen purge gases. Frost density was assumed to be 900 kg/m^3 (56 pcf) for carbon dioxide and 640 kg/m^3 (40 pcf) for nitrogen. The same value of thermal conductivity was used for both frosts, 0.115 W/m·K (0.8 BTU in./ft^{2}hr° F). In all cases longer ground holds result in higher weights and carbon dioxide purged systems are heavier than those that use nitrogen. The weight increase with ground hold time are asymptotic and the differences in the unit weights of the TPS at various airframe locations decrease as ground hold time increases. In fact, for long ground hold times the insulation thickness reaches a constant value regardless of location. The weight differences are attributable to the amounts of frost that are evaporated during flight and also the amount of hydrogen fuel boil off during flight. The higher weights of the carbon dioxide designs are due to the higher condensation temperature of this purge gas as compared to nitrogen.

Closed Cell - Mass diffusion through closed cell insulation is negligible, therefore, frost deposition can be avoided by maintaining the interface of the outer and inner insulations at a temperature above the freezing point of the purge gas during ground hold. With this constraint, in conjunction with the other constraints set forth in the study guidelines, conventional transient conduction analysis methods were used to determine the required thicknesses of the outer and inner insulations such that the weight of the thermal protection system is minimized. Since no cryodeposit is formed when the closed cell insulation is used, the system weight becomes the sum of the weights of the two insulation materials and the average hydrogen boil off during flight.

The external temperature constraint of 273K (32°F) dictated a total insulation thickness of 2.7 cm (1.1 inch) under steady state ground hold with an ambient temperature of 283K (50°F) and a heat flux of 284 W/m^2 (90 BTU/ft^{2}hr). The effect of the maximum temperature of the impermeable insulation on TPS weight and total insulation thickness (outer plus inner) is shown in

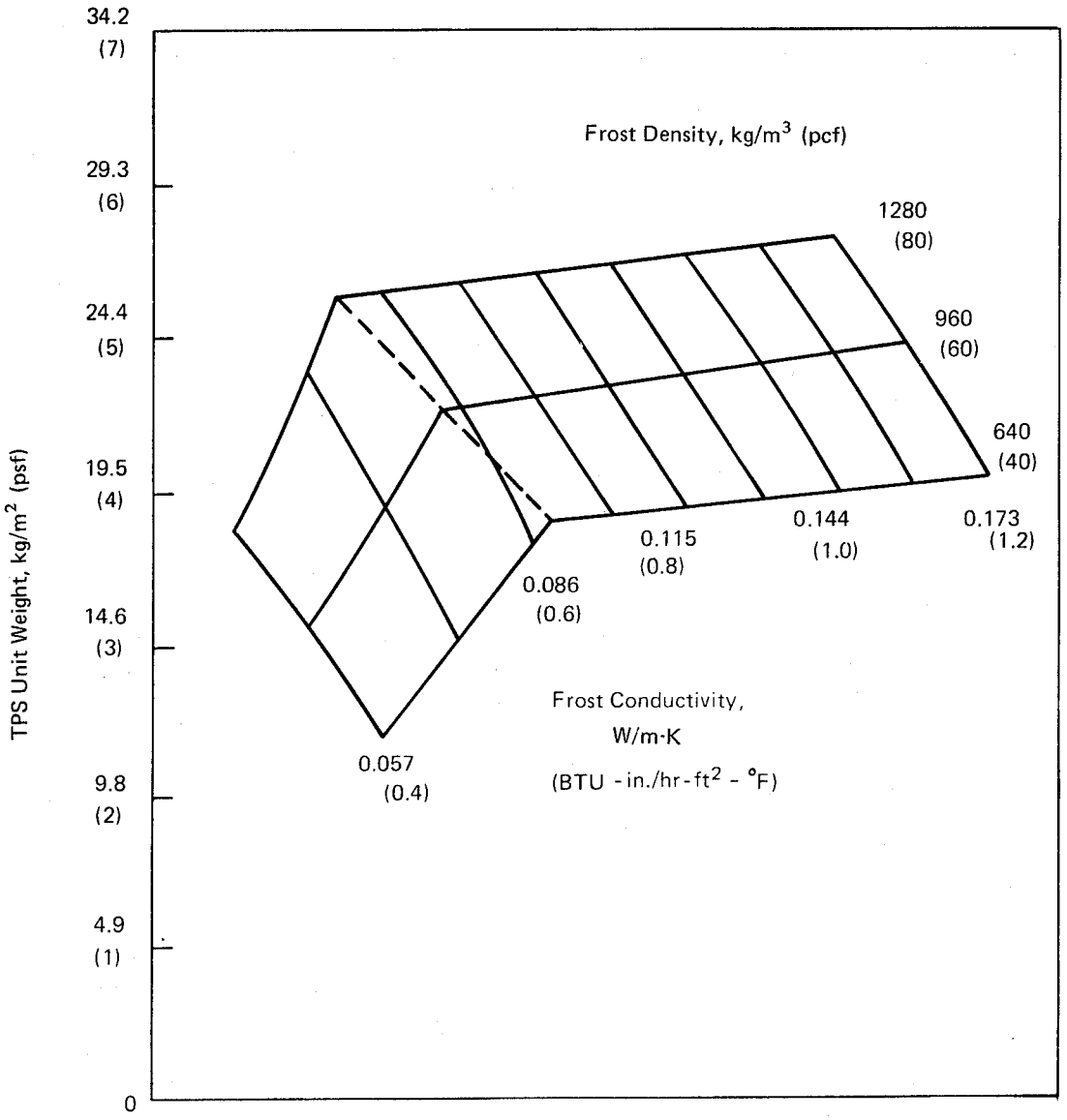

Figure 6. Effect of Nitrogen Frost Density and Thermal Conductivity on TPS Weights for Hypersonic Transport Tankage, Ground Hold = 6 Hours, Ground Heat Flux = 284 W/m² (90 BTU/ft² - hr), Fuselage Lower Centerline, Wet Tank

TABLE I
OPTIMIZED TPS WEIGHTS FOR HYPERSONIC TRANSPORT TANKAGE,
AMBIENT HEAT FLUX = 283 W/m^2 (90 BTU/HR-FT^2), TS = 273 K (32°F)

Location	Wall Status	Ground Hold Time Hours	Weight kg/m^2 (psf)				Insulation Thickness cm (in.)							
			Carbon Dioxide		Nitrogen		Carbon Dioxide				Nitrogen			
							Total		Microtherm		Total		Microtherm	
Fuselage		3	18.1	(3.70)	14.8	(3.03)	2.03	(0.80)	2.03	(0.80)	2.92	(1.15)	1.75	(0.69)
Lower	Wet	6	23.4	(4.79)	19.2	(3.94)	3.56	(1.40)	3.30	(1.30)	3.30	(1.30)	2.49	(0.98)
		12	31.0	(6.35)	24.9	(5.10)	5.46	(2.15)	4.93	(1.94)	4.82	(1.90)	2.34	(0.92)
Fuselage		3	13.5	(2.76)	10.6	(2.18)	2.92	(1.15)	2.59	(1.02)	2.41	(0.95)	1.98	(0.78)
Lower	Dry	6	19.7	(4.03)	16.8	(3.45)	4.19	(1.65)	3.71	(1.46)	3.30	(1.30)	2.49	(0.98)
		12	28.3	(5.79)	23.4	(4.80)	5.84	(2.30)	5.23	(2.06)	4.82	(1.90)	2.33	(0.92)
Fuselage		3	13.8	(2.82)	11.5	(2.36)	2.92	(1.15)	2.62	(1.03)	2.28	(0.9)	2.28	(0.9)
Upper	Dry	6	19.9	(4.07)	17.4	(3.56)	4.19	(1.65)	3.70	(1.46)	3.30	(1.30)	2.49	(0.98)
		12	28.8	(5.90)	24.9	(5.10)	5.84	(2.30)	5.23	(2.06)	4.82	(1.90)	2.33	(0.92)

Figures 7 and 8, respectively, for the three tank wall cases examined previously for the permeable material. The density of the inner insulation has little influence on TPS weight or total insulation thickness. For the wet tank wall, a minimum weight is found at about 420K (300°F). Weights for dry tank walls continue to decrease as the maximum temperature increases because the thickness of the denser outer insulation decreases as the temperature of the lighter inner insulation is allowed to increase. Thickness data of Figure 8 indicate that flight, rather than ground hold, conditions dictate insulation requirements at all locations when maximum foam temperatures are below about 505K (450°F). This is in contrast to results with the permeable insulation where ground hold was dominant. As the allowable maximum temperature is increased the 2.7 cm (1.1 inch) thickness dictated by ground hold is reached first at the wet bottom centerline, about 505K (450°F), then at the dry upper centerline about 535K (500° F), and finally at the dry bottom centerline.

Comparison of TPS Concepts

The TPS weights for each of the four hydrogen tanks in a typical hypersonic transport are shown in Table II and Table III. Comparison of the average unit weights shows that: 1) a system that uses a closed cell insulation is as much as two-thirds lighter than a system that uses the denser permeable insulation for the inner insulation layer, 2) a nitrogen purged insulation system is 15% lighter than a carbon dioxide purged system, and 3) an increase of the maximum service temperature of the closed cell foam from 366K (200°F) to 477K (400°F) will reduce the system weights by as much as 20%. Figure 9 shows the average unit weight of the thermal protection system for the individual tanks and the integrated average for the four tanks of the hypersonic transport as a function of the maximum service temperature of the foam. For the purposes of this study the tanks were emptied in the same order as in Reference 15. The greatest weight savings are realized by the tanks which are emptied early in the flight.

It should be noted that the weights presented in the tables for the system with permeable insulation were based on a ground hold time for six hours and use of Microtherm insulation which has a density of 384 kg/m^3 (24 pcf). A reduction in either of these parameters would make the permeable insulation more promising. However, it would require a ground hold time of less than one hour if the density is 384 kg/m^3 (24 pcf) or it would require a density of less than 96 kg/m^3 (6 pcf) if the ground hold time is 6 hours to make the permeable insulation weight equal to the closed cell system. Therefore, the experimental portion of the study concentrated on reducing the permeability and density of the permeable insulation and on increasing the maximum service temperature of the closed cell foam insulations.

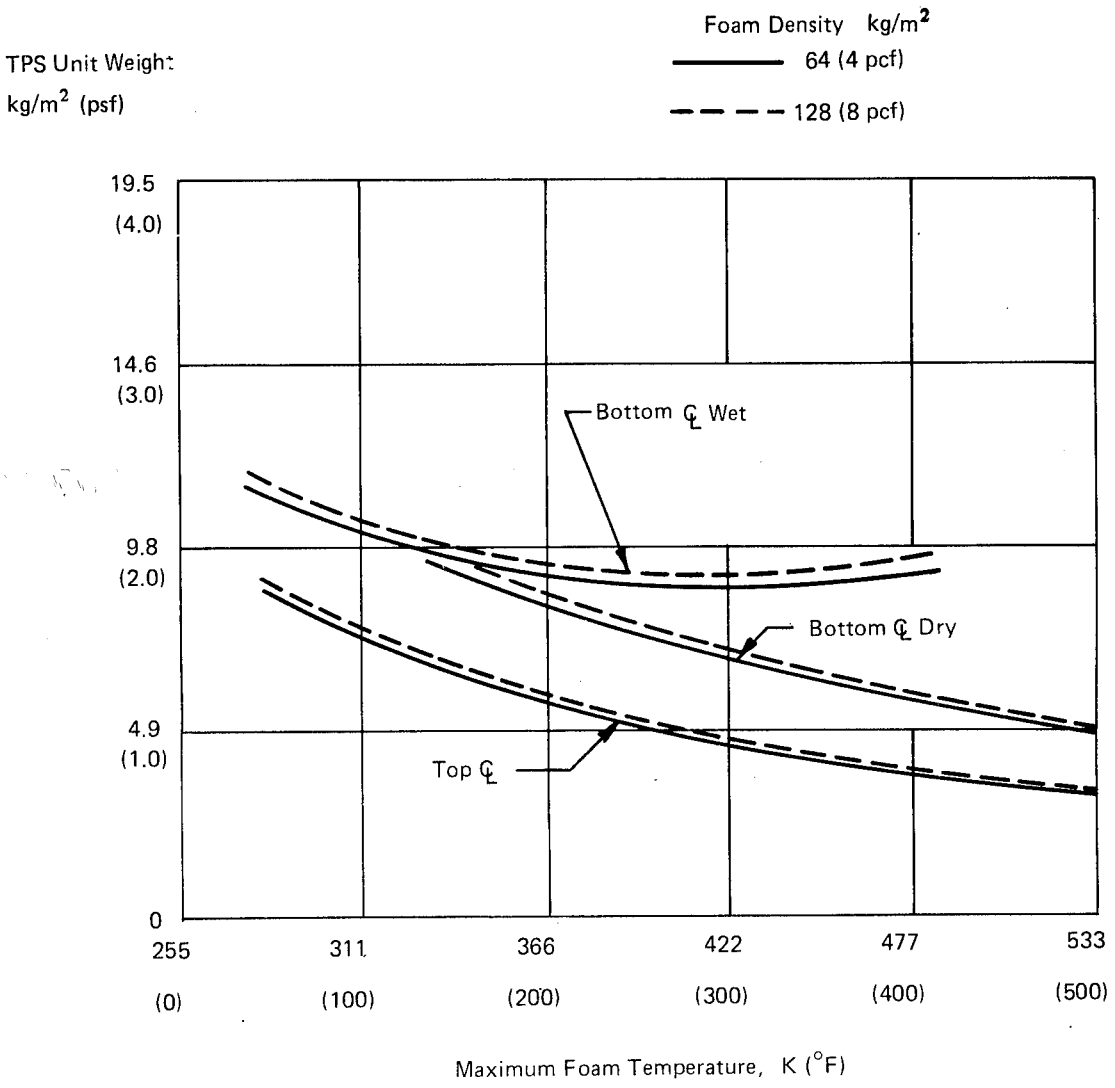

Figure 7. TPS Weight for a Closed Cell Innermost Insulation System
Nitrogen Purge Gas

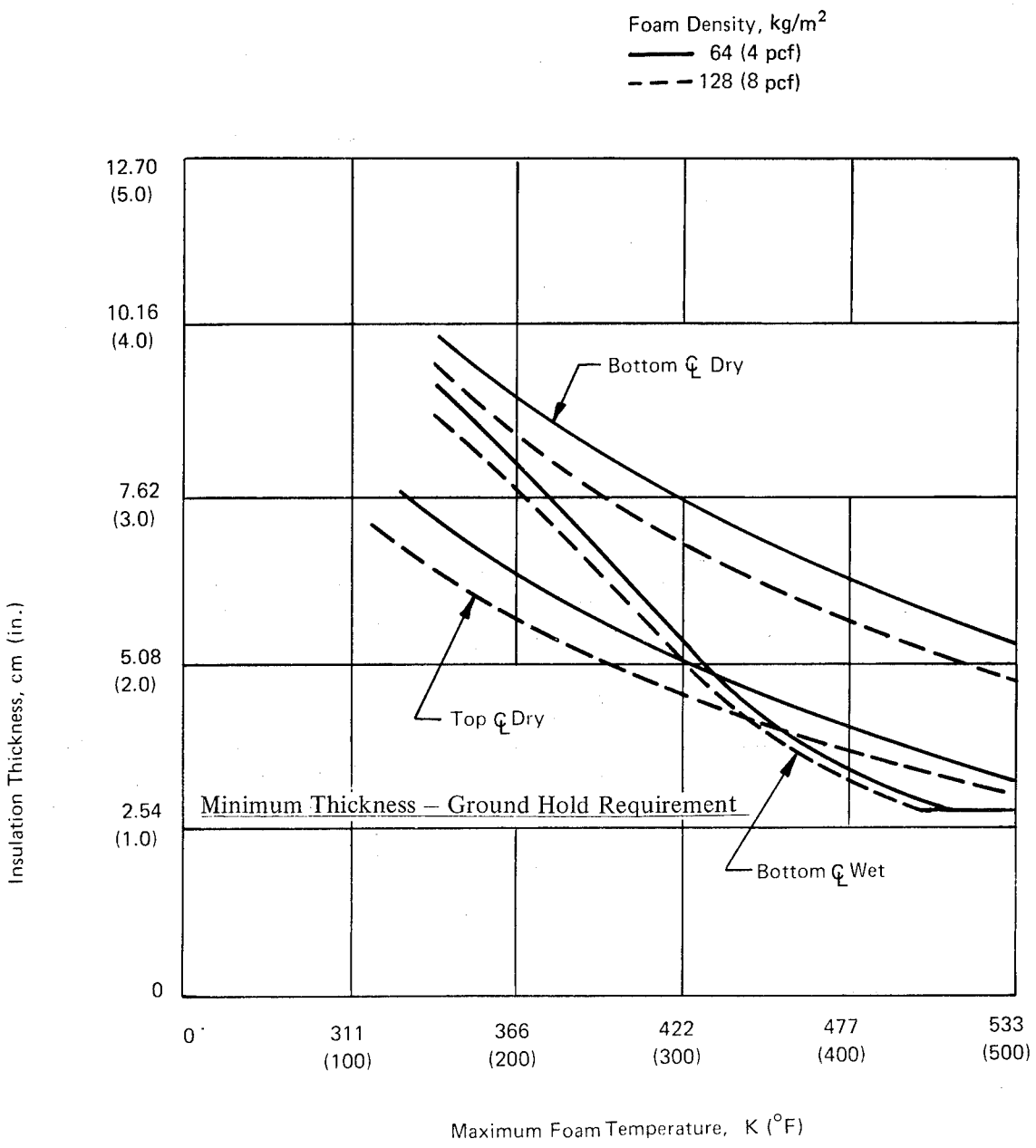

Figure 8. Total Insulation Thickness for a Closed Cell Innermost Insulation System, Nitrogen Purge Gas

TABLE II
COMPARISON OF HYDROGEN TANKAGE TPS WEIGHTS FOR HYPERSONIC TRANSPORT
GROUND HOLD TIME = 6 HR, METRIC UNITS

Tank	Location & Condition	Area (m^2)	Closed Cell Foam Interface Temperature				Microtherm			
			366K		477K		N_2 Purge		CO_2 Purge	
			W/A (kg/m^2)	W (kg)	W/A (kg/m^2)	W (kg)	W/A (kg/m^2)	W (kg)	W/A (kg/m^2)	W (kg)
Forward	Wet Bottom	170.7	9.42	1608	9.03	1541	19.2	3277	23.4	3994
	Dry Bottom	0	8.39	0	6.35	0	16.8	0	19.7	0
	Dry Top	33.6	5.71	192	3.81	128	17.4	585	19.9	668
Forward Center	Wet Bottom	144.6	9.42	1362	9.03	1305	19.2	2776	23.4	3383
	Dry Bottom	43.6	8.39	365	6.35	277	16.8	733	19.7	859
	Dry Top	188.2	5.71	1074	3.81	717	17.4	3275	19.9	3745
Aft Center	Wet Bottom	153.0	9.42	1441	9.03	1382	19.2	2937	23.4	3580
	Dry Bottom	0	8.39	0	6.35	0	16.8	0	19.7	0
	Dry Top	153.0	5.71	874	3.81	582	17.4	2662	19.9	3045
Aft	Wet Bottom	0	9.42	0	9.03	0	19.2	0	23.4	0
	Dry Bottom	131.5	8.39	1103	6.35	835	16.8	2209	19.7	2590
	Dry Top	131.5	5.71	750	3.81	501	17.4	2288	19.9	2617
Total - Four Tanks		1,151.7		8,769		7,268		20,742		24,483
Average unit weight			7.61		6.31		18.0		21.3	

TABLE III
COMPARISON OF HYDROGEN TANKAGE TPS WEIGHTS FOR HYPERSONIC TRANSPORT
GROUND HOLD TIME = 6 HR, ENGLISH UNITS

Tank	Location	Area ft^2	Closed Cell Foam Interface Temperature				Microtherm Purged System			
			200° F		400° F		N_2 Purge		CO_2 Purge	
			W/A (psf)	W (lb)	W/A (psf)	W (lb)	W/A (psf)	W (lb)	W/A (psf)	W (lb)
Forward	Wet Bottom	1,838	1.93	3,547	1.85	3,400	3.94	7,241	4.79	8,804
	Dry Bottom	0	1.72	0	1.30	0	3.45	0	4.03	0
	Dry Top	358	1.17	422	0.78	279	3.56	1,274	4.07	1,457
Forward Center	Wet Bottom	1,541	1.93	2,974	1.85	2,850	3.94	6,071	4.79	7,381
	Dry Bottom	464	1.72	798	1.30	603	3.45	1,601	4.03	1,869
	Dry Tank	2,005	1.17	2,345	0.78	1,563	3.56	7,138	4.07	8,160
Aft Center	Wet Bottom	1,630	1.93	3,145	1.85	3,015	3.94	6,422	4.79	7,808
	Dry Bottom	0	1.72	0	1.30	0	3.45	0	4.03	0
	Dry Top	1,630	1.17	1,907	0.78	1,271	3.56	5,802	4.07	6,634
Aft	Wet Bottom	0	1.93	0	1.85	0	3.94	0	4.79	0
	Dry Bottom	1,400	1.72	2,408	1.30	1,820	3.45	4,830	4.03	5,642
	Dry Top	1,400	1.17	1,638	0.78	1,092	3.56	4,984	4.07	5,698
Total - Four Tanks		12,266		19,184		15,893		45,363		53,450
Average Unit Weight			1.56		1.29		3.69		4.35	

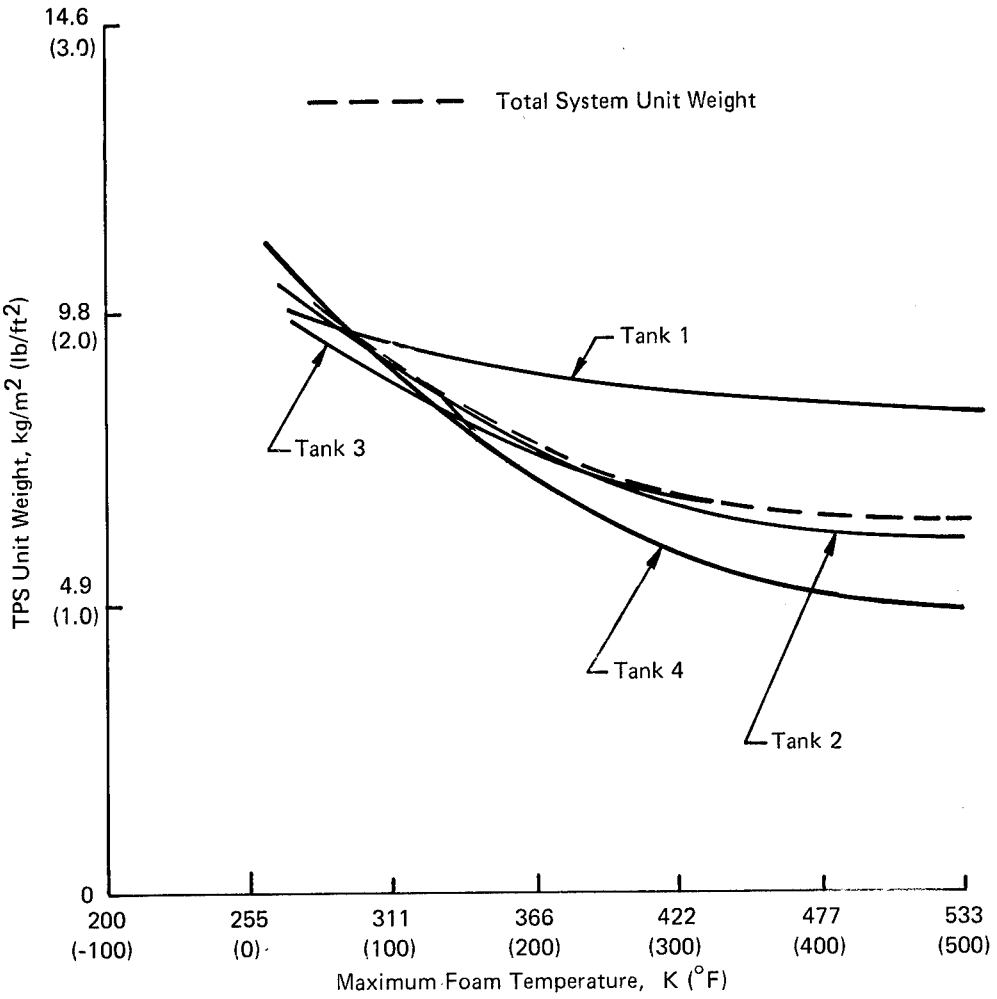

Figure 9. Variation of Hydrogen Tankage TPS Unit Weights with Maximum Foam Temperature, Hypersonic Transport Tankage

MATERIAL SELECTION

The previous selections showed that the TPS weights of a purged insulation system are highly dependent upon the properties of the insulation material that contacts the tank wall. Initially the study focused on materials that would not restrict the operating temperature level of the fuel tank. Later in the program, analytical studies showed that the tank wall would not exceed 311K (100°F), so emphasis was shifted to lower temperature, less permeable insulations. Regardless of the temperature range of interest, insulation properties of importance included permeability, thermal conductivity, density, and strength.

High Service Temperature Materials

In the initial attempts to find a high-temperature, low permeability insulation for the inner layer, a large number of commercially available materials were screened. In general, these materials were limited to those with a maximum service temperature of 1144K (1600°F) or greater; however, the permeability characteristics of some lower temperature materials were also examined. Results of these studies are summarized in the following sections and discussed in more detail in Appendix B.

Permeability Tests – The initial permeability tests indicated that the best high temperature insulating materials available exceeded acceptable levels of permeability for successful use in purged insulation systems for liquid hydrogen tanks. A number of techniques were investigated for reducing the pore size of commercially available materials so as to decrease permeability. Techniques that were tried included recrystallization of magnesium sulfate from saturated aqueous and alcohol solutions, filling the pores with submicron colloidal silica particles, depositing smoke particles, and increasing density by compression. Only the compression approach provided a substantial improvement. By increasing the density of Min-K from 320 kg/m^3 (20 pcf) to 670 kg/m^3 (42 pcf), the permeability was decreased from about 4 millidarcies to less than 2 millidarcies. However, this permeation was not as low as that of a special high density insulation later obtained from the manufacturer which had a permeability of 0.6 millidarcies.

Liquid Retention – Unlike carbon dioxide, nitrogen has a liquid phase at pressures below 5 atmospheres. Thus, a continuous pumping action of the purge gas to the tank wall could be established if the liquid flows from the insulation. For a nitrogen purge system to function properly, the capillary forces must be greater than the dynamic forces from the expected acceleration levels. Therefore, the liquid retention characteristics of the promising, permeable insulations had to be defined. The materials included Min-K 2000, Microtherm and Grumman CPI. Tests with Min-K 2000, which was shown to have a permeability of less than 4 millidarcies, indicated that an acceleration of at least several hundred times the gravitational acceleration was required to dislodge the liquid drops from the insulation. Since the pore size of this insulation is comparable to the other permeable insulations, it was concluded that any insulation that satisfies the permeability requirement will also retain liquid nitrogen. Appendix B describes the test apparatus used to obtain these results and also presents the test results.

Low Service Temperature Materials

After the search for a lightweight, low permeability, high temperature insulation proved unsuccessful and the analytical predictions showed that the tank wall would never exceed 311K (100°F) with an optimum weight thermal protection system, the maximum operating temperature limit of the insulation was reduced. This opened the study to include the benefits derivable from using closed cell plastic foams. Because of the modest temperature limit of these insulations, 366K (200°F), they require an added thickness of the higher temperature insulation to limit their temperature during high speed flight. This additional weight was more than offset by reduction in the innermost insulation weight and the cryodeposited purge gas. Even further reductions were possible by increasing the maximum upper temperature limit of the insulation as previously shown in Figure 7. Considering the nature of polymeric materials, a target temperature of 450K (350°F) was set with aging at elevated temperatures as the primary means for attaining this goal.

Candidate Materials – Contacts with a number of American and European vendors resulted in a list of candidate materials as presented in Table IV. The ADL cryogenic urethane foam specimens which were reinforced with chopped glass fibers were of two variations. One had integral plastic skins formed during the foaming process whereas the other was devoid of skins as a result of being cut from a thicker block of lower density insulation with fewer voids. In addition, a polybenzimidazole foam developed by the Ames Research Center of NASA was included in this series of screening evaluations. It should be noted that most of the materials evaluated were not developed specifically for the insulation of cryogenic tanks, and that none of the suppliers made any claims in this regard. Furthermore, the inability of some materials to meet the requirements of this program should not be construed in any way to detract from their ability to perform the functions for which they were developed.

Thermal Effects – Many of the closed cell insulations have a modest upper temperature limit established by thermal distortion. The effect of elevated temperature on some of the candidate insulations is shown in Figure 10. (It should be noted that these specimens were not originally of identical size.) The Last-A-Foam and Rohacell materials exhibited the greatest dimensional stability through the two thermal cycles. They also exhibited no degradation in performance from thermal exposure up to 450K (350°F).

It was known that the thermal distortion effects of some of the materials can be alleviated by aging (i.e., curing) at elevated temperatures while the material is restrained against thermal expansion. (For example see Ref. 16.) Therefore, both aged and unaged specimens of some of the foams were examined in subsequent testing.

Screening Tests – Three types of screening tests were conducted on the candidate foams: (1) permeability, (2) liquid nitrogen cold shock, and (3) high temperature limit. The permeability testing involved exposure of a small sample 0.63 x 2.5 x 2.5 cm (0.25 x 1 x 1-inch), to a helium gas pressure differential of 103 kN/m^2 (15 psi). The opposite side of the test apparatus was connected to a helium mass spectrometer. In the shock test a sample at room temperature was plunged into a bath of liquid nitrogen, left immersed for about 5 minutes, and returned to the room temperature environment; this process was repeated several times. During the first immersion, the sample was flexed with hand tongs to check for brittleness. In addition to shocking flat samples, some specimens consisted of two pieces of insulation bonded to form a butt joint and bonded to aluminum alloy plates. The upper temperature limit was determined by heating samples with a planform

TABLE IV
CANDIDATE CLOSED CELL PLASTIC FOAMS

Name	Supplier	Material	Density Range kg/m^3 (psf)
ADL Cryogenic Urethane Foam	Formulated by A.D. Little, Inc.	Polyurethane Reinforced with chopped glass fibers	64 to 110 (4 to 7)
Klegecell H917	L'Air Liquide Sassenage, France	Rigid Polyvinylchloride	32 to 87 (2 to 5.5)
Stepan Foam G-302	Stepan Chemical Company	Polyester	32 (2)
Sablon	Solar Division of International Harvester	Polyimide	8 to 640 (0.5 to 4.0)
Last-A-Foam FR-3604-HF	General Plastics Manufacturing Co.	Polyurethane	24 to 40 (1.5 to 2.5)
Rohacell	ROHM Gmbh Kirchen-Allee, Germany	Polymethacrylimide	30 to 80 (1.8 to 5.0)
Ames	Formulated by NASA/ARC	Polybenzimidazole	24 to 32 (1.5 to 2.0)

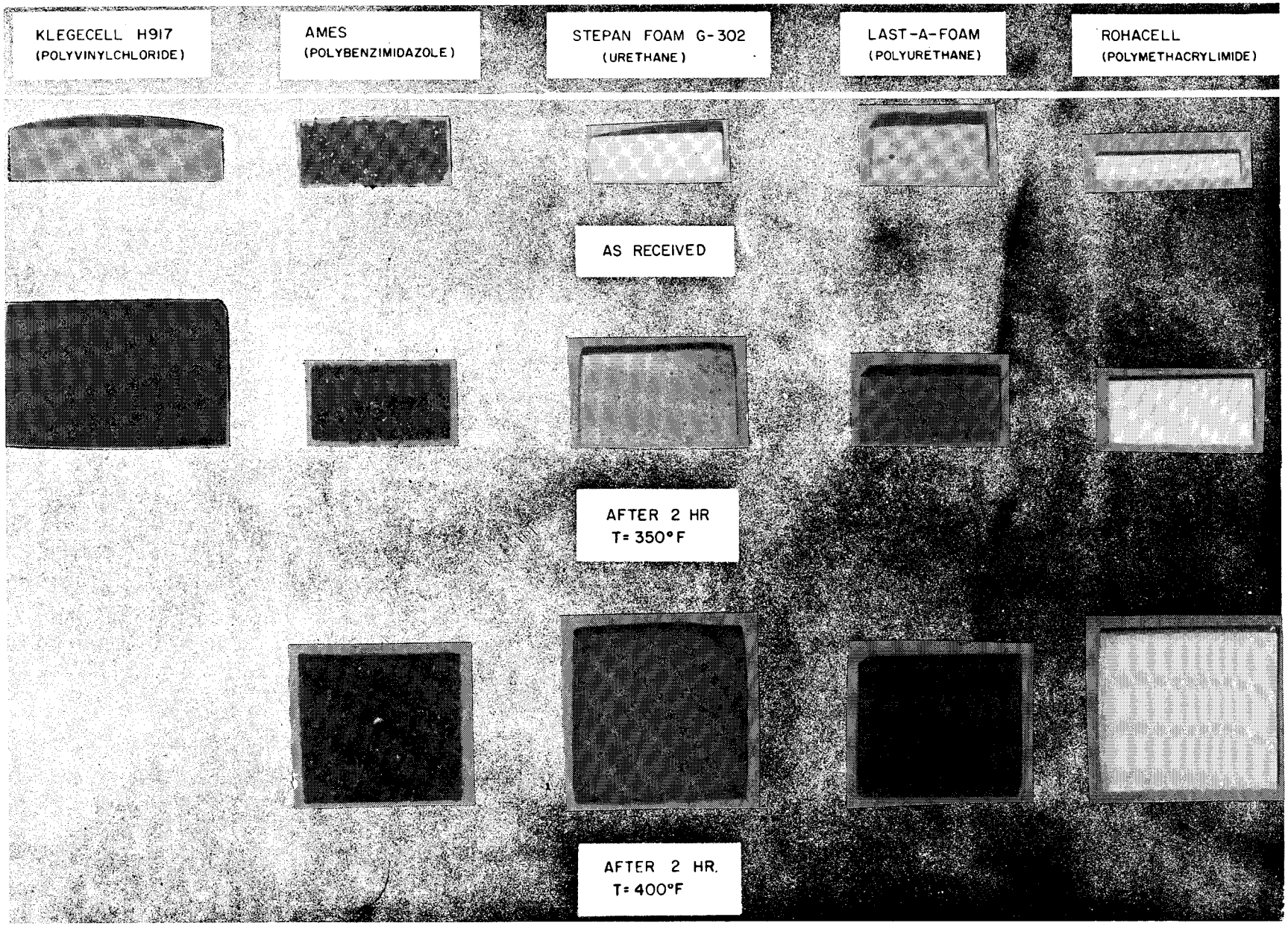

Figure 10.- Cryogenic Insulation Foam

area of between 33 and 64 cm^2 (5 to 10 in^2) in an electrical oven. Dimensions were measured periodically to check for shrinkage, and when a change of about 1% was noted, the heating was stopped.

The ADL foam with integral skins withstood the liquid nitrogen cold shock test and passed the permeability tests, both before and after a short time exposure to 422K (300°F), although the color changed as a result of the thermal exposure. The foam cut from a thick slab, and consequently without skins, passed the liquid nitrogen cold shock, but became brittle during exposure at 450K (350°F). Subsequent testing showed that aging of the ADL foam (6 hours at 400K (260°) and 6 hours at 450K (350°F)) with and without skins had an undesirable effect on its permeability. The Sablon and Ames polybenzimidazole foams failed both types of permeability tests and were eliminated from further consideration. The Klegecell material was eliminated on the basis of its relatively low maximum temperature capability, about 394K (250°F). The Stepan Foam G-302 passed the permeability tests and appeared useful at temperatures below 422K (350°F). However, it was eliminated in preference to Last-A-Foam FR-3600 HF and Rohacell, both of which indicated possible use of temperatures slightly in excess of 450K (350°F). These two materials were subjected to simulated purge cycling conditions at low and high temperatures. A 5 x 5 x 18 cm (2 x 2 x 7 inch) open aluminum vessel was covered on five sides by bonding insulation material to its exterior. The insulated area was enclosed by a plastic bag and exposed to carbon dioxide gas while the vessel was filled with liquid nitrogen. The filled vessel was then placed into an oven set at 422K (300°F) while the liquid nitrogen boiled away. This was repeated three times. No problems were encountered with either material.

Since both the Last-A-Foam (polyurethane) and the Rohacell (polymethacrylimide) indicated good performance under all of the screening tests, the choice of which material to use for large scale testing was based on visual examination. The cell structure of the Rohacell insulation was small and uniform while the Last-A-Foam contained a few quite large cells or voids; consequently, the Rohacell was selected.

LARGE SCALE TESTING

The primary purpose of the large scale testing was to subject a large insulation specimen to the pressure/temperature/purge gas characteristics that would be experienced by a liquid hydrogen fuel tank during service. Since hydrogen fuel tanks are expected to be of relatively large diameter a flat specimen configuration was considered to be acceptable. Testing was limited to closed cell plastic foam materials because screening tests and analytical predictions indicated a superiority of impermeable materials despite their low maximum temperature limits.

Apparatus and Procedures

A specimen diameter of 76 cm (30 inches) was selected which led to an apparatus shown schematically in Figure 11, having an outside diameter of 99 cm (39 inches). The upper shell of the apparatus contains the cryogen tank which is protected by ADL cryogenic urethane foam with chopped glass fibers; the specimen is mounted on the lower surface of the upper shell. The detachable bottom shell forms the container for the purge gas and encloses an electrical heating blanket which is installed against the insulation. A controlled purge gas supply and a vacuum pump are provided to simulate altitude conditions. Even though the test vessel was designed to incorporate a trunnion such that the test insulation could be horizontal downward, vertical, or horizontal upward, only the downward facing condition was evaluated since it represented the wet tank wall where the characteristics of the insulation system are most critical. Details of the test apparatus, which was orginally designed as a more complex guarded calorimeter, are described in Appendicies F, G and H.

The test procedure involved replacement of the air in the purge chamber with purge gas, cool down of the apparatus by flowing the test cryogen into the simulated tank under a pressure of about 5.5 kN/m^2 (8 psig), and operation of the heater blanket to produce the desired temperature of the warm side of the insulation. The pressure altitude history of the purge gas was controlled by adding or removing gas so that the vehicle mission conditions were simulated. Figure 12 shows the calculated temperature history of the warm side of the insulation, the nominal test cycle and the range of test data. The duration of the experimental heat-up and cool-down periods were designed to be shorter than for the actual flight for test expediency since a simplified stress analysis indicated that the duration had only a slight effect on stress level. The pressure history of the purge gas is shown in Figure 13.

Materials Tested

Closed cell plastic foams of two different compositions, polyurethane and polymethacrylimide were evaluated. The polyurethane specimens which were formulated by Arthur D. Little, Inc. included unaged specimens with integral plastic skins formed at the interface of the mold when the material was foamed and aged specimens with the skins intact and with the skins removed.

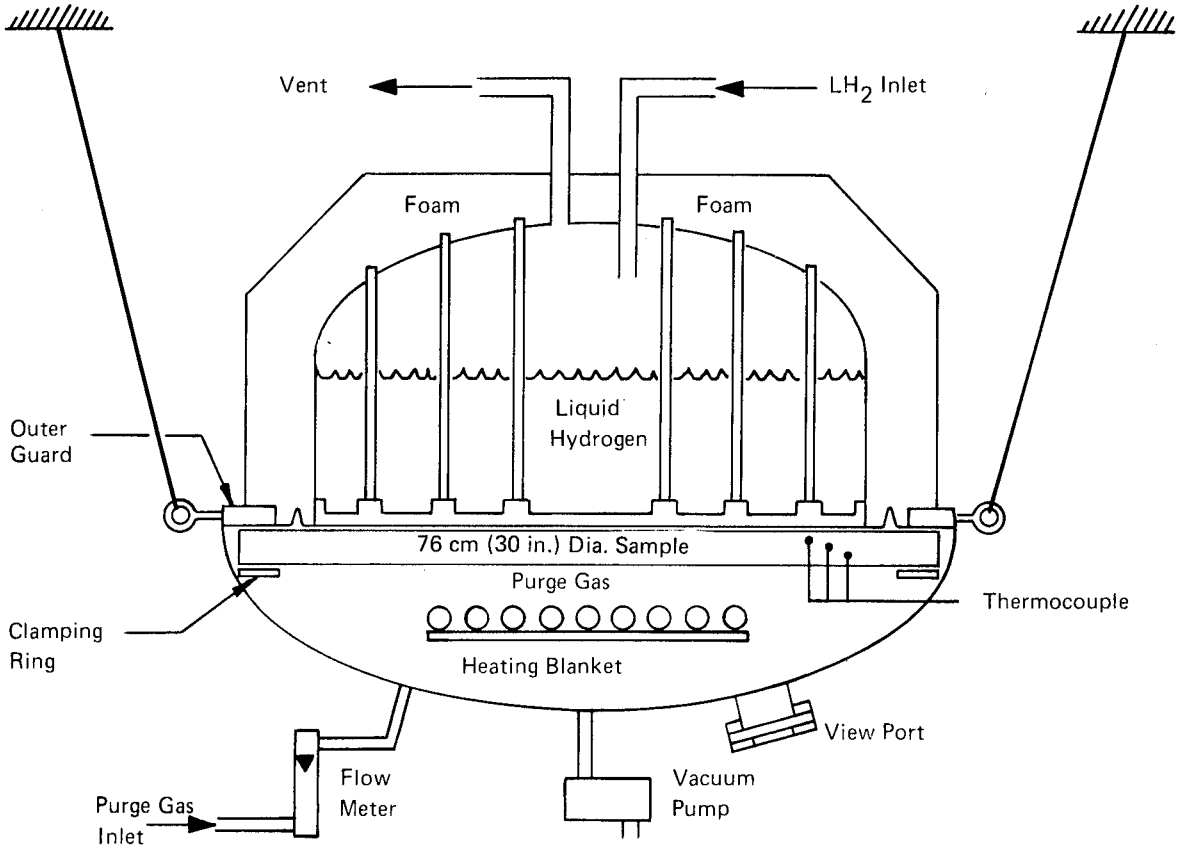

Figure 1.1. Life Cycle Test Apparatus

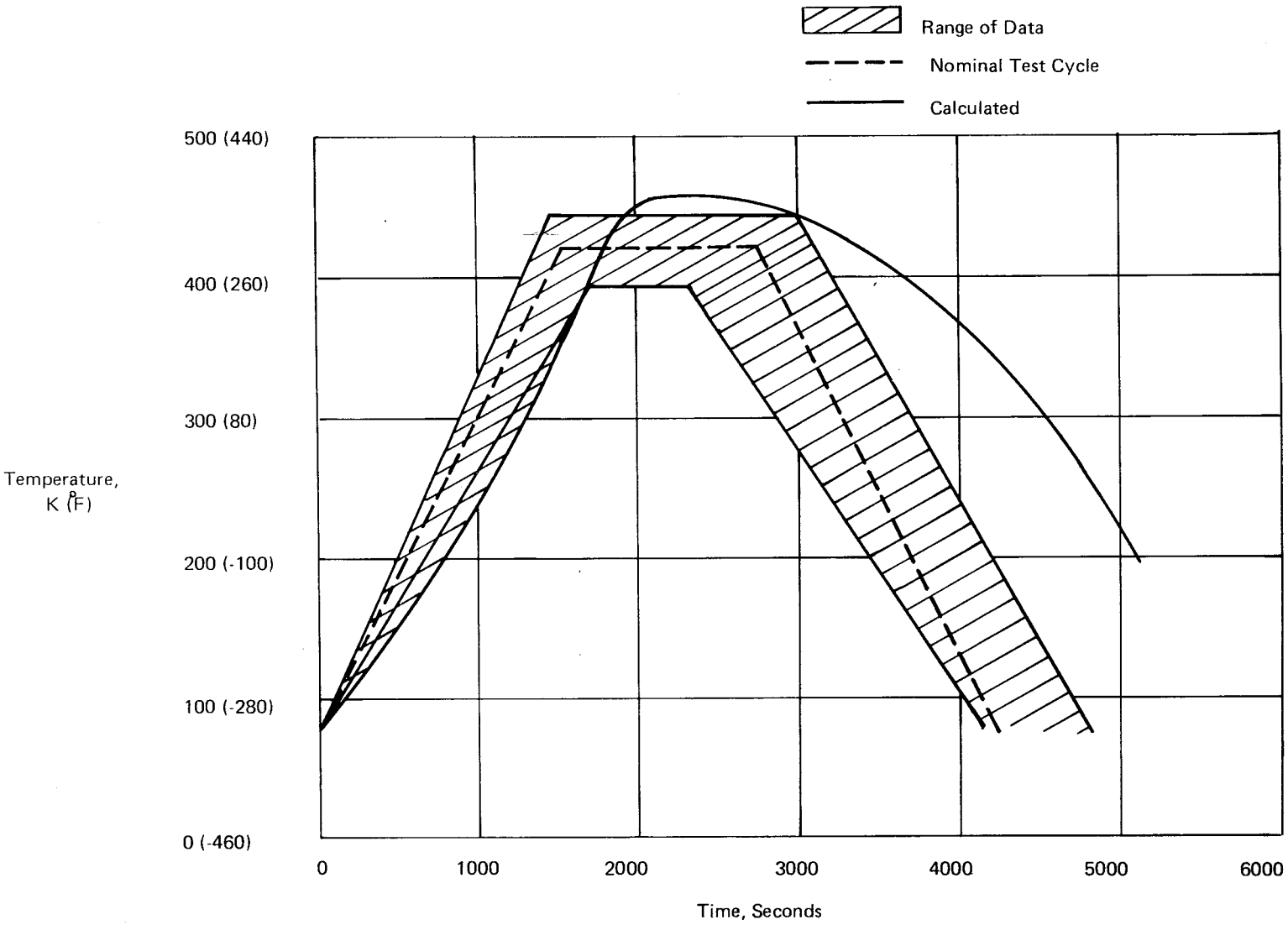

Figure 12. Temperature History of Interface between Insulation Layers

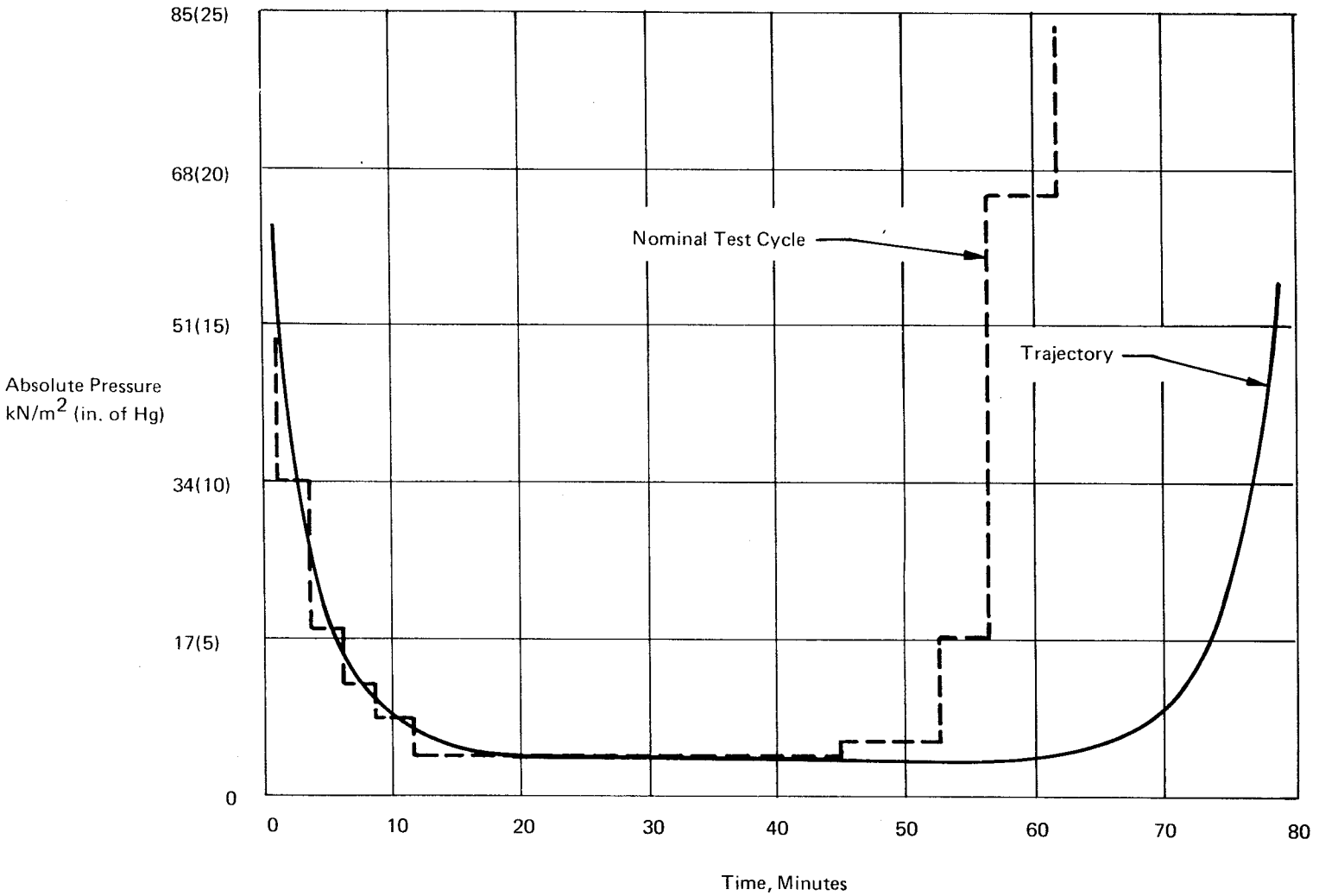

Figure 13. Ambient Pressure History

Test Results

Three unaged glass fiber reinforced polyurethane specimens with integral skins were tested with a carbon dioxide purge and a liquid nitrogen cryogen. Two of these specimens were damaged perfecting the test technique (see Appendix H); the third, which was bonded to the tank with crest 7343 adhesive, was successfully subjected to a cryogenic environment for a period of approximately 2.5 hours during which time the temperature of the insulation went from ambient to that of liquid nitrogen on the cold side and from ambient to the freezing point of carbon dioxide on the warm side. (Approximately 20 minutes were required for cool down to liquid nitrogen temperatures with an additional 1.5 hours required before purge gas deposition began, i.e., the warm surface reached the freezing point of carbon dioxide.) There was no apparent damage to the insulation as evidenced by the pre and post test photographs of Figures 14 and 15.

Two aged glass fiber reinforced polyurethane specimens one without integral skins and one with were also tested with carbon dioxide and liquid nitrogen. (The aging process, which was to increase the maximum service temperature of the foam and thereby reduce the system weight, consisted of curing the specimen at 400K (260°F) for 6 hours and 450K (350°F) for 6 hours while the material was completely constrained against thermal expansion.) Both specimens showed evidence of diffusion of purge gas into the insulation and both were extensively damaged either during testing or during the warm-up period following the tests (apparently from outgassing). See Figure 16. Although prior permeability tests indicated the aging process did not change permeability, subsequent permeability tests with several samples indicated that the aging process caused the material to become permeable and that additional heating cycles increased the permeability. Therefore, it was concluded that the aged material was not suitable for this application.

In the initial tests of polymethacrylimide insulation, a 30 kg/m^3 (1.9 pcf) density specimen was severely damaged, apparently because of improper bonding to the tank. Subsequently, a 60 kg/m^3 (3.8 pcf) specimen was bonded to the tank and subjected to the series of tests summarized in Table V.

As indicated in Table V during the first carbon dioxide/liquid nitrogen test cracking occurred and a circular ring separated from the central disk (Figure 17). This failure apparently was the result of binding between the specimen and the clamping ring which attached the specimen to the outer guard (see Figure 11). (The ring was intended to provide a slip fit so as to accommodate differential thermal expansion between the tank and the outer guard.) Since the central portion of the specimen appeared to be in good condition, the crack was repaired with annular segments of aluminum foil cemented to the surface of the insulation with crest adhesive (Figure 18). This repair, which successfully maintained a pressure of 5 mm Hg in the slot between the tank and guard under cryopumping conditions, provides a potential solution to the problem of sealing joints between adjacent pieces of insulation in an actual application.

After several additional thermal cycles, with CO_2 and LN_2, confirmed the suitability of the repair, the specimen was tested with nitrogen as the purge gas and liquid hydrogen as the cryogen. Eight thermal cycles were imposed in accordance with the temperature and pressure schedules of Figures 12 and 13 with no apparent damage. However, when the specimen was re-examined after a weekend shutdown, there was evidence of damage over a small area which extended from the edge to a position near the center of the specimen.

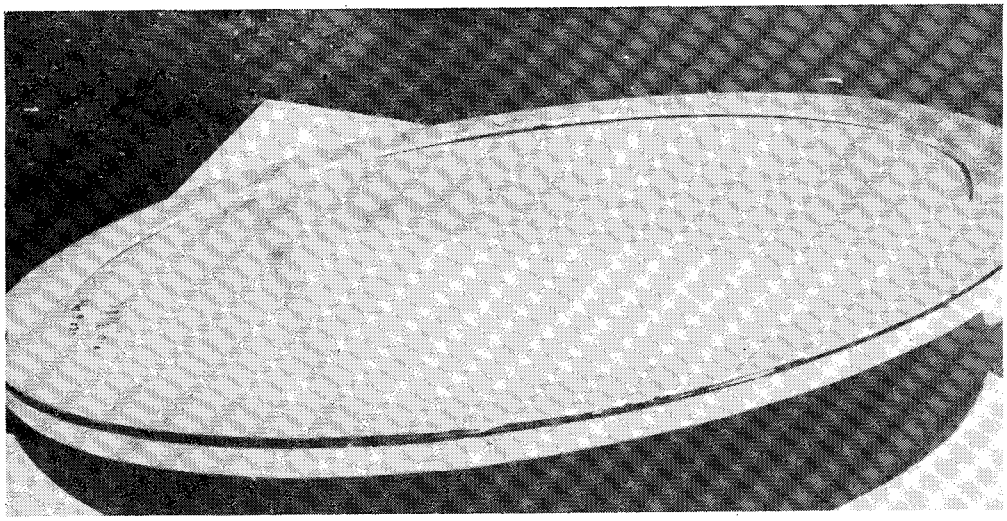

Figure 14.- ADL Cryogenic Polyurethane Foam with Skins

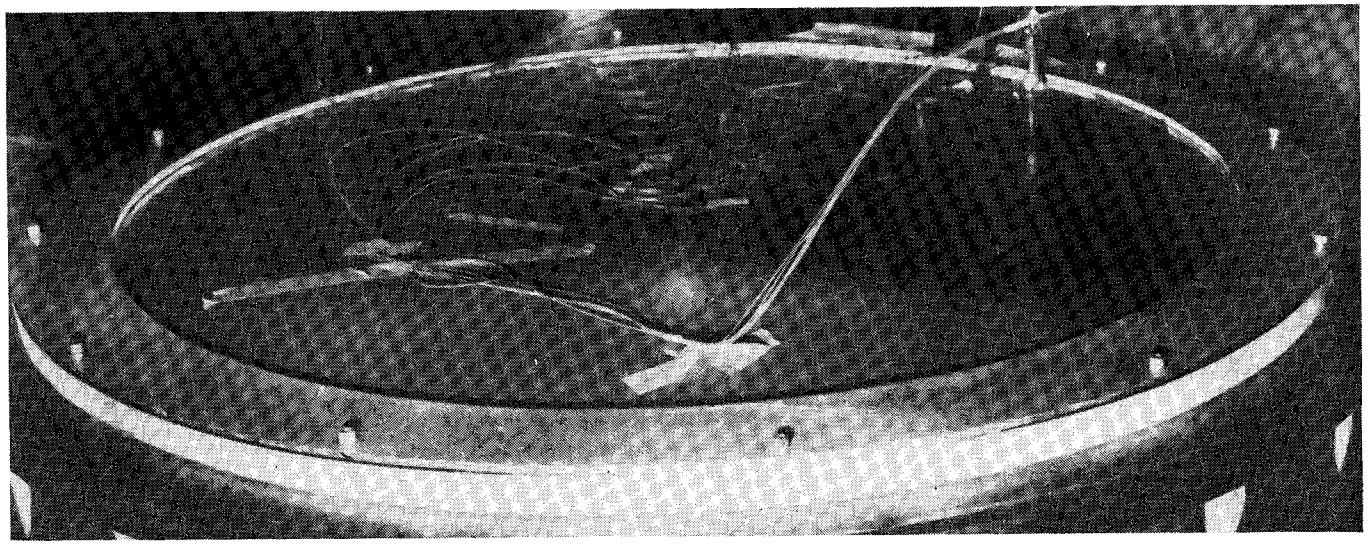

Figure 15.- ADL Cryogenic Polyurethane Foam With Skins After One Cycle

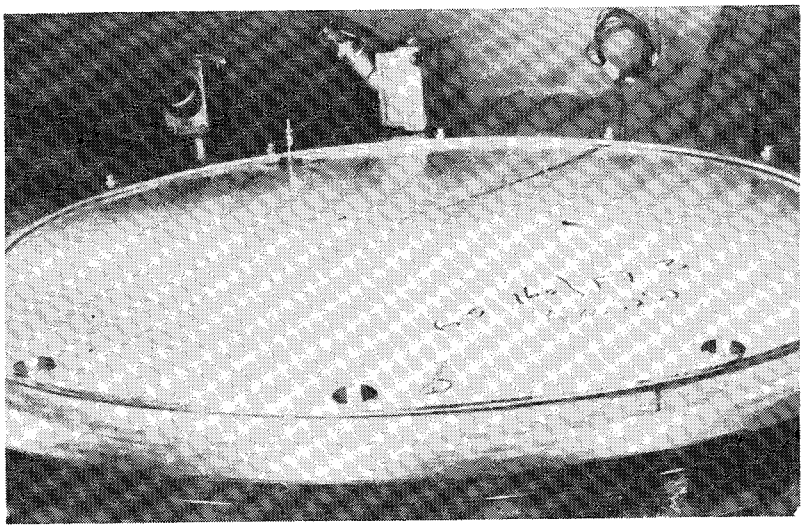

Immediately After Test

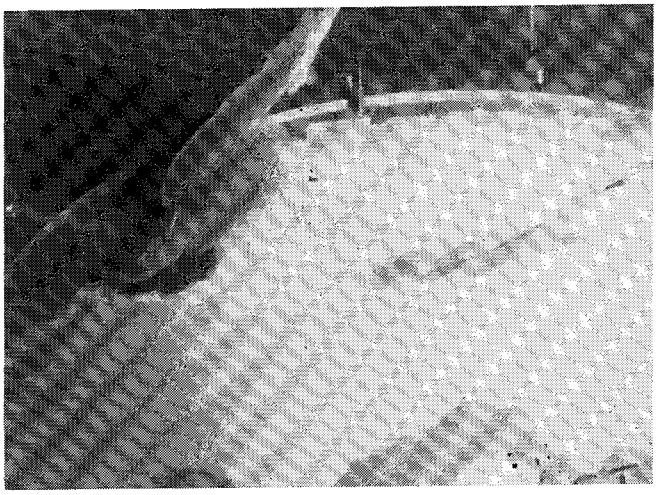

After Warm Up

Figure 16.- Aged ADL Cryogenic Polyurethane Foam After One Cycle

TABLE V

76 cm (30 IN.) ROHACELL 51 SAMPLE TESTS

Date	Test Conditions	Sample Condition and Remarks
	LN_2 CRYOGEN – CO_2 PURGE GAS	
2/15/74	Amb. to 163K (-167° F) to amb.	Lost slot vacuum. Post inspection - complete circular crack in sample at slot location, because of differential expansion of test apparatus which is not representative of flight conditions. No apparent damage to 76 cm (30 in.) diameter center section.
	REPAIRED CRACK WITH 0.05 mm (0.002 in) ALUMINUM FOIL	
3/5/74	Amb. to 166 to 422K (-160 to + 300°F) No altitude simulation.	Post inspection - indication of surface discontinuity at center where frost had caused heating blanket to adhere to sample.
3/7/74	Test aborted, LN_2 cart's burst disc ruptured during initial calorimeter fill.	Only 20 minutes of exposure to cryogen.
3/8/74	3 flight cycles 189K (120°F) to 422K (+300°F) with altitude simulation.	Post inspection - no visible change.
	LH_2 CRYOGEN – N_2 PURGE GAS	
3/9/74	Amb. to 77K (-320° F) amb. No altitude simulation.	Crack repair leaked prior to tests, but slot cryopumped to and maintained an absolute pressure of 5 mm Hg. with no evidence of cryodeposition during tests.
4/11/74	2 flight cycles 77K (-320°F) to 433K (+320°F) with altitude simulation.	
4/12/74	2 flight cycles.	Post inspections - no visible changes.
4/17/74	4 flight cycles.	
	Re-examination after weekend revealed the loss of a shallow section of foam over a 3.8 cm x 5 cm (1½" x 2") area near the slot and two small surface flaws near the center of the specimen. Foam removed from a 51 cm x 21 cm (20" x 8½") area and small sections of Rohacell 31, 61S, and 51 with water behind it were installed.	
5/3/74	1 flight cycle	Aborted testing. Short in heater circuit during start of second cycle. Problems during run: 1) Heater control T.C. shorted. 2) Warm T.C. open at switch. 3) Variations in heater volt and amp. with constant setting. Post inspection - indication of temp. in excess of 477K (+400°F) on warm side. Crack in Rohacell 61S. No major failures were detectable.
5/9/74	4 flight cycles	
5/14/74	4 flight cycles	Post inspection - 5 cm (2 in.) section of Rohacell 51 starting to lift at center.
5/15/74	3 flight cycles .	
5/15/74	4 flight cycles.	Post inspection - 5 cm (2 in.) shallow section of 51 broke off at center.
5/17/74	4 flight cycles.	Post inspeciton - 51 insulation surface cracks in several places 61S color changed to dark brown from start of tests.

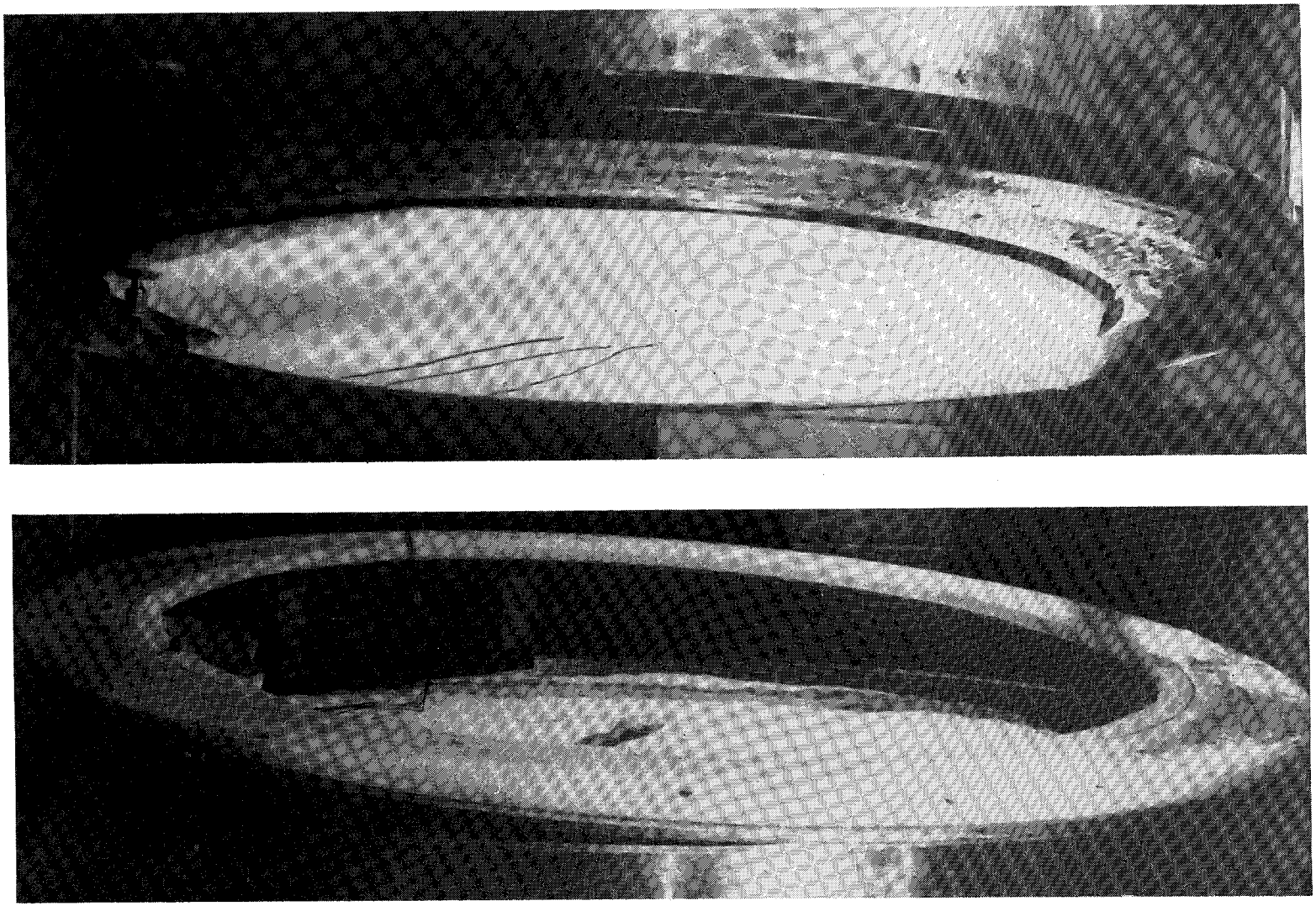

Figure 17.- Circumferential Failure During Initial Cooldown With Rohacell 51 Foam

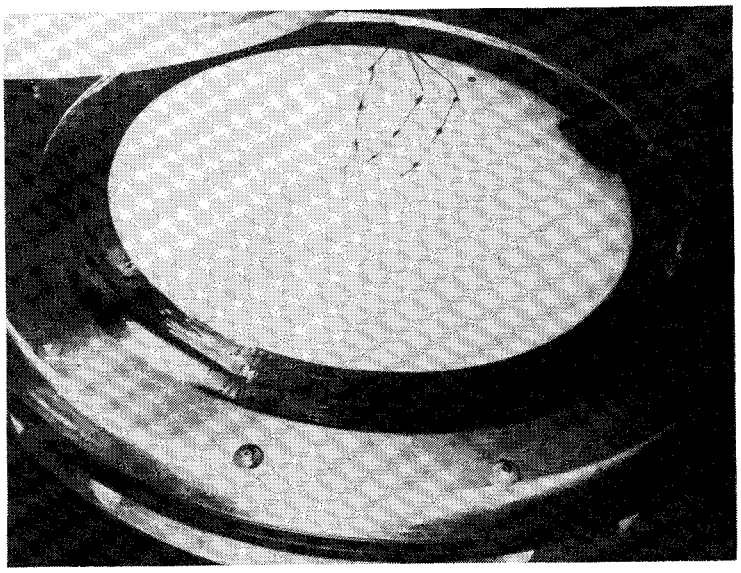

Figure 18.- Joint Repair of Rohacell 51

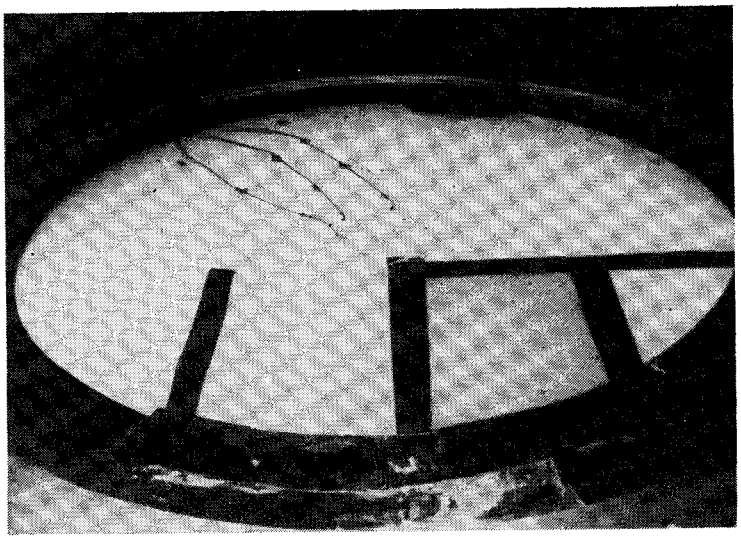

Figure 19.- Repair of Rohacell 51 To Eliminate Minor Surface Cracks

It was postulated that the damage was the result of moisture freezing in an area near the edge of the specimen where the bond was defective. The moisture had entered the slot which was vented to atmosphere after the test and diffused into the defective bond while the tank and specimen were still cold. This experience and the previous one indicate the criticality of having a continuous bond between the tank and insulation.

The insulation was removed from an area slightly larger than the damaged area and samples of the lower density insulation (R-31), insulation with a fire retardant (R-61S), and insulation (R-51), with a small amount of water behind it were bonded to the tank and all but one edge sealed using the technique developed previously (Figure 19). The remaining tests were plagued by malfunctions of the heater and control thermocouples which permitted the hot surface of the insulation to reach a temperature in excess of 477K (400°F). Damage initiated by the over temperature was progressive but at a relatively low rate to the end of the tests as shown by Figure 20. It is interesting to note that the over temperature damage appeared to be most severe in the specimen with the fire retardant additive. Similiar effects of fire retardant additives have been experienced with other insulations (Ref. 17).

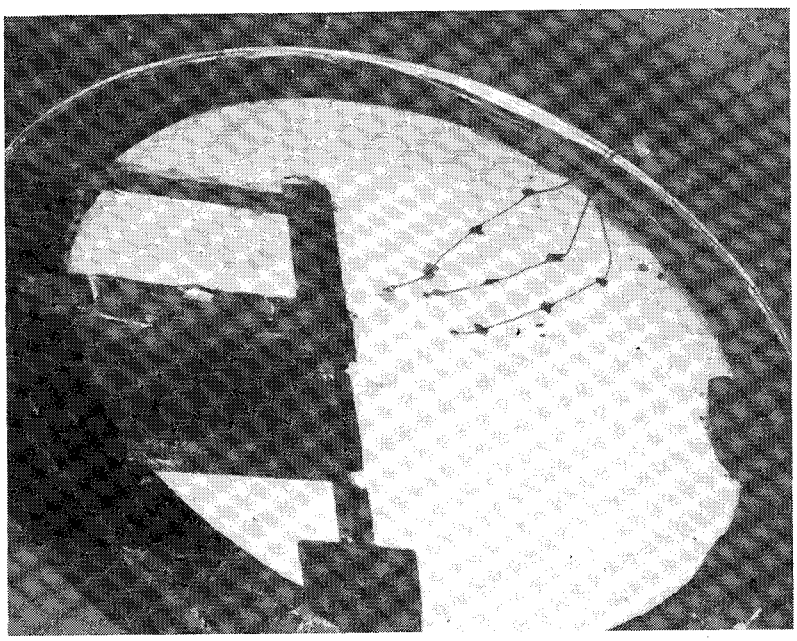

After

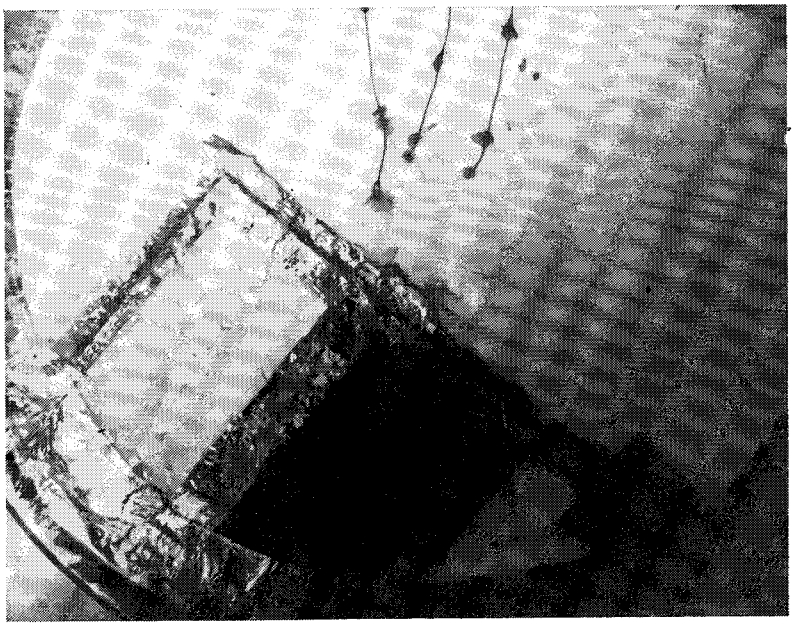

Before

Figure 20.- Rohacell 51 Specimen Before and After 28th Cycle

CONCLUDING REMARKS

The objective of the analytical and experimental investigation was to develop and validate a lightweight purged insulation system for a hypersonic cruise vehicle with hydrogen tanks which would require minimum preflight preparation and would offer dependable reusability. The data developed during the investigation and the following concluding remarks are for a Mach 8 hypersonic aircraft with a 35 minute cruise time and ground hold times of 3 to 12 hours. Results of the analysis, verified by material screening and later thermal cycling tests, indicated that a nitrogen purge system with a closed cell, nonpermeable innermost insulation layer provide the lightest weight system for the prescribed design conditions.

Some specific conclusions derived from this study are as follows:

1. The cryodeposition rate of a purge gas within a permeable insulation is initially diffusion limited and subsequently heat transfer limited. The period of time that the system is diffusion limited depends on the permeability of the insulation.

2. A diffusion limited process is required to avoid excessive buildup of cryodeposits during ground hold. Permeabilities of less than 1 millidarcy for a carbon dioxide purge and less than 0.8 millidarcies for a nitrogen purge are required to limit the cryodeposit 4.86 kg/m^2 (1.0 lb/ft^2) in three hours.

3. The only high temperature insulations that satisfied the above permeability requirement were dense ($\geqslant$ 384 kg/m^3 (24 pcf)). The average unit weight of an optimized nitrogen purge insulation system using these insulations and based on a 6 hour ground hold was 18.0 kg/m^2 (3.69 psf).

4. The average unit weight of a nitrogen purged system using a 477K (400°F), 51.3 kg/m^3 (3.2 pcf), closed cell foam was 6.31 kg/m^2 (1.29 psf).

5. The total system weight of the low temperature low density, closed cell insulations can be decreased by as much as 20 percent if the foam temperature limit can be increased from 366K (200°F) to 477K (400°F).

6. Nitrogen purged systems were always lighter than carbon dioxide purged systems.

7. A 76 cm (30 inch) diameter specimen of polymethacrylamide foam survived 5 thermal cycles with carbon dioxide purge gas and liquid nitrogen as a cryogen and an additional 8 cycles with nitrogen as the purge gas and liquid hydrogen as the cryogen without apparent damage. (In the latter tests the temperature of the hot surface was cycled between 77K (-320°F) and 422K (300°F).) The specimen was also exposed to an additional 20 thermal cycles with progressive damage after it had inadvertently been exposed to a temperature in excess of 477K (400°F).

8. A technique for sealing joints between adjacent pieces of insulation was developed and successfully demonstrated.

REFERENCES

1. Hammond, M.B., Jr.; "An Analytical Model for Determining the Thermal Conductivity of Closed Cell Foam Insulations," Advances in Cryogenic Engineering, Vol. 15, Plenum Press, 1970, pp 332-342.

2. Norton, Francis J.; "Thermal Conductivity and Life of Polymer Foams," Journal of Cellular Plastics, Vol. 3, No. 1, January 1967, pp 23-37.

3. Bennett, R.B., "A Structural Plastic Foam Thermal Insulation for Cryogenic Service," Advances in Cryogenic Engineering, Vol. 18, Plenum Press, 1973, pp 393-399.

4. Heathman, John H., and Kelley, Larry G.; "Hydrogen Tankage for Hypersonic Cruise Vehicles," AIAA/ASME Seventh Structures and Materials Conference, April 1966, pp 430-438.

5. Jackson, L. Robert, Davis, John G., Jr., and Wichorek, Gregory R.; "Structural Concepts for Hydrogen-Fueled Hypersonic Airplanes," NASA TN D-3162, 1966.

6. Norton, Allan M., "Advanced Structural Concepts, Experimental Program - Project ASCEP," Volume II, AFFDL-TR-67-146, June 1968.

7. Jackson, L.R., and Anderson, M.S.; "A Carbon Dioxide Purge and Thermal Protection System for Liquid Hydrogen Tanks of Hypersonic Airplanes," Advances in Cryogenic Engineering, Volume 12, Plenum Press, Inc., 1967, pp 146-156.

8. Sharpe, Ellsworth L.; "The Control of Carbon Dioxide Cryodeposits," NASA TN D-7334, 1973.

9. Clay, John P.; "Carbon Dioxide Frost as Insulation for Hypersonic Spacecraft. Insulation-Materials and Processes for Aerospace and Hydrospace Applications," Soc. Aerospace Materials Process Engineering, May 1965.

10. Sharpe, Ellsworth L., and Jackson, L. Robert; "Performance of a Hypersonic Hot Fuselage Structure with a CO_2 Frost Purged Cryogenic Tank," NASA TND-7799, March 1975.

11. Jackson, L. Robert and Sharpe, Ellsworth L., "A Carbon Dioxide Purge and Thermal Protection System for Liquid Hydrogen Tanks," Conference on Hypersonic Aircraft Technology NASA SP-148, 1967, pp 501-513.

12. Lees, L.; "Laminar Heat Transfer over Blunt-Nosed Bodies at Hypersonic Flight Speeds," Jet Propulsion, Vol. 26, No. 4, April 1956, pp 259-269.

13. Spalding, D.B. and Chi, S.W., "The Drag of a Compressible Turbulent Boundary Layer on a Smooth Flat Plate With and Without Heat Transfer," Journal of Fluid Mechanics, Vol. 18, Part 1, January 1964, pp 117-143.

14. Neal, Luther, Jr., and Bertram, Michael H.: "Turbulent-Skin-Friction and Heat-Transfer Charts Adapted from the Spalding and Chi Method," NASA TN D-3969, 1967.

15. Helenbrook, R. G.; McConarty, W. A.; and Anthony, F. M.: "Evaluation of Active Cooling Systems for a Mach 6 Hypersonic Transport Airframe," NASA CR-1917, December 1971.

16. Lemons, C. R.; Salmassy, O. K.; and Watts, C. R.: "Advances in Cryogenic Foam Insulations," McDonnell-Douglas Corporation. MDAC paper WD 1765, September 1971 (Presented at the SAMPE Conference, Huntsville, Alabama, 5-7 October 1971).

17. Atallah, S. and Buccigross, H.: "Investigation and Evaluation of Nonflammable, Fire Retardant Materials." Final Report prepared by Arthur D. Little, Inc., USAAMRDL Technical Report 72-52 (1971).

18. Helenbrook, R. G. and Anthony, F. M.: "Design of a Convective Cooling System for a Mock 6 Hypersonic Transport Airframe." NASA CR-1918, December 1971.

APPENDIX A

ANALYTICAL APPROACH TO THE PURGE GAS CRYODEPOSITION PROCESS

This Appendix describes the analytical background for the computer program used to compute the purge gas flowrates along with the assumptions that were necessary to derive the controlling equations.

Mass and Heat Transfer Mathematical Models

The one-dimensional model used for the thermal analysis shown in Figure 1 represents a portion of the insulated tank wall. The insulation consists of an outer layer of high permeability insulation and an inner layer of low permeability or non-permeable insulation. The problem was to determine the weight characteristics of a purged insulation system where the weight includes the weights of the cryodeposited frost, the fuel boiloff and the weight of the insulation. Analysis of the transient behavior for this type of insulation system, i.e., with gas flow, is more complex than the analysis of a static insulation system because of the interactions between gas flow, condensate formation, and heat transfer. The operation of the thermal protection system can be divided into the ground operation phase and flight operation phase. During ground operation, the purge gas is considered to be continually deposited within the insulation until the frost line reaches the saturation temperature line within the insulation. During the flight operation, the frost will absorb a major fraction of the incoming aerodynamic heat as it evaporates hence reducing the fuel boiloff during flight. Since the controlling heat transfer and mass diffusion equations are somewhat different for the two operational phases, the analytical approaches for each phase are presented separately

Ground Operation - The analysis of the purge gas thermal protection system must provide for the interactions between the diffusion process and the heat transfer process; however, initially and terminally the interaction is negligible. When purge gas is first supplied, no frost layer exists, the flow path length is maximum and the resistance to gas flow is at a minimum. The equation used to predict the diffusion flowrate during the initial phases is Fick's equation:

$$\dot{w} = \left[\frac{B_o \rho_g \Delta p}{\mu}\right]\left(\frac{1}{x-z}\right) \tag{1}$$

where z is given by the relationship

$$z = t_i - \sqrt{t_i^2 - 2\left[\frac{B_o \rho_g \Delta p}{\mu \upsilon \rho_f}\right]\theta} \tag{2}$$

The relationship for z assumes that the purge gas is deposited at the frost line at a uniform density and that quasi steady-state conditions exist at all times.

Substituting (2) in (1) the equation for diffusion controlled cryodeposition becomes

$$\dot{w} = \frac{\phi}{\sqrt{t_i^2 - 2\theta\psi}} \tag{3}$$

where

$$\phi = \left[\frac{B_o \rho_g \Delta p}{\mu}\right] \quad \text{and} \quad \psi = \left[\frac{B_o \rho_g \Delta p}{\mu \upsilon \rho_f}\right]$$

are related to both the purge gas properties and the inner insulation characteristics and were determined empirically. As such, the interaction of the heat transfer with the diffusion processes will be accounted for in the analyses. These quantities are essentially constants when diffusion predominates; therefore, equations (1) and (3) show that the purge gas flowrate increases with time since the amount of insulation effective in resisting gas flow decreases. However, as the frost thickness increases, the heat flow from the frost interface to the hydrogen tankage decreases and the amount of purge gas that can be condensed also decreases. Therefore, a point exists where heat transfer limits the purge gas flowrate.

The controlling equations for the heat transfer process must be determined from an energy balance at the pseudo steady-state frost line. Considering both convection due to the purge gas and conduction through the insulation, the equation for temperature on the hot side of the frost line is given by

$$T = C_1 e^{(\dot{w}c_p x/k_i)} + C_2 \tag{4}$$

where C_1 and C_2 are integration constants which must be evaluated from the boundary conditions of

$$T = T_f \text{ at } x = \ell - z \tag{5}$$

and

$$-k_i \frac{dT}{dx} = h(T_\infty - T) \text{ at } x = 0 \tag{6}$$

Applying these boundary conditions the equation for temperature becomes

$$T = T_\infty + \frac{(T_\infty - T_f)\left[\frac{\dot{w}c_p}{h} - 1 + e^{(\dot{w}c_p x/k_i)}\right]}{1 - \frac{\dot{w}c_p}{h} - e^{(\dot{w}c_p(\ell - z)/k_i)}} \tag{7}$$

Now that the temperature distribution is known, it is possible to perform a heat balance at the frost interface, that is

$$-k_i \frac{dT}{dx}\bigg|_{x = \ell - z - \Delta x} + \dot{w}(h_{fg})_g = -k_f \frac{dT}{dx}\bigg|_{x = \ell - z + \Delta x} \tag{8}$$

If we assume that the frost conductivity is reasonably constant over the temperature ranges of interest this equation becomes

$$\frac{\dot{w}c_p (T_\infty - T_f)}{1 - (1 + \dot{w}c_p/h)\, e^{(-\dot{w}c_p (\ell - z)/k_i)}} + \dot{w}(h_{fg})_g = k_f \frac{(T_f - T_c)}{z} \tag{9}$$

Under pseudo steady-state conditions, this relationship can be solved iteratively for the purge gas flowrate and the frost thickness can be evaluated from the following

$$z = \frac{1}{\rho_f \upsilon} \int_0^{\theta_g} \dot{w} d\theta \tag{10}$$

If the interaction between the mass diffusion process and heat transfer process is considered to be negligible at all times during the ground hold operation, the diffusion flowrate can be compared with the condensation rate and if it is greater, the later value must be employed to evaluate the frost thickness. The accumulation of frost as a function of time must be performed numerically because there is no simple closed form solution for the heat transfer limited flowrate, therefore the equation for the frost thickness becomes

$$z' = z + \frac{\dot{w}\Delta\theta}{\rho_f \upsilon} \tag{11}$$

if the problem becomes heat transfer limited. Frost will continue to build up until either an equilibrium frost level is established or the vehicle enters into the flight regime.

Experimental data presented in Appendix B show that for the low permeable insulations the purge gas flowrate is very small and nearly independent of time. In this case the frost thickness can be approximated as

$$\overline{z} = \frac{\dot{w}\theta}{2\upsilon\rho_f} \tag{12}$$

and the heat flow equation simplifies to

$$\frac{k_f (T_f - T_c)}{z} = \dot{w}\,(h_{fg})_g \tag{13}$$

Combination of these two equations shows the limiting value of the heat transfer flowrate to be

$$\dot{w} = \sqrt{\frac{\upsilon \rho_f k_i (T_f - T_c)}{2(h_{fg})_g \quad \theta}} \tag{14}$$

Because of the large difference between the specific volumes of the purge gas and its frost, the pressure at the frost interface is much less than the external pressure, hence Δp in equations (1) and (2) is nearly equal to the external pressure. The resulting mass flux for the diffusion limited case as a function of the permeability constant is shown in Figure 4. The figure shows that a permeability coefficient less than 1 millidarcy for CO_2 or .8 millidarcy for N_2 is required to maintain mass fluxes to less than 4.86 kg/m^2 (1.0 lb/ft^2) for a 3 hour period which was an initial ground rule established because of purge gas supply requirements.

Flight Operation - During Flight, the vehicle experiences aerodynamic heating and the heat shield temperature will reach 1144K (1600°F) on the lower centerline and 866K (1100°F) on the upper vehicle centerline. These surface temperatures will result in a substantial heat flow to the hydrogen tank. If the hydrogen is in contact with the tank wall, this heat flow will cause the hydrogen to boil off. This condition will be subsequently referred to as a "wet tank." If only hydrogen gas is in contact with the tank wall, an adiabatic condition essentially exists. Thus, the incoming heat flow will result in an increase in tank wall temperature. This condition will subsequently be referred to as a "dry tank." With the exception of the areas near the liquid interface, lateral conduction in the tank wall is essentially negligible, hence, the heat flow is only one dimensional.

For a wet tank, the heat input initially boils off the deposited frost until the equilibrium temperature level is reached at which time the frost vaporization process ceases. Since the weight of the frost as well as the fuel boiloff weight are different during each of these phases, the time required to reach this equilibrium condition (θ_1) must be computed before the weight of the TPS can be estimated. At time θ_1, the temperature distribution will be established and a heat balance at the frost line yields

$$\frac{k_f (T_f - T_c)}{z_1} = \frac{k_i (T_s - T_f)}{\ell - z_1} \tag{15}$$

which can be solved directly for z_1,

$$z_1 = \frac{\ell}{\left(\frac{T_s - T_f}{T_f - T_c}\right)\left(\frac{k_i}{k_f}\right) + 1} \tag{16}$$

Assuming that the rate of frost boiloff is constant during the initial phase, the purge gas flowrate can be approximated as

$$\dot{w} = \frac{\upsilon \rho_f (z_o - z_1)}{\theta_1} \tag{17}$$

With this value of flowrate, the heat flow to the frost line during this period of time can be approximated from the relationship

$$Q = \frac{\upsilon \rho_f c_p (z_o - z_1)(T_s - T_f)}{1 - e^{[\upsilon \rho_f c_p (z_o - z_1)(\ell - \frac{1}{2}(z_o + z_1))/k_i \theta_1]}} \tag{18}$$

This relationship assumes that the average frost thickness can be used to estimate the heat flow through the frost layer. An equation with θ_1 as the only dependent variable is obtained if a heat balance is performed at the frost line. The resulting equation is

$$Q = \frac{k_f (T_f - T_c)\theta_1}{\frac{1}{2}(z_o + z_1)} + \upsilon (z_o - z_1)\rho_f (h_{fg})_g \tag{19}$$

Once θ_1 has been determined, the time average frost thickness for the complete flight is evaluated. If the flight time is less than θ_1, the average frost thickness is given by

$$z_m = z_o \left[1 - \frac{1}{2}\left(\frac{\theta_T}{\theta_1}\right)\right] + \frac{1}{2}\left(\frac{\theta_T}{\theta_1}\right) z_1 \tag{20}$$

whereas if the flight time is greater than θ_1, the average frost thickness is given by

$$z_m = \frac{1}{2}\left(\frac{\theta_1}{\theta_T}\right) z_o + z_1 \left[1 - \frac{1}{2}\left(\frac{\theta_1}{\theta_T}\right)\right] \tag{21}$$

Using the appropriate value for the mean frost thickness, the weight that must be assessed against the thermal protection system is

$$W_f = \rho_f z_m \tag{22}$$

and the weight of hydrogen boiloff is

$$W_B = \frac{k_f (T_f - T_c)\theta_T}{z_m (h_{fg})_{H_2}} \tag{23}$$

Addition of these weights to the insulation weight, yields the total weight that is accountable to the thermal protection system for regions of the hydrogen tank, in which liquid hydrogen is in contact with the wall at all times during the significant heating phases of the flight.

For the dry tank condition, the heat input must be absorbed by increasing the heat content of the thermal protection system as well as vaporizing the frost. Before the weight of the thermal protection system can be calculated, the time required to boiloff all of the frost (θ_2) must be estimated.

At time θ_2, the tank wall will be at the frost vaporization temperature. Assuming again that the frost boiloff and heat flow to the frost line vary linearly during the time interval θ_2, the cumulative heat input to the frost line can be estimated by utilizing the heat flux at time $\theta_2/2$ given by

$$\dot{q} = \frac{\upsilon \rho_f c_p z_o / \theta_2 (T_s - T_f)}{1 - e^{(\upsilon \rho_f c_p z_o (\ell - z_o/2) k_i \theta_2)}} \tag{24}$$

Equating the total heat input during time θ_2 to the increase in internal energy of the insulation system plus the heat vaporization of the complete frost thickness the equation for θ_2 is obtained as

$$\theta_2 = \frac{\upsilon \rho_f c_p z_o (\ell - z_o/2)}{k_i \ln \left[\frac{1 + \upsilon \rho_f c_p z_o (T_s - T_f)}{\upsilon \rho_f c_p z_o (T_f - T_c)/2 + \rho_w c_{pw} t_w (T_f - T_c) + \upsilon \rho_f z_o h_{fg}} \right]} \tag{25}$$

On the basis of this value, the time averaged frost weight can be computed. If the flight time is less than θ_2, the mean frost thickness is given by

$$z_m = z_o \left[1 - \tfrac{1}{2} \left(\frac{\theta_T}{\theta_2} \right) \right] \tag{26}$$

whereas if the flight time is greater than θ_2, it is given by

$$z_m = \tfrac{1}{2} \left(\frac{\theta_2}{\theta_T} \right) z_o \tag{27}$$

The frost weights can now be computed from equation (19). Since the hydrogen is not in contact with the tank wall, the fuel boiloff weight will be negligible hence the total system weight includes only this frost weight and the insulation weights.

In the case of the dry tank, the tank wall temperature is increasing during flight and if it exceeds the maximum allowable temperature of the material, the operating life of the vehicle will be reduced from design expectations. Consequently, a wall temperature constraint must be applied to the dry tank. Assuming that the heat flow to the tank wall varies linearly with time, the tank wall temperature can be obtained from the solution of the following equation.

$$\left[\frac{\rho_o c_{po} y^2}{2\ell} + \frac{\rho_i c_{pi} [y + (t_i/2)]}{\ell} + \rho_w c_{pw} t \right] (T_w - T_f) = \frac{U_o (\theta_T - \theta_2)}{\ell} \left[T_s - \tfrac{1}{2} (T_w - T_f) \right] \tag{28}$$

This equation must be solved by an iteration technique, since the overall conductance is dependent on each of the insulation thermal conductivity values which are related to the mean temperature level of the insulation which, in turn, are dependent on the wall temperature. If the computed wall temperature exceeds the specified maximum temperature, a weight penalty will be incurred from increasing

the insulation thickness to reduce the heat input to the tank wall, due to an increase in insulation thickness for purposes of reducing the heat input to the tank wall.

General Solution Technique - For given values of the outer and inner insulation thickness, the weight of the thermal protection system can be computed from the above relationships; however, it is unlikely that the system weight is a minimum. Because of the complicated form of the weight equation, differentiation and subsequent solution for the insulation thicknesses is nearly impossible and a systematic searching technique is necessary to determine the optimum system specifications. The approach selected was to evaluate the system weights and temperatures for several values of inner insulation thicknesses and one value of outer insulation thickness. The weight data, ground surface temperature data, and the interface temperature data were each fit by a least-square polynomial curve with inner insulation thickness as the independent variable.

Utilizing these equations with the differentiated form of the polynomial weight equation, it is possible to determine the inner insulation thickness that results in the least weight while satisfying the ground surface temperature and interface temperature constraints. By repeating this procedure for several outer insulation thicknesses, it is possible to find the one combination of outer and inner insulation thicknesses that will result in the lowest weight thermal protection system for any set of conditions.

APPENDIX B
PERMEABILITY OF INSULATIONS

In Appendix A the accumulation of frost within the insulation was shown to be dependent on the insulation permeability; therefore, before the weights of the system can be evaluated, it was first necessary to determine the permeability of the promising permeable insulations. In this Appendix, the test apparatus and procedure employed to measure the permeability of the insulation are described and the test results are presented.

Apparatus and Test Procedure

Appendix A of this volume showed that gas flow through a porous medium is related to the pressure gradient by a characteristic of the material called the permeability coefficient B_o. An apparatus was designed to measure this permeability at room temperature. The permeability apparatus shown in Figure 21 used an O-ring compression seal fitted with the sample holder ring and an O-ring cover seal. Individual insulation samples were cut into disks 5.1 cm (2 in.) in diameter and 2.5 cm (1 in.) thick and sealed with Stycast Epoxy within a metal ring. Nitrogen or carbon dioxide gas pressurized one side of the insulation sample, flowed through it, and was exhausted through a calibrated flow meter. The pressure drop across the sample was measured by a manometer. The permeability coefficient B_o of each sample was determined from the flow rate, the pressure drop across the sample, and the properties of the gas, as follows:

$$B_o = \frac{Gt\mu}{\Delta P}$$

where the following nomenclature and units are used:

- G – volumetric flux in $cm^3/sec \cdot cm^2$
- ΔP – pressure drop in N/m^2
- t – thickness in cm
- μ – viscosity in poise
- B_o – permeability coefficient in cm^2

with the further convention that for the permeability coefficient:

1.013 darcy = 10^{-8} cm^2 or

1.013 millidarcy = 10^{-11} cm^2

Permeability is a characteristic of the natural structure of insulation materials and is almost independent of temperature. The gas flow through the sample is a function of pressure, gas density, and gas viscosity, all of which are temperature dependent. To determine the gas flow characteristics in other temperature and pressure ranges of interest, the measured permeability at room temperature and known relationships between density, pressure, viscosity, and temperature were used.

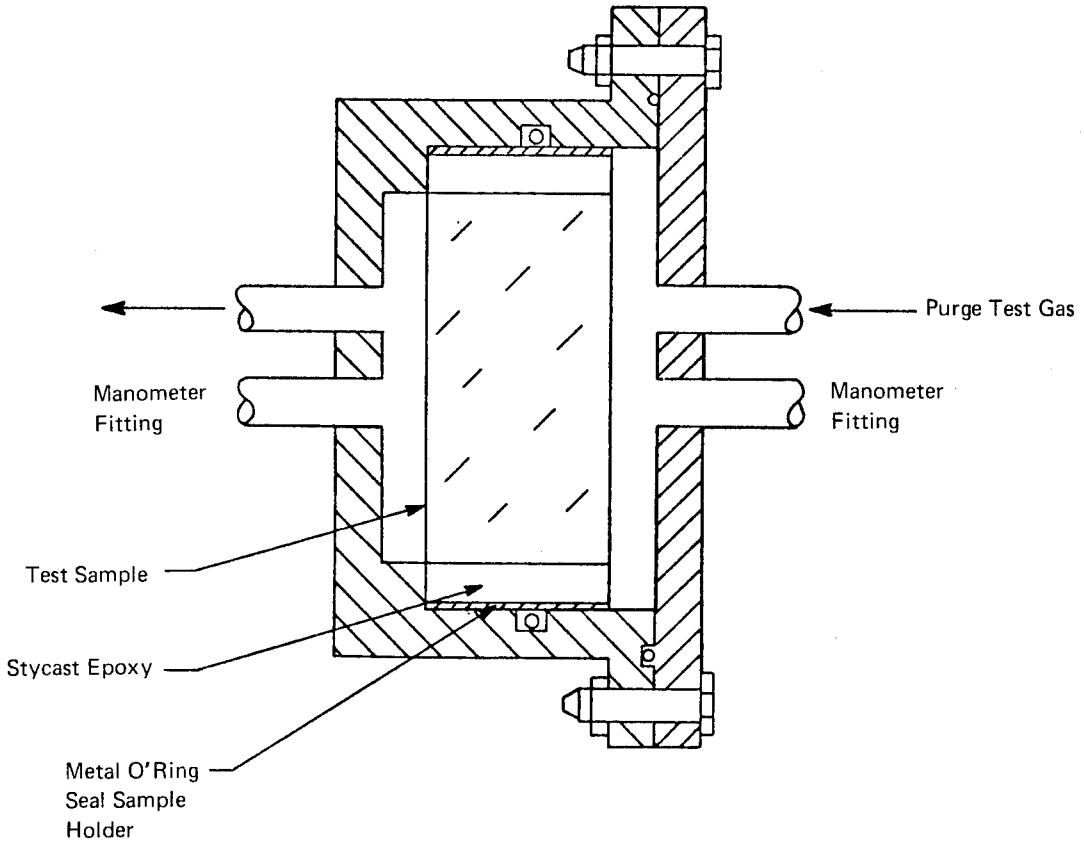

Figure 21. Permeability Apparatus

Results

Table VI presents the permeability coefficient of each of the insulation materials tested in both the as-received condition and after modification. The techniques used to modify the permeability of the high-temperatue insulations (1144K (1600° F)) included recrystallization of magnesium sulfate from saturated aqueous and alcohol solutions, filling the pores with sub-micron colloidal silica particles, depositing smoke particles, and increasing density by compression. Table VI indicates that increasing the density of Min-K 2000 by compression was by far the most successful technique for lowering the permeability of a material.

Table VII lists those materials with permeability coefficients low enough for consideration for the thermal protection system of interest. This table clearly shows the effect of compression on the permeability; however, it should also be noted that the density increases by a factor somewhat greater than 2 for a reduction in permeability from 3.21 to 1.29 millidarcies. Consequently, these insulations were included because of their low permeability in full realization that the weights would be prohibitive.

The permeability properties of Min-K 2000 were found to be nonisotropic. The permeability in a direction parallel to the sheet is more than an order of magnitude greater than the permeability normal to the sheet.

TABLE VI
SUMMARY OF PERMEABILITY TESTS

Material	Modification	Maximum Service Temperature		Density		Permeability B_o
		K	°F	(kg/m^3)	(lb/cu ft)	(millidarcies)
Min-K	Test No. 1	1255	1800	320	20	3.62
	Test No. 2	↓	↓			3.83
	Test No. 3					3.21
	Test No. 4					4.70
	a. Sample No. 2 average permeability			320	20	10.25
	No. 2 soaked in methanol P = 15 cm			320	20	12.55
	No. 2 soaked in methanol P = 27 cm			320	20	17.60
	No. 2 soaked in methanol P = 16.5 cm			320	20	10.35*
	Smoked with NH_3CL			320	20	7.20
Min-K	Soaked with $MgSO_4$ and methanol			320	20	20.00
	Smoked with NH_3CL			320	20	13.10
Min-K	Soaked with $MgSO_4$ and ethanol			320	20	5.40
Min-K	Vibrated with CAB-O-SIL			320	20	2.95
Min-K	Cross-section (parallel to layers)			320	20	45.0
Min-K	Cross-section (parallel to layers)			320	20	110.0
Min-K	CAB-O-SIL ethanol sol. with compressed cycles			320	20	139.0
Min-K	Treated with $H_2O + MgSO_4$			320	20	1,500.00
Min-K	Compressed to 830 N			574	35.8	1.96
	Machined epoxy bond			574	35.8	2.26
Min-K	Compressed to 1660 N			670	41.8	1.045*
	Compressed to 1660 N			670	41.8	1.290
	Compressed to 1600 N			670	41.8	1.335
	Compressed to 1660 N			670	41.8	1.475
	Compressed to 1660 N	1255	1800	670	41.8	1.58
Kalowool	Red Block	1533	2300	449	28	463
	Pass NH_4CL Smoke-through			449	28	260
Kalowool Castable	Gray block, compressed			1762	110	163
Kalowool/ microtherm	Kalowool fiber and propanol and microtherm compressed to 690 N			461	28.8	5.5
Kalowool-CAB-O-SIL	Kalowool fiber and CAB-O-SIL compressed			-	-	130
Fiberfrax				256	16	8,500
Fiberfrax Block				256	16	8,500
Fiberfrax Block	$MgSO_4$ and methanol			256	16	3,010
Fiberfrax Paper F	.25 mm			248	15.5	960
Fiberfrax Paper J	2.5 mm			248	15.5	2,170
Fiberfrax Paper J	2.5 mm with microtherm			248	15.15	300
Fiberfrax Paper A	.64 mm	1533	2300	308	19.2	680

*Tested with CO_2

TABLE VI (CONTD)

Material	Modification	Maximum Service Temperature		Density		Permeability B_o
		K	°F	(kg/m^3)	(lb/cu ft)	(millidarcies)
Refrasil A-100	Batt 1.27 mm	1366	2000	50	3.1	1,000
A-100	Batt 2.54 mm	↓	↓	50	3.1	1,000
C-100	Batt 1.27 mm			64	4.0	1,000
B-100	Batt 12.7 mm			50	3.1	12,000
Thermoflex	Density felt	1477	2200	64	4	1,000
Thermoflex	Felt	↓	↓	128	8	6,000
Thermoflex	Felt			192	12	
ADL Lightweight Ceramic		1533	2300	784	49	19,000
ADL-Lightweight Ceramic	No surface finish	↓	↓	785	49.0	19,000
Zircar Board				320	20	6,200
Zircar Block		1811	2800	1218	76	6,200
Microquartz Felt		1477	2200			250
Closed Cell Urethane Foam		394	250	57.9	3.6	0.0
Lo-Con Felt	3.81 mm	-	-	64	4.0	6,800
Fiber-film	1 layer Teflon	533	500	-	-	0.54
7-106-6N	Impregnated 2 layers each .038 mm					
Dexter paper	1 layer, .25 mm	-	-	-	-	250
Dexter paper	3 layers, 90° rotation, .76 mm	-	-	-	-	400
Mylar	Test sample	-	-	-	-	4.25×10^{-3}
Sil. Temp. 25 m	6.35 mm	1366	2000	34	2.1	6,000
Haveg No. 84	.635 mm	-	-	74	4.6	600

TABLE VII
SUMMARY OF LOW PERMEABILITY MATERIALS FOR
THE INNERMOST INSULATION LAYER

Material	Density		Permeability
	(kg/m^3)	(lb/ft^3)	(millidarcies)
Min-K 2000			
normal to the sheet	320	20	3.21
parallel to the sheet			45 to 110
compressed to 830 N	574	35.8	2.0
compressed to 1660 N	670	41.8	1.3
	670	41.8	1.045*
High Density Min-K	560	35	0.6
Microtherm			
parallel to the sheet	384	24	1.3
normal to the sheet	384	24	0.4
ADL Cryogenic Foam Insulation	57.9	3.6	0.0

* Tested With CO_2

APPENDIX C
MATHEMATICAL MODEL VERIFICATION

Before the thermal protection system weights of the purged insulation concept could be computed, the validity of the mathematical models, developed in Appendix A, had to be established by comparison with experimental results. Test conditions were that of cryogenic temperatures on a simulated tank wall side of the insulation specimen and the introduction of a condensable inert purge gas to the other side of the insulation system. Test apparatuses were designed and built to evaluate annular and flat plate specimens. The cryodeposition rate of the purge gas was measured and compared with the analytical results. In addition to being used as a means for establishing the validity of the thermal models, this flat plate apparatus was also used to investigate the performance of the more promising insulation samples defined in Appendix B when exposed to a condensable purge gas in a cryogenic environment. This appendix describes the test apparatuses, the test procedures and the comparison of the results.

Cylindrical Test Apparatus

The small cylindrical insulation calorimeter shown in Figure 22 was designed and built to validate the cryodeposition rate of purge gas within permeable insulation specimens. The cylindrical copper vessel, capable of holding 2.6 liters of cryogen, was insulated with annular test specimens. These annular sections were cut from a 5.1 cm (2 inch) thick sheet of test insulation. They were attached to the copper vessel and bonded to one another with low temperature polyurethane adhesive. Polyurethane foam insulation was placed at the top and bottom of the cryogenic vessel container to limit heat and condensate flow to the test specimens. Thermocouples were placed radially within the insulation layers at the mid-level of the 20.3 cm (8 inch) stack of insulation.

The flow system used to provide the purge gas and measure boil-off in this test apparatus is shown in Figure 23. The vacuum line was used to evacuate the test chamber and to remove noncondensable gases that could inhibit the condensation process when pure purge gas was introduced to the chamber. When the test volume had been evacuated sufficiently, the vessel was filled with liquid nitrogen through the fill tube and when full, the boil-off was measured with a calibrated flowmeter. This established the heat flux without purge gas. The purge gas (carbon dioxide) was then admitted to the chamber and the increase in boil-off resulting from cryopumping of carbon dioxide was measured. The purge gas inflow was also measured and maintained at a level necessary to maintain a slight positive chamber pressure.

The first specimen tested with this apparatus was Min-K 2000. The cryotank was filled with liquid nitrogen while the surrounding chamber was held at a vacuum. Three hours and ten minutes later, after thermal equilibrium had been reached in the specimen, the chamber was pressurized with carbon dioxide. After one and one-half hours of cryopumping (first CO_2 fill), the carbon dioxide supply was shut off and the chamber was allowed to cryopumped to a vaccum. Four hours and twenty minutes later the chamber was again pressurized with carbon dioxide (Second CO_2 fill).

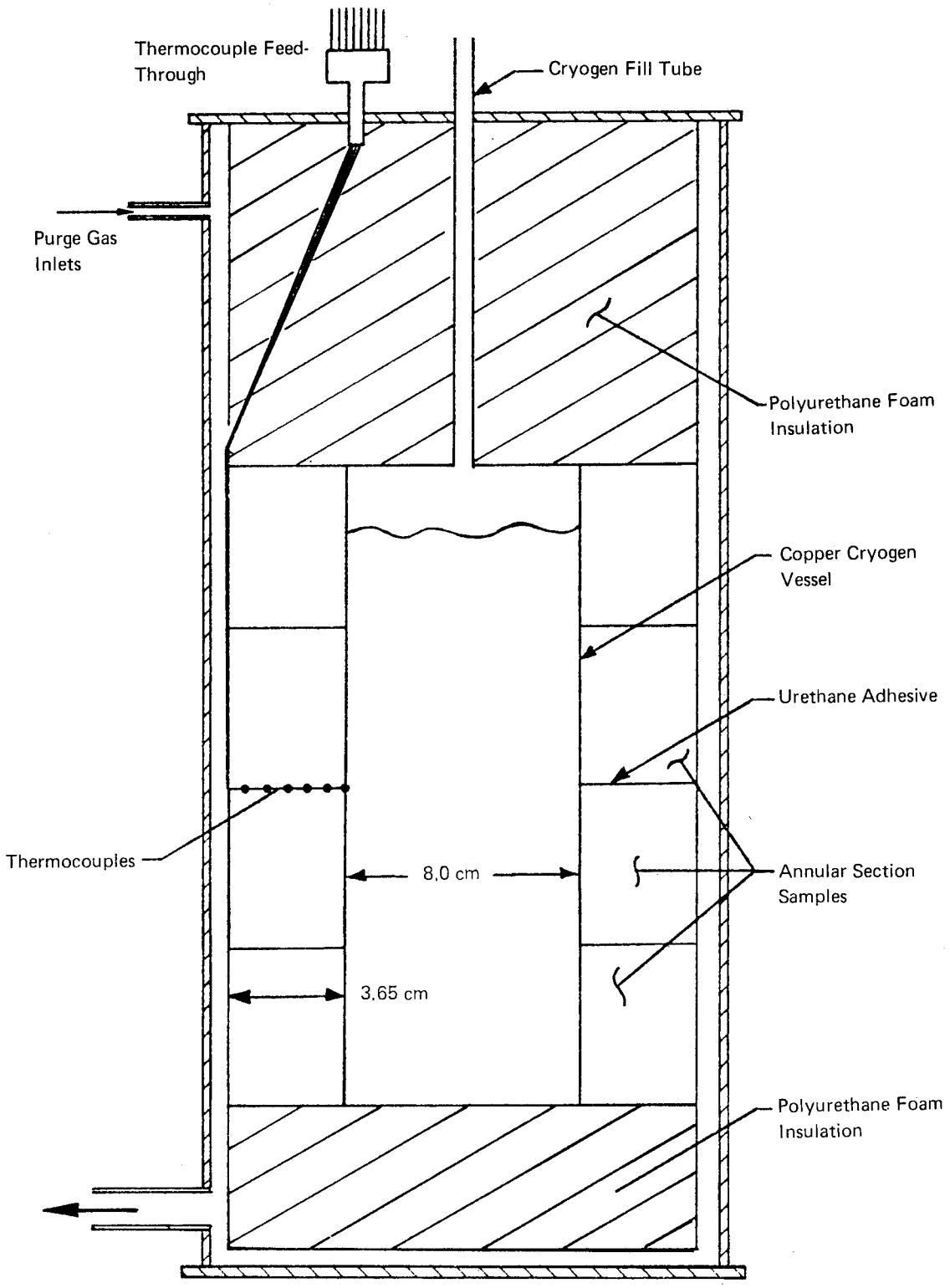

Figure 22. Cylindrical Laboratory Test Chamber

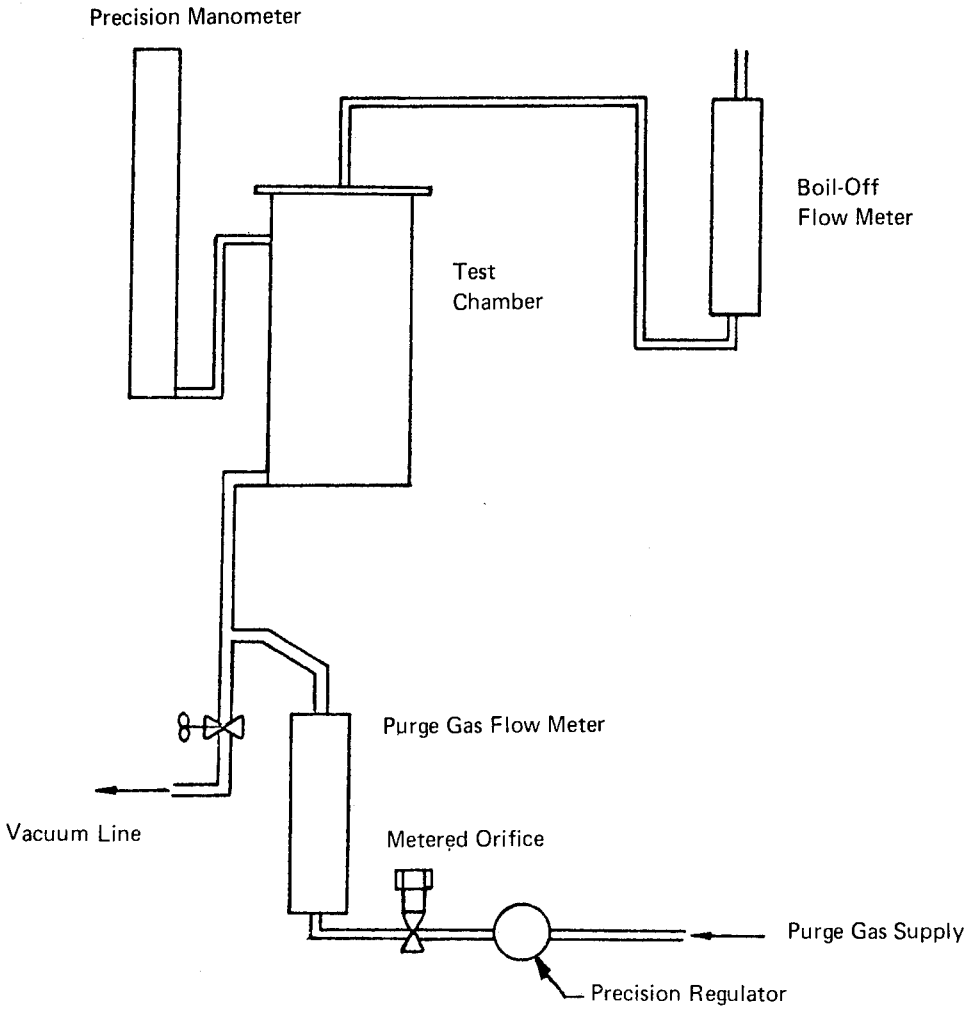

Figure 23. Cylindrical Laboratory Test Apparatus Flow Schematic

Thermocouples placed at .32 cm (.125 in) radial increments through the insulation measured the temperature distribution through the thickness. At the end of the first carbon dioxide fill, temperatures below the carbon dioxide cryodeposition temperature existed from the cryosurface out to 1.52 cm (.6 in) into the insulation. During the second carbon dioxide fill, which lasted 1.5 hours, the frost line temperature moved out only .18 cm (.07 in) which suggests that the cryodeposition was primarily within the frost layer, a conclusion previously reached in the investigation of Reference 8.

Table VIII presents the results of the tests with the sample varification apparatus. The last two columns of this table present values of heat transfer rates obtained by two different methods. The last column values were calculated using the boil-off rate of liquid nitrogen and represent the total heat flux to the cryotank. The next to the last column is the heat flux due to the carbon dioxide cryodeposition only. Total heat flux obtained by adding the cryodeposition flux and the tare flux (obtained while the specimen was in a vacuum) are within 4% of the measured value in all cases.

TABLE VIII

INSULATION SAMPLE VERIFICATION TESTS

INSULATION	TEST CONDITION	CO_2 DEPOSITION RATE, g/s (lb/hr)	HEAT FLUX, W/m^2 (BTU/hr-ft^2)	
			(1)	(2)
Min-K-2000				
ρ_i = 320 kg/m^3 (20 pcf)	Evacuated	—	—	77.5 (24.6)
t_i = 3.56 cm (1.4 in)	First CO_2 Purge	.088 (0.70)	718 (228)	771 (245)
	Second CO_2	.091 (0.72)	724 (230)	838 (266)
ADL Foam				
ρ_i = 64 kg/m^3 (4 pcf)	Evacuated	—	—	252 (80)
t_i = 1.3 cm (0.5 in)	CO_2 Purge	8.4×10^{-4} (6.7×10^{-3})	—	299 (95)

(1) Based on CO_2 Flow

(2) Based on LN_2 Boil Off

The measured CO_2 deposition rates for the Min-K-2000 were approximately 40% higher than rates that were originally predicted based on a permeability coefficient of 0.63 g/s (.6 lb/hr). Subsequently it was learned that the permeability of the insulation perpendicular to the thickness was significantly higher than that through the thickness (see Appendix B). For the higher permeability the deposition process was heat transfer limited. Calculations based on the heat transfer limited model predicted deposition rates that were within 10% of the measure values. However, since the design of the cylindrical test apparatus was such that the purge gas penetration was perpendicular to the thickness and, therefore, not representative or the actual thermal protection system it was not used for further tests of permeable insulation.

Testing with the impermeable ADL cryogenic foam indicated a slight carbon dioxide purge flow which was credited to cryodeposition at joints between the samples and also between the top and bottom isolation insulation pieces. The tare heat flux for the ADL cryogenic insulation after being corrected for the different insulation thicknesses is approximately 5% greater than Min-K which agrees with thermal conductivity data for the two insulations. No degradation of either insulation occurred during this testing.

Flat Plate Apparatus

Since the cylindrical apparatus did not simulate the flow path through the insulation correctly, a flat plate apparatus which isolated the ends of the sample from the purge gas was designed and built. This apparatus is shown in Figure 24. It consisted of a 15.3 cm (6 in.) cold plate which was cooled by the flow of a cryogen through a tube soldered to its back surface. The cold plate and tubing were surrounded by closed cell polyurethane foam which was foamed in place. A cavity was provided on the front surface in which samples of insulation were mounted by bonding to the foam with polyurethane adhesive. The cold plate and sample were placed within a pressure-tight vessel into which purge gas was introduced. For tests with dry nitrogen purge gas, helium was the cryogen; for carbon dioxide purge gas, liquid nitrogen was the cryogen. Thermistors and thermocouples were used for measuring temperatures on the cold plate and through the insulation.

The flow schematic is shown in Figure 25. The purge gas flow was controlled by a throttle valve and was monitored by one of three calibrated flow meters selected for the purge gas flow rate. The flow of purge gas was controlled manually by the test operator as he monitored the pressure within the chamber. The greater the permeability of an insulation, the greater was the purge gas flow requirement to maintain positive purge gas pressure. Typically, the test procedure was to introduce cryogen to the cold plate, and then introduce purge gas to the chamber surrounding the insulation. The purge gas flow rate was measured as a function of time, for 6 hours or until frost was noted on the outside of the sample.

Table IX summarizes the results of the flat plate apparatus tests. Visual examination after the first exposure to a condensing purge gas indicated that all of the basic permeable insulations were susceptible to surface cracks. Only the impermeable glass fiber reinforced polyurethane foam and the microtherm insulation with wire stitching survived the tests without cracking. Cryodeposition rates for the various insulations are presented and compared with analytical predictions in Figures 26 to 31.

For the bare flat plate, the cryodeposition rate is solely heat transfer limited. Thus, the analytical results, based on Equation 14, should closely approximate the experimental results. However, although the analytical results predict the trend of the data, the experimental deposition rates presented in Figure 26 are approximately twice the analytical values. The only rational explanation for this discrepancy, is that purge gas was leaking around the edges of the cavity and was deposited on the back side of the apparatus as well as the front. (It should be noted that the bare plate tests were run after the apparatus had been exposed to several thermal cycles.) The extremely low deposition rates encountered during subsequent tests in which the cavity was sealed with mylar covered polyurethane foam, tend to confirm this hypothesis (see Figure 27). Although this leakage would alter the results obtained in a heat transfer limited process, it should not significantly effect the deposition rate in a diffusion controlled process.

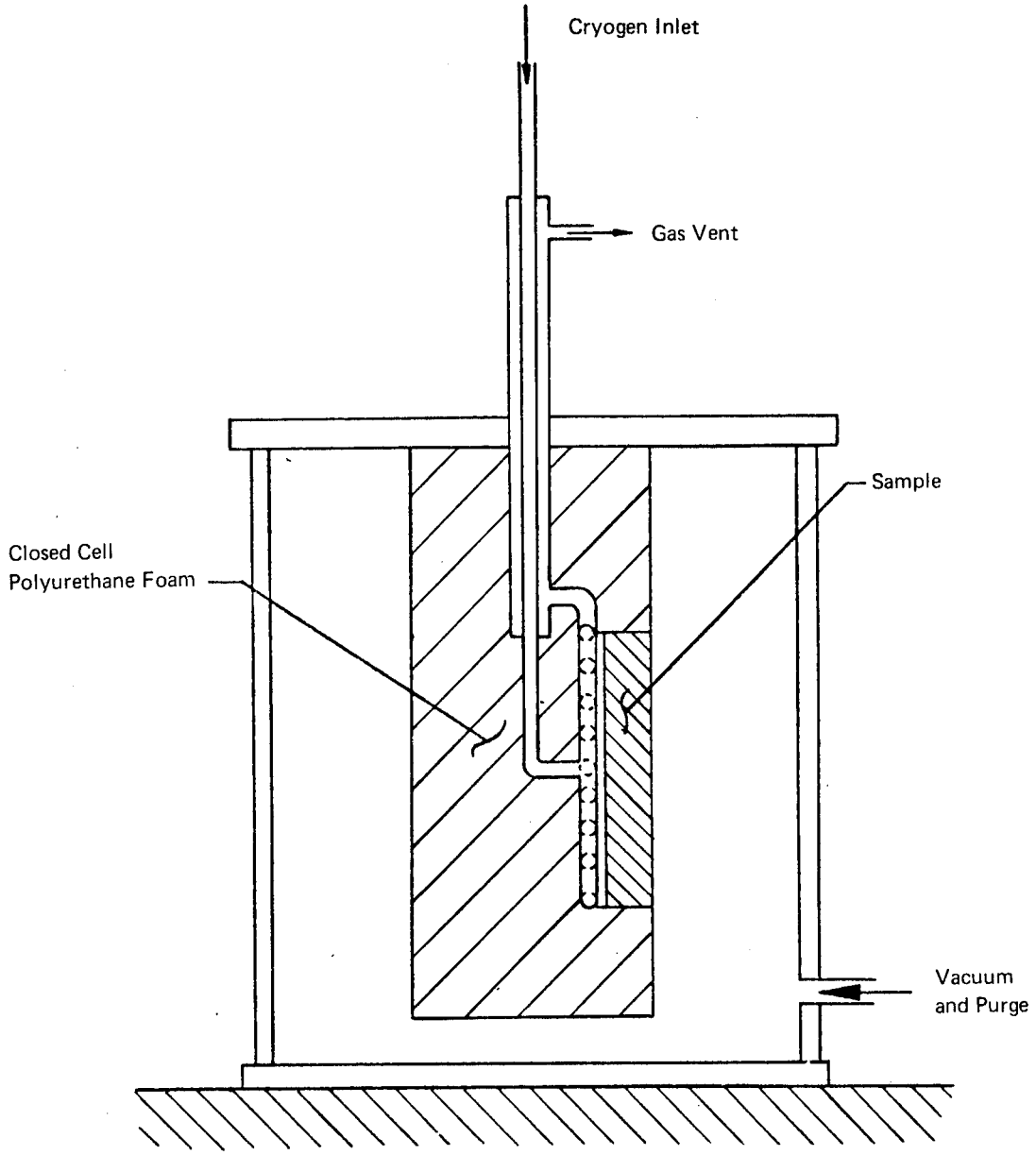

Figure 24. Flat Plate Test Apparatus

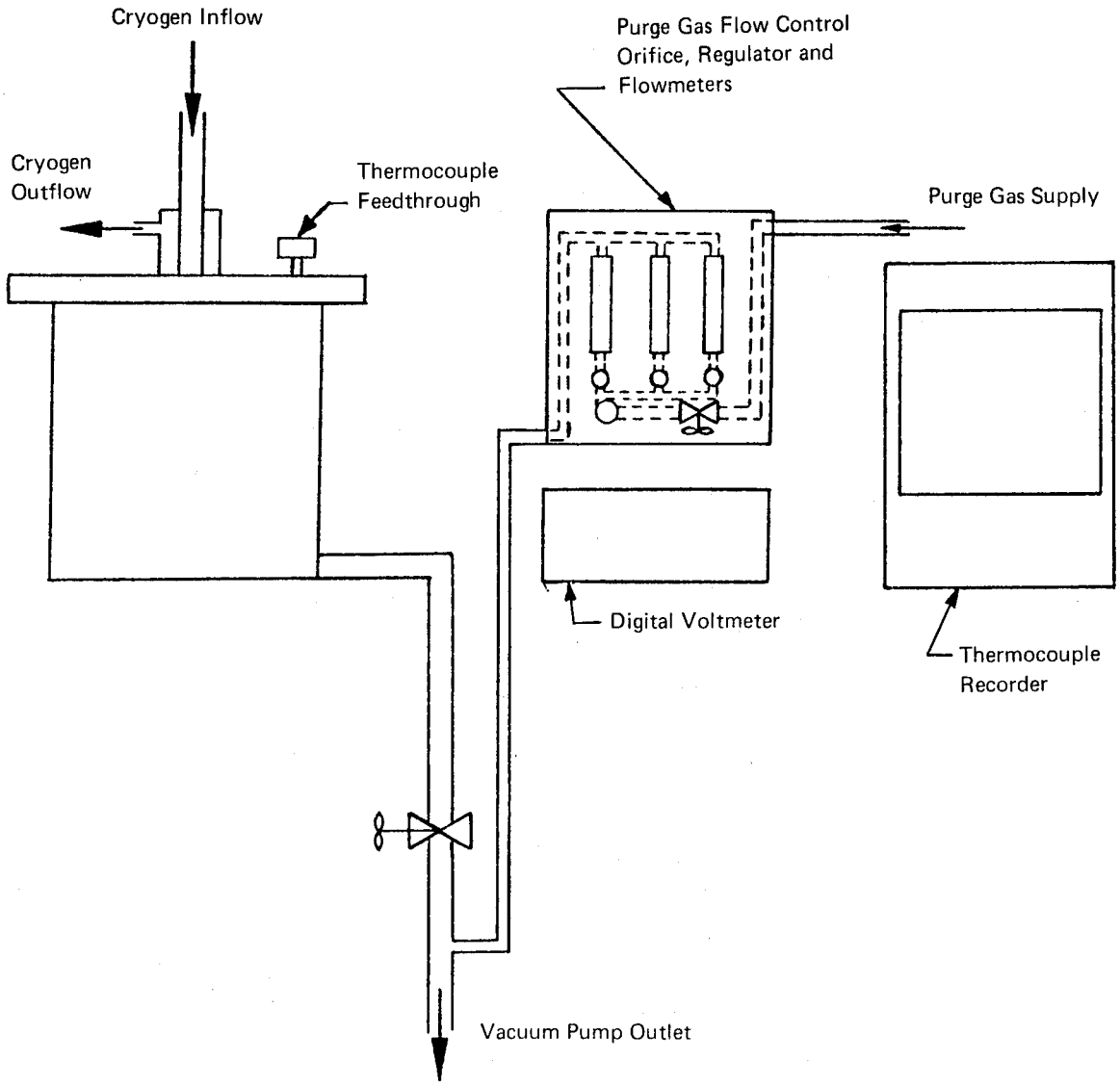

Figure 25. Flat Plate Test Apparatus Flow Schematic

TABLE IX
INSULATION SAMPLES INVESTIGATED WITH THE FLAT PLATE APPARATUS,
INSULATION THICKNESS = 2.54 cm (1.0 in.)

Test Order	Sample	Cryogen	Purge Gas	Comments
1	Min-K 2000	LHe	N_2	After test hairline crack in insulation observed
2	Min-K 2000	LN_2	CO_2	Audible cracking during warm-up - large crack observed after warm-up
3	Bare Plate	LN_2	CO_2	Honeycomb pattern of cracks formed in solid CO_2 - cracking audible during deposition
4	ADL Cryogenic Foam Covered with Mylar	LN_2	CO_2	No detectable problem
5	Microtherm	LN_2	CO_2	Small hairline crack developed during warm-up
6	High Density Min-K	LHe	N_2	Large rupture developed near center of sample during warm-up
7	Stitched Microtherm	LN_2	CO_2	Front face heated after test - No evidence of damage
8	Stitched Microtherm	LN_2	CO_2	Same sample as preceeding test - backface heated after test - No evidence of damage.

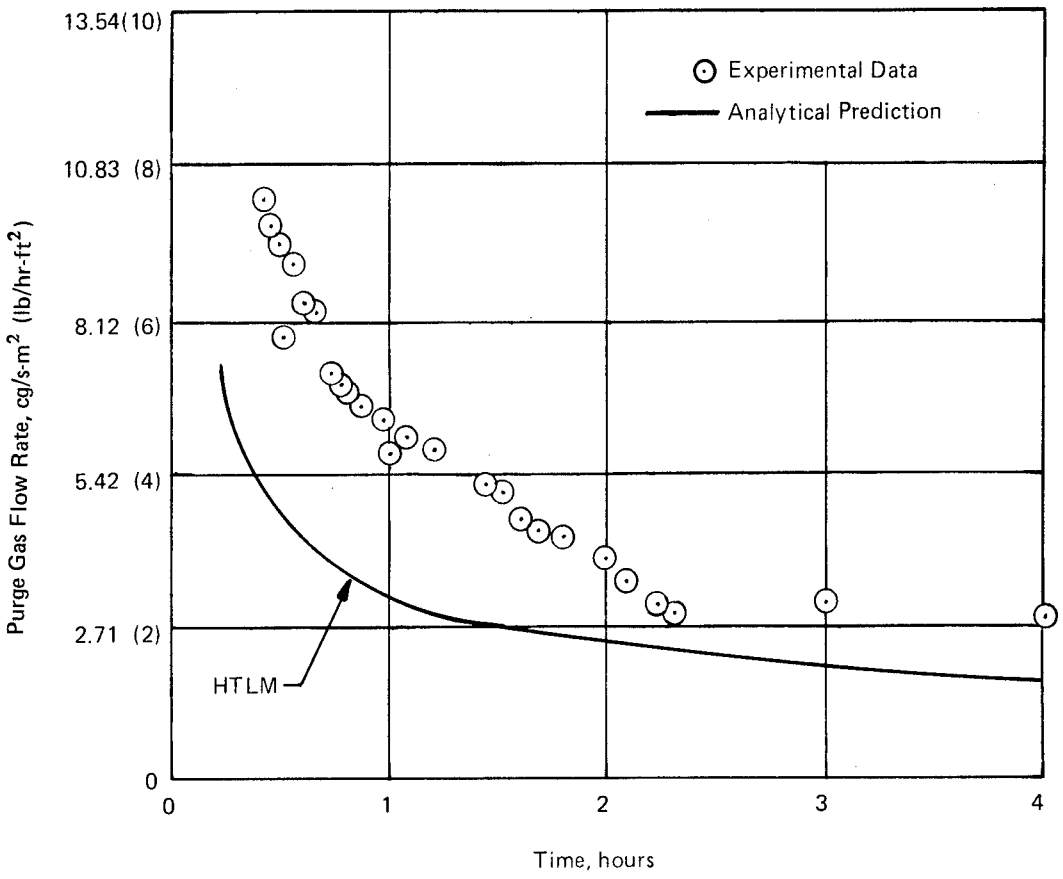

Figure 26. Cryodeposition Rate of Carbon Dioxide on the Test Apparatus without Insulation Sample, Liquid Nitrogen Cryogen

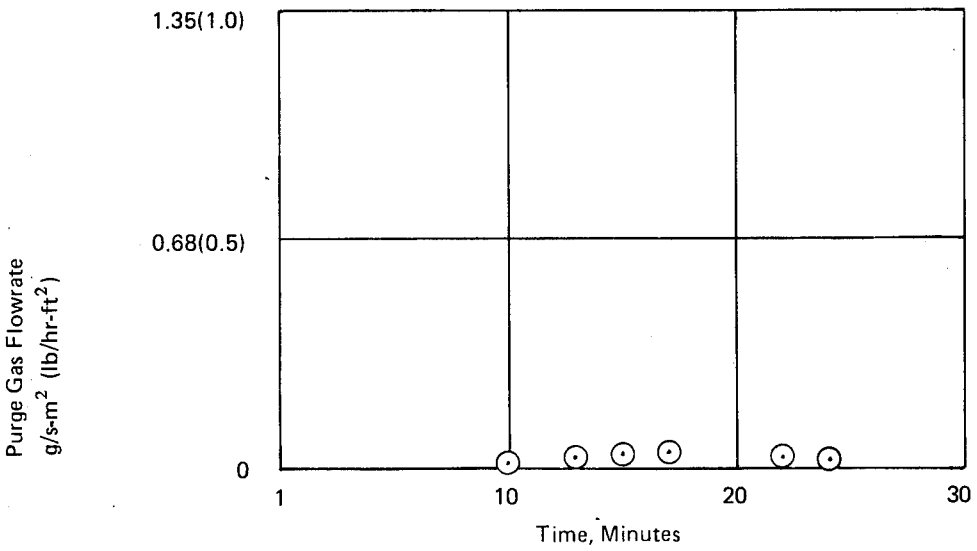

Figure 27. Cryodeposition Rate of Carbon Dioxide with Mylar Covered ADL Cryogenic Foam Insulation; Liquid Nitrogen Cryogen

Figure 28 demonstrates the permeability limited process. Microtherm was tested and the deposition rate of carbon dioxide was recorded as a function of time. The agreement between experiment and analysis was excellent. Visual examination, after the sample was warmed to room temperature, revealed that the sample was cracked. The absence of any sudden increase in the deposition rate indicates that the crack must have occurred during warm-up.

Figure 29 illustrates the transition with time from a permeability to a heat transfer controlled process. In this test with CO_2 and LN_2, the permeability of the Min-K-2000 is sufficiently low to control the deposition process initially; however, in less than one hour, heat transfer becomes the controlling factor. As with the microtherm sample, the specimen was damaged during the test.

In an earlier section of this report, it was shown that the most effective way to decrease the permeability of an insulation was to compress it (thereby also increasing the density). The effect of this change on deposition rate is shown in Figure 30. In these tests with nitrogen and liquid helium, the deposition rate for Min-K-2000 (320 kg/m^3 (20 lb/ft^3)) was first permeability, then heat transfer limited, as in the previous figure. With high density Min-K (560 kg/m^3 (35 lb/ft^3)), the deposition rate was diffusion controlled throughout the test and was much lower than that for the Min-K 2000, and somewhat lower than the analytical prediction. The damage incurred by the higher density material was more severe.

In an attempt to overcome the cracking problem, a special sample was fabricated with microtherm. This sample had fiberglass cloth attached to both surfaces of the insulation with 0.025 cm (0.01 in.) diameter copper wire stitching through the insulation. The 0.64 cm (0.25 inch) long stitches, which formed a 2.54 cm (1-inch) square grid, provided reinforcement for the insulation and vent paths through which cryodeposites could out-gas. It was postulated that because of the high conductivity of the copper, the vent path would seal rapidly with solid cryodeposits during cryodeposition and open rapidly during heating. The cryodeposition rate in the initial tests of this specimen with carbon dioxide and liquid nitrogen (Figure 31), was approximately twice that of the unstitched specimen (see Figure 28); although in the second test, the rate was comparable to that of the unstitched specimen. The reason for this discrepancy is unknown. The important aspect of this test, however, is the fact that the specimen survived two thermal cycles with no evidence of damage, even though heating was applied (see Table IX) to increase the severity of out-gassing following the tests.

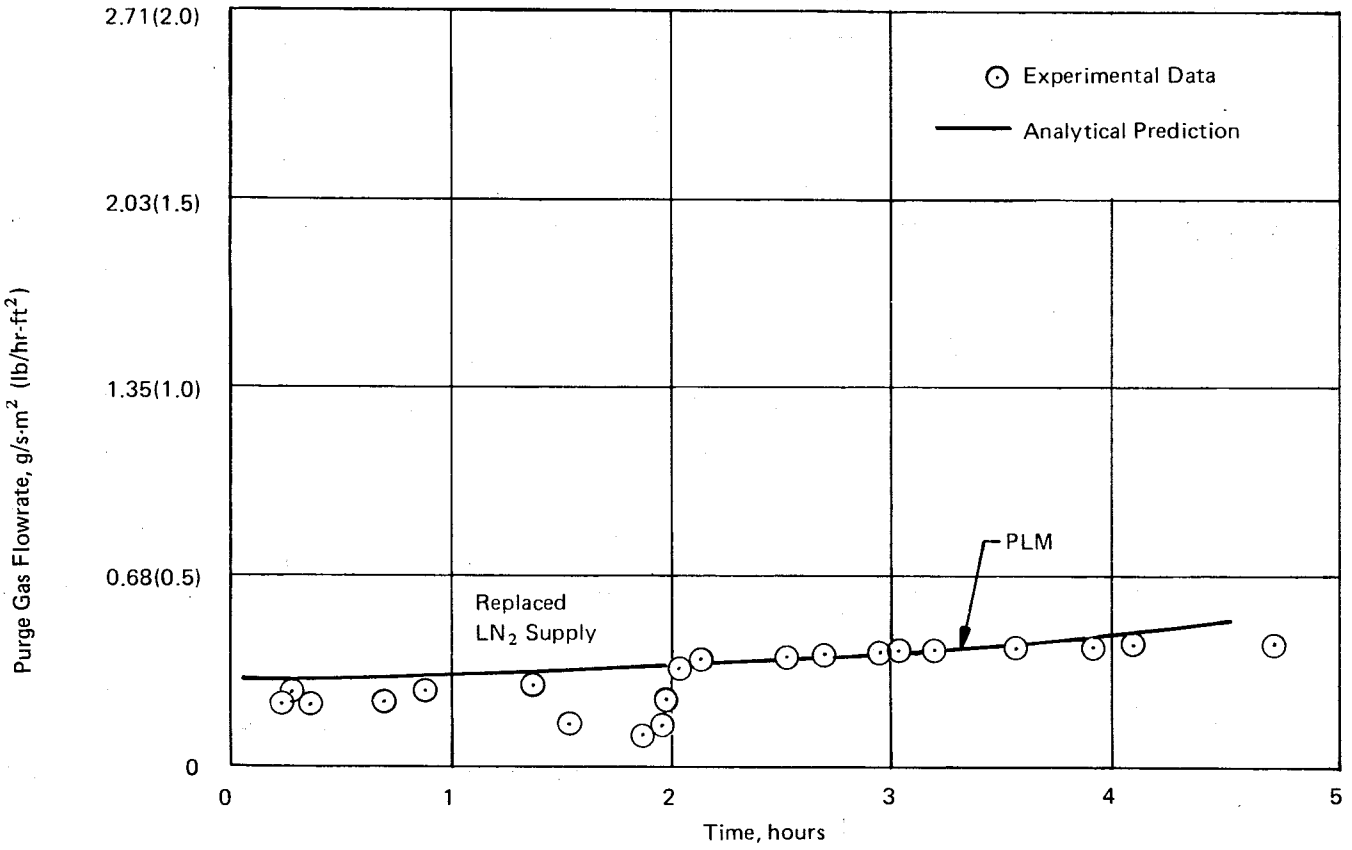

Figure 28. Cryodeposition Rate of Carbon Dioxide within Microtherm; Liquid Nitrogen Cryogen

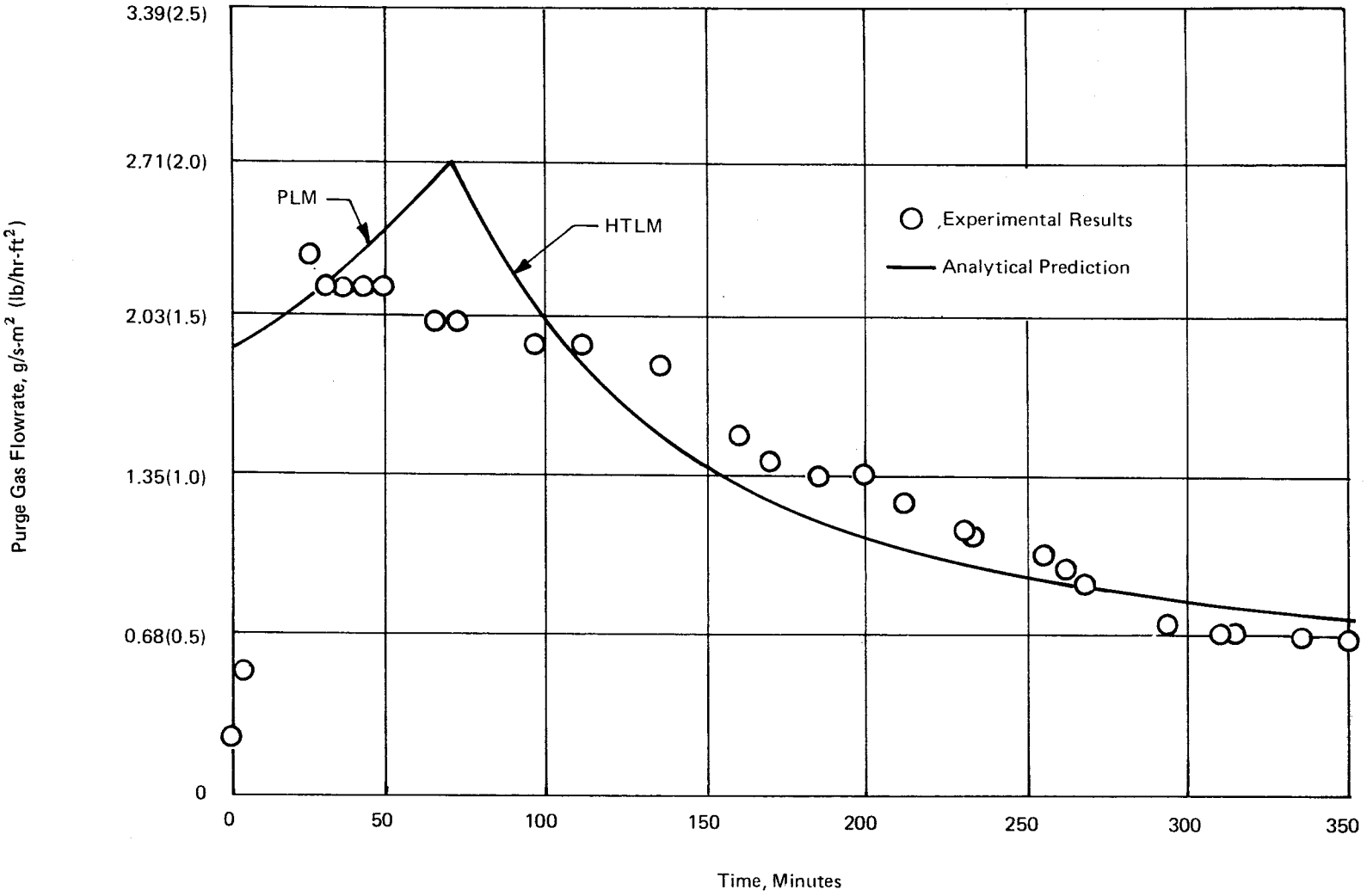

Figure 29. Crodeposition Rate of Carbon Dioxide in Min K-2000; Liquid Nitrogen Cryogen

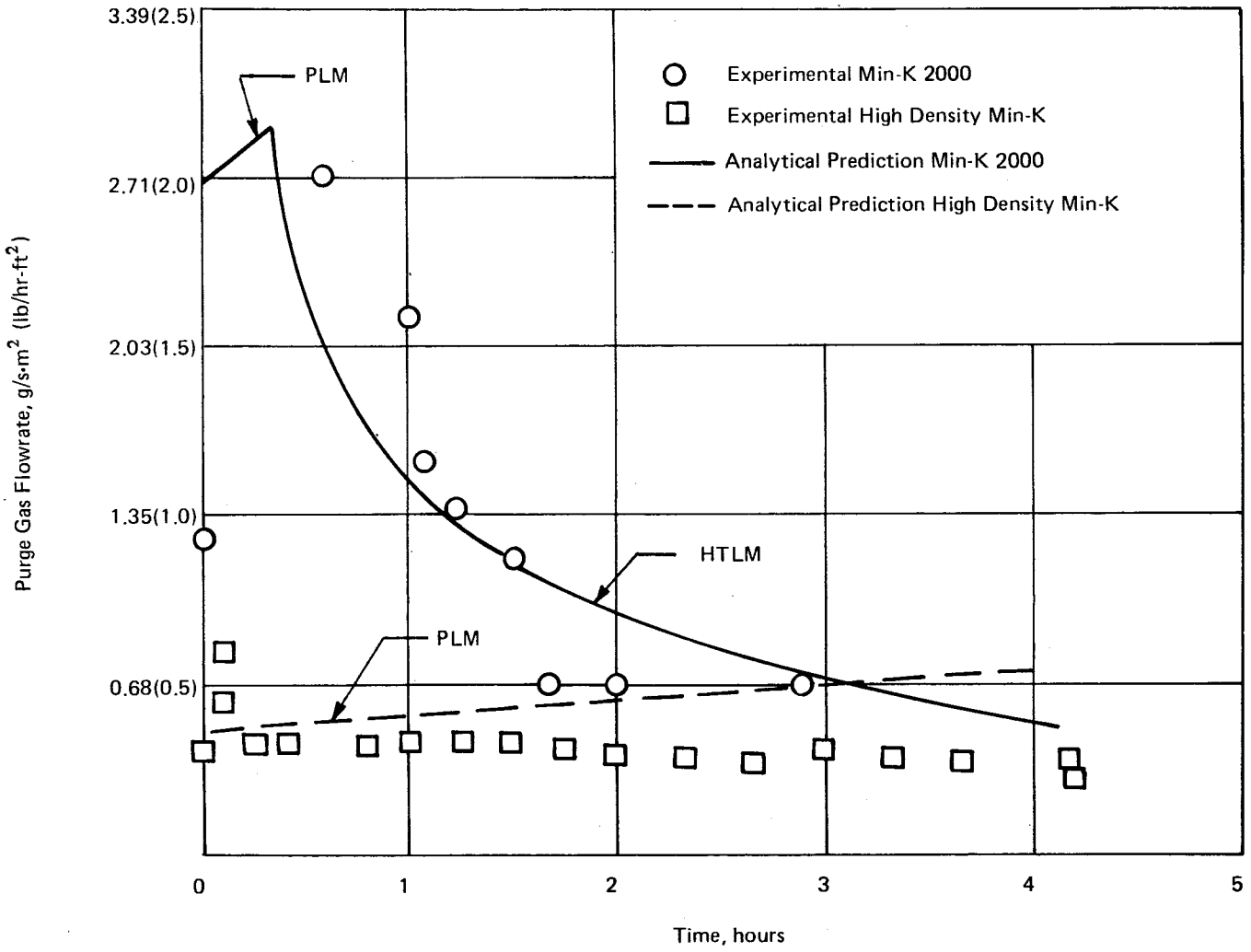

Figure 30. Cryodeposition Rate of Nitrogen within Min-K 2000 and High Density Min-K; Liquid Helium Cryogen

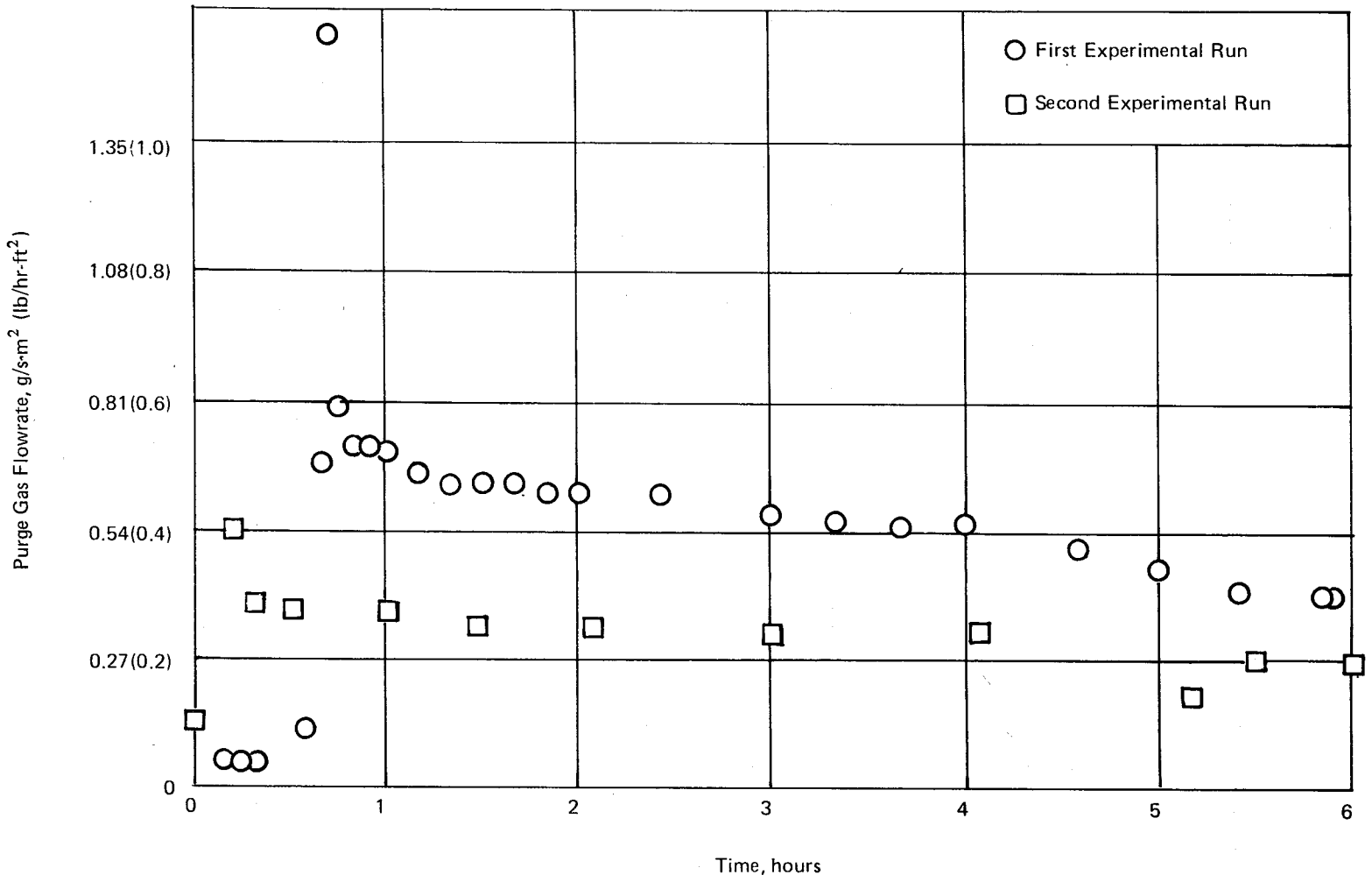

Figure 31. Cryodeposition Rate of Carbon Dioxide in Microtherm with 0.24 mm (0.010 inch) Diameter Copper Wire Stitching Spaced 6.8 mm (0.25 inch) on a 2.54 cm (1.0 inch) Grid; Liquid Nitrogen Cryogen

APPENDIX D
WEIGHT STUDIES

In the previous appendices, a mathematical model of the purged insulation system was developed and experimentally verified. In addition, it was determined that Microtherm insulation was the only permeable insulation that had an acceptable permeability and was not seriously degraded by exposure to liquid hydrogen temperature. In this appendix, the thermal protection system unit weights are presented for both an insulation system with a 384kg/m^3 (24 pcf) Microtherm inner insulation layer and an insulation system with a closed cell plastic foam inner layer. For these studies the outer layer was 96.2 kg/m^3 (6 pcf) Dynaflex. After the unit weights are presented, the total TPS weights for the tankage of a hypersonic transport are discussed.

Environmental Boundary Conditions

Before the weight of the purged insulation system can be determined from the equations listed in Appendix A, it was necessary to define the thermal and physical properties of each element in the system and the heating conditions during ground operation and flight operations.

A summary of the properties used for the weight sensitivity studies are listed in Table X and shown in Figure 32.

When the vehicle is being readied for takeoff, it is assumed to be in an external environment with natural convection to the external surface as the primary heat transfer mode. As long as the fuel boiloff on the ground is reasonable, the most severe operating condition is a low ambient temperature, a high humidity, and still air. In this situation the surface temperature will be lowest and ice buildup due to water vapor in the air will be a potential problem. For these studies, the ambient temperature was specified as 283K (50°F) and the external heat transfer coefficient was assumed to vary between 5.7 J/m^2 -sec-K (1.0 and 10.0 BTU/hr-ft^2 -°F) which corresponds to still air and a reasonable wind velocity, respectively. The duration of this type of heating condition was assumed to be greater than 3.0 hours but less than 12.0 hours.

During high-speed flight, heating of the external surface is defined by the vehicle shape and trajectory. Because of previous studies (References 15 and 18), the hypersonic transport was selected as the baseline vehicle (the tanks of the transport in this study were larger then the tanks in the previous studies because the Mach number was increased from 6 to 8). The mission profile of the hypersonic transport and the radiation equilibrium temperature data for several regions on the tankage surface were previously shown in Figures 1 and 2.

On the basis of the above property data and heating conditions the optimum thermal protection system weights were predicted. For this investigation, locations on both the lower and upper vehicle centerline were studied. Since each tank will have an ullage requirement, the study region on the upper centerline was always considered to be a dry tank condition, i.e., the tank wall is not in contact with liquid hydrogen. On the lower centerline, both the wet and dry tank conditions were investigated. The wet tank condition corresponds to a tank which is full during the heating phases of the flight, whereas the dry tank condition corresponds to a tank which is emptied during the early stages of ascent. For analysis purposes, the dry tank corresponds to an adiabatic tank wall, hence any heat input will result in a temperature rise of the system, whereas the wet tank corresponds to a constant tank wall temperature of 22K (-420°F).

TABLE X
DIFFUSION AND THERMAL PROPERTIES OF VARIOUS COMBINATIONS OF INSULATIONS AND PURGE GASES

A. Metric Units

Insulation Type	Purge Gas	Insulation		Purge Gas		Diffusion Parameters		Frost	
		Density kg/m^3	Specific Heat J/g-C	Specific Heat J/g-C	Latent Heat J/g	ϕ cg/hr-m	Ψ cm^2/hr	Density kg/m^3	Specific Heat J/g-C
Dynaflex	N_2	96	0.84	1.05	-	-	-	-	-
Dynaflex	CO_2	96	0.84	0.84	-	-	-	-	-
Microtherm	N_2	385	0.84	1.05	197	0.68	0.47	640	1.05
Microtherm	CO_2	385	0.84	0.84	581	0.27	0.24	896	0.84
ADL Cryogenic Foam		64	1.68		-	-	-	-	-

B. English Units

Insulation Type	Purge Gas	Insulation		Purge Gas		Diffusion Parameters		Frost	
		Density pcf	Specific Heat BTU/lb-°F	Specific Heat BTU/lb-°F	Latent Heat BTU/lb	ϕ lb/in/hr-ft^2	Ψ in^2/hr	Density pcf	Specific Heat BTU/lb-°F
Dynaflex	N_2	6	0.2	0.25	-	-	-	-	-
Dynaflex	CO_2	6	0.2	0.20	-	-	-	-	-
Microtherm	N_2	24	0.2	0.25	85	0.55	0.074	40	0.25
Microtherm	CO_2	24	0.2	0.20	250	0.22	0.038	56	0.2
ADL Cryogenic Foam		4	0.4	-	-	-	-	-	-

*Diffusion parameters are defined in Appendix A.

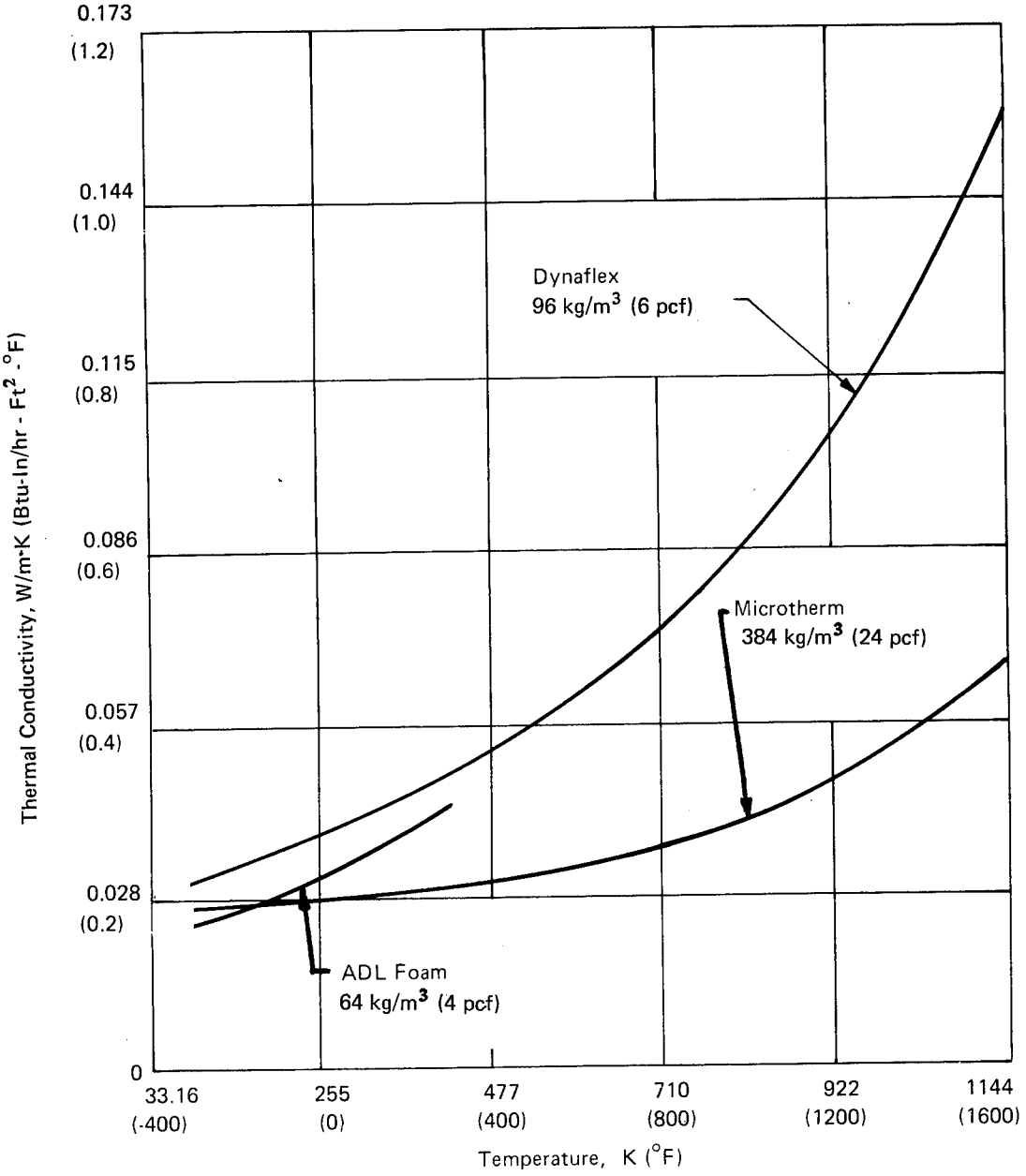

Figure 32. Insulation Thermal Conductivity in Air at an Absolute Pressure of 10 mm of Hg.

Permeable Inner Insulation Weight Studies

The unit weights of a purged insulation system with a permeable inner insulation using either nitrogen or CO_2 as the purge gas are presented in Tables XI and XII. The effect of ground hold time as well as location on the tank are indicated. The weight shows a strong dependence on ground hold time. This is mainly due to frost conductivity being significantly higher than the insulation thermal conductivity. As the frost layer builds with time, more insulation is required to maintain the outer surface temperature at or above 273K (32°F).

The weights of the wet tank are greater than the dry tank weights since they include the weight of the fuel boiloff. Comparison of the results for a dry tank on the lower surface to a dry tank on the upper surface shows that the insulation thicknesses are exactly the same but the weights are different. For the dry tank, the insulation thicknesses are sized by the ground hold heat flux and skin temperature requirement, but the weight is dependent on the amount of frost evaporated during flight. Since the lower surface is exposed to a more severe heating environment, more frost is evaporated and the time averaged frost weight is less. Comparison of the carbon dioxide system weights with the nitrogen weights reveals that the nitrogen weights are at least 2.44 kg/m^2 (0.5 psf) lighter than the CO_2 system. Nitrogen has a lower freezing point than carbon dioxide; therefore, the thickness of both the frost and the denser inner insulation are less for nitrogen, consequently, the lower unit weights.

The above comparison was based on constant values of frost thermal conductivities, and densities as well as ground hold heat flux; therefore, a sensitivity study of these parameters was required in order to establish the validity of these weight comparisons. Since the nitrogen system indicated the least weight, it was selected as baseline for these studies. The ground hold time was selected as 6 hours. Figures 6, 33, and 34 present the sensitivity of the TPS weights to frost density and the effective thermal conductivity of the frost and insulation combination. These results are for locations on both the bottom and top centerline of the vehicle and are specificially for a ground hold time of 6 hours and an external heat flux of 283 W/m^2 (90 BTU/hr-ft^2) during ground hold. The knee in the curve is associated with a change in the constraint which controls the system sizes. At high values of frost conductivity, the insulating efficiency of the frost layer is poor, hence the least weight system occurs when the frost thickness is minimized. By eliminating all of the Dynaflex, the flow path length for the purge gas is at a maximum and the system is diffusion limited during the full duration of ground hold operation. As the effective conductivity of the frost layer is reduced, the weight penalty related to using Microtherm over the much lighter weight Dynaflex insulation to impede the frost buildup exceeds the boiloff weight penalty; therefore, it becomes advantageous to minimize the Microtherm thickness. The minimum thickness of Microtherm is that required to maintain the interface between the Microtherm and the Dynaflex at least equal to the condensation point of the purge gas during ground hold.

Comparison of the curves for the wet bottom and dry bottom indicates that the weight of wet tank is more sensitive to changes in frost conductivity. As a matter of fact for frost conductivities in excess of 0.086 W/m - K (0.6 BTU-in/hr-ft^2 -°F), the dry tank results are nearly independent of frost conductivity. For a dry tank, the additional heat flow through the frost during flight as a result of the high frost conductivity only increases the tank wall temperature, whereas for a wet tank, it increases the fuel boiloff. In either case, however, the total thickness of insulation is controlled by the requirement that the outer vehicle surface temperature must be equal to or greater than 273K (32°F) during ground hold operation so that ice buildup is prevented.

TABLE XI
UNIT WEIGHTS FOR A NITROGEN PURGED INSULATION SYSTEM WITH AN INNER LAYER OF MICROTHERM, GROUND HEAT FLUX = 283 W/m^2

(90 BTU/hr-ft^2)

Peripheral Location on Fuselage	Wall Status	Ground Hold Time hr	Unit Weight		Insulation Thickness			
					Overall		Microtherm	
			kg/m^2	lb/ft^2	cm	in.	cm	in.
Bottom	Wet	3	14.7	3.03	2.92	1.15	1.75	0.69
Bottom	Wet	6	19.2	3.94	3.30	1.30	2.49	0.98
Bottom	Wet	12	24.8	5.10	4.83	1.90	2.34	0.92
Bottom	Dry	3	10.6	2.18	2.41	0.95	1.98	0.78
Bottom	Dry	6	16.8	3.45	3.30	1.30	2.49	0.98
Bottom	Dry	12	23.4	4.80	4.83	1.90	2.34	0.92
Top	Dry	3	11.5	2.36	2.29	0.9	2.29	0.90
Top	Dry	6	17.4	3.56	3.30	1.30	2.49	0.98
Top	Dry	12	24.9	5.10	4.83	1.90	2.34	0.92

TABLE XII
UNIT WEIGHTS FOR A CARBON DIOXIDE PURGED INSULATION SYSTEM WITH AN INNER LAYER OF MICROTHERM, GROUND HEAT FLUX = 283 W/m^2

(90 BTU/hr-ft^2)

Peripheral Location on Fuselage	Wall Status	Ground Hold Time	Weight		Insulation Thickness			
					Overall		Microtherm	
			kg/ml^2	lb/ft^2	cm	in.	cm	in.
Bottom	Wet	3	16.5	3.70	2.03	0.80	2.03	0.8
Bottom	Wet	6	23.3	4.79	3.55	1.40	3.30	1.30
Bottom	Wet	12	30.9	6.35	5.46	2.15	4.93	1.94
Bottom	Dry	3	13.4	2.76	2.92	1.15	2.59	1.02
Bottom	Dry	6	19.6	4.03	4.19	1.65	3.71	1.46
Bottom	Dry	12	28.2	5.79	5.84	2.30	5.23	2.06
Top	Dry	3	13.7	2.82	2.92	1.15	2.62	1.03
Top	Dry	6	19.8	4.07	4.19	1.65	3.71	1.46
Top	Dry	12	28.8	5.90	5.84	2.30	5.23	2.06

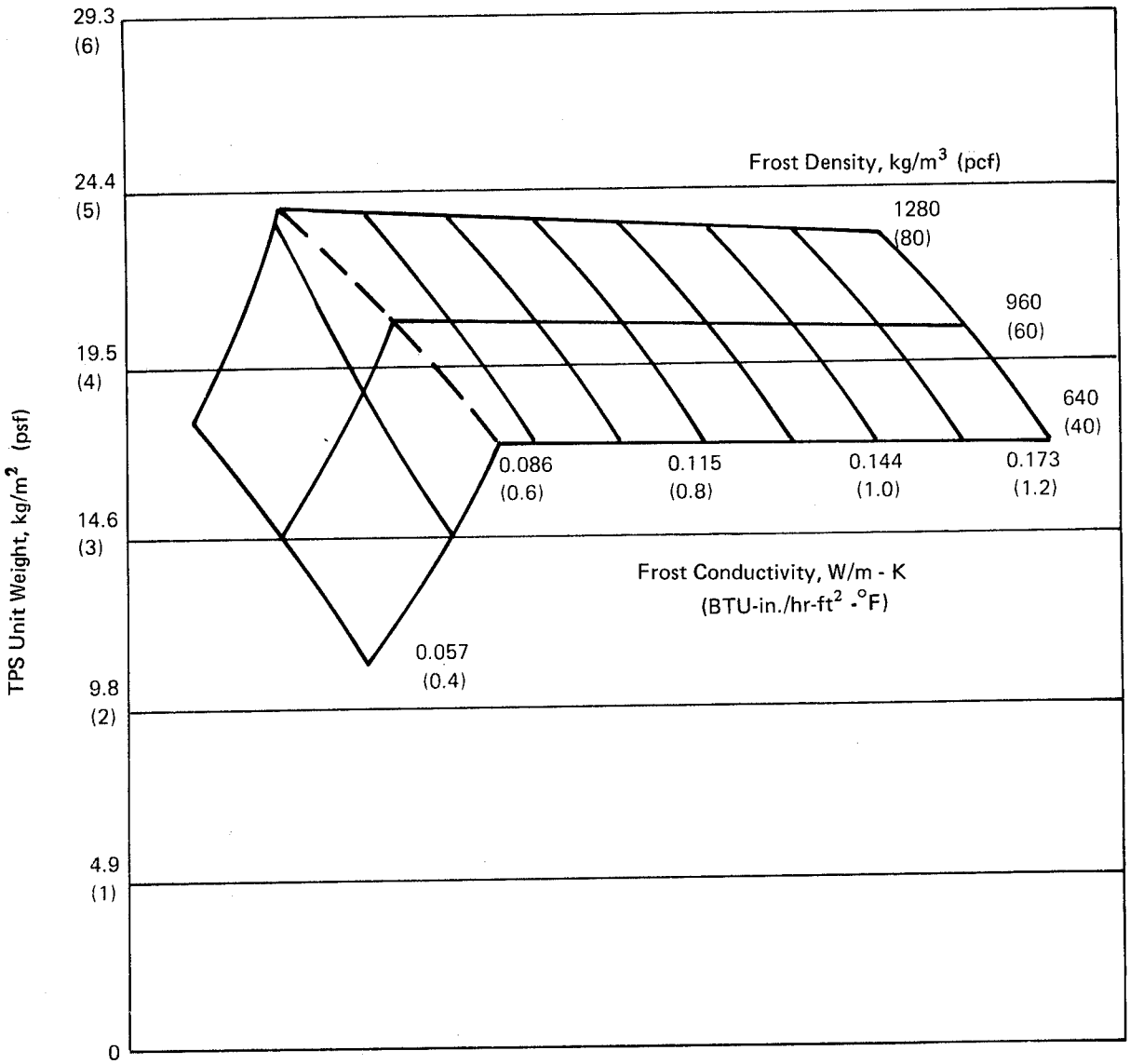

Figure 33. Effect of Nitrogen Frost Density and Thermal Conductivity on TPS Weights for Hypersonic Transport Tankage, Ground Hold = 6 Hours, Ground Heat Flux = 284 W/m² (90 BTU/ft²-hr), Fuselage Lower Centerline, Dry Tank

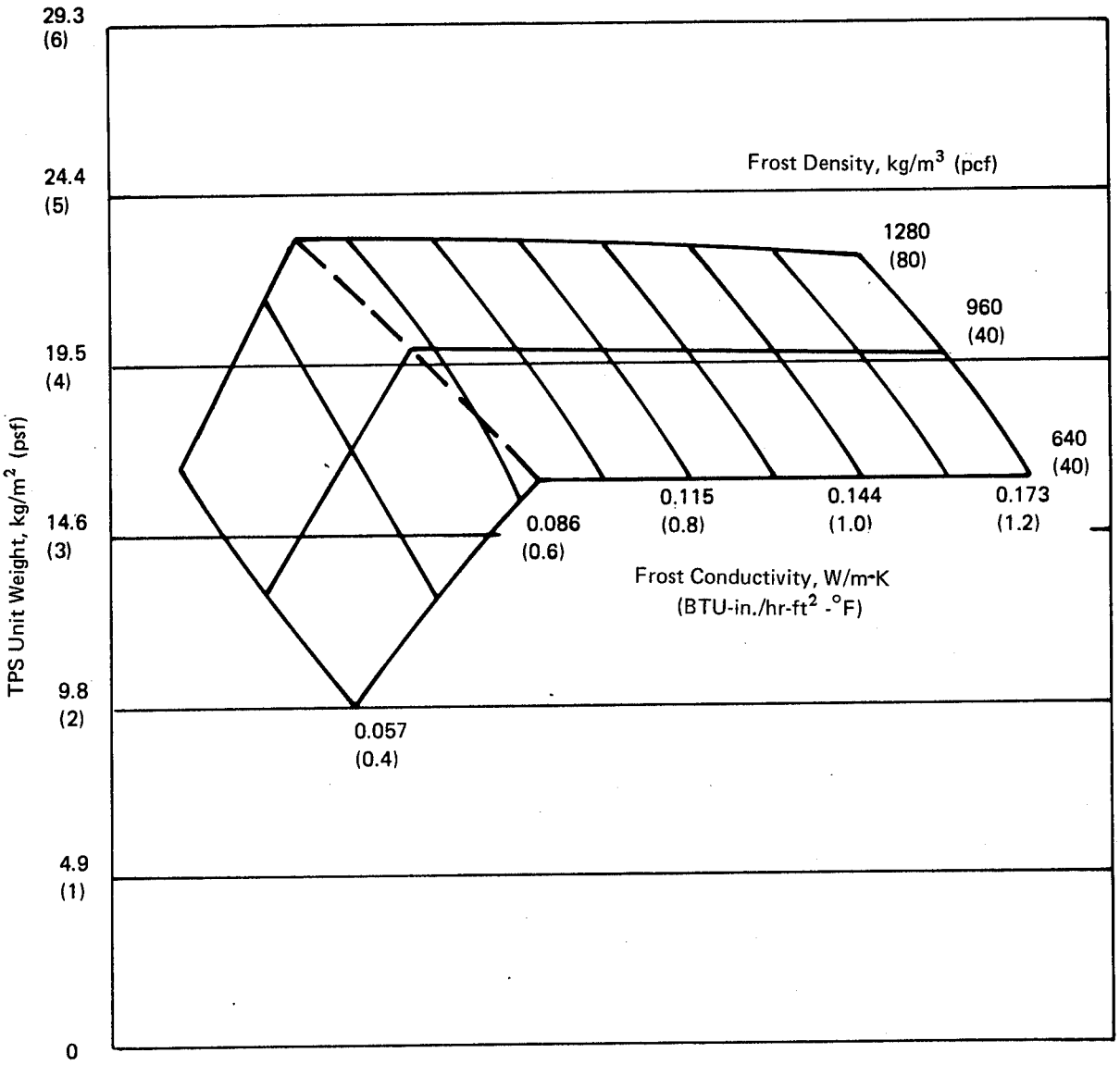

Figure 34. Effect of Nitrogen Frost Density and Thermal Conductivity on TPS Weights for Hypersonic Transport Tankage, Ground Hold = 6 Hours, Ground Heat Flux = 284 W/m² (90 BTU/ft²-hr) Fuselage Upper Centerline, Dry Tank

The effect of the ambient heat flux on TPS weight is shown in Figure 5. The heat flux is defined as

$$q = h\ (T-T_s)$$

where h is the heat transfer coefficient

T is the ambient temperature

T_s is the minimum outer surface temperature

At very low heat fluxes, large insulation thicknesses are required to insulate the outer skin from the cold tank wall. Because the thicknesses are large, the frost layer can be very thick, hence it pays to employ all Microtherm to minimize the frost buildup during ground operation. As the external heat flux increases, the insulation requirements decrease and so does the thickness of insulation below the purge gas condensation point. Once the frost weight becomes small enough, it is advantageous to use the least amount of Microtherm. This change in constraint is noted as the break in the curve. For the wet tank another break in the curve occurs at heat fluxes greater than 535 W/m^2 (170 BTU/ft^2 -hr) At the higher heat fluxes, flight conditions rather than ground conditions size the insulation system.

Closed Cell Inner Insulation Weight Studies

By its inherent nature, mass diffusion through the insulations towards the tank wall is negligible for the closed cell inner insulation. Frost deposition is prevented by maintaining the interface between the outer and inner insulation layer at a temperature above the purge gas condensations point, and ice deposition due to water vapor in the air is prevented by maintaining the outer surface temperature above the freezing point. During flight, the interface between the insulations must be maintained at a temperature less than the insulation's maximum service temperature so that the inner insulation is not degraded.

During the ground hold operation, the two ground hold temperature constraints which must be applied to the problem can be written in equation form as

$$y \geqslant \frac{k_o\,(T_s - T_f)}{h\ (T_\infty - T_s)}$$

$$x \geqslant \frac{k_i\,(T_f + 420)}{h\ (T_\infty - T_s)}$$

In these equations, the thermal conductivity was evaluated at the mean temperature. Once the minimum thicknesses are established, a parametric study with both insulation thickness as the variables is performed and the minimum weight thermal protection system, which satisfies the interface constraint, is determined. The analysis is completed with the aid of a general finite element transient heat transfer program. Each insulation layer was subdivided into a minimum of 10 elements and the heat fluxes as determined from the aerodynamic heating analysis are applied as external boundary conditions. The inner boundary condition depends on the tank wall condition. For the wet tank,

it was assumed that the wall remained at a constant temperature of 22K (-420°F), whereas for the dry tank, it was assumed that the wall absorbed all of the heat. The computer program integrates the amount of fuel boiloff and averages it over the flight period. This weight penalty is added to the insulation weight to obtain the total thermal protection system weight.

The weights for a closed cell insulation system are shown in Figure 7. These weights include the inner insulation at 64 or 128 kg/m^2 (4 or 8 pcf), the outer dynaflex insulation at 96 kg/m^3 (6 pcf), and the average weight of fuel boiloff during flight. With the exception of the wet tank at temperatures in excess of 422K (300° F), the weights continually decrease with an increase in temperature, because of the reduction in dynaflex insulation thickness required to insulate the foam. The wet tank results begin to increase at higher temperatures because the fuel boiloff weight increases with a decrease in insulation thickness.

In contrast to the permeable insulation system, the thickness and weight of the closed cell foam system are dictated by flight rather than ground hold conditions. Ground hold constraints, in particular the outer surface temperature, dictate that the total overall insulation thickness must be at least 2.8 cm (1.1 inch). This assumes an ambient temperature of 283K (50° F), a moisture freezing point of 273K (32° F) and an ambient heat transfer coefficient of 28.4 W/m^2 - K (5.0 BTU/hr-ft^2 -°F). However, it can be seen from Figure 8 that the thickness of the optimized system will less than 2.8 cm (1.1 inch) only if the maximum use temperature of the foam is greater than 533K (500°F). This means that the maximum service temperature capability of the foam controls the insulation sizing. Recalling that the only reason for employing the foam is to prevent freezing of the purge gas within the insulation, this suggests that the ratio of the foam thickness to the overall thickness should be minimized, which is the same as fixing the interface temperature between the two insulations at the condensation point of the purge gas. For nitrogen, the interface temperature is 77K -320° F) and the foam thickness is 17 percent of the overall thickness.

APPENDIX E

THERMOPHYSICAL PROPERTIES TESTS

This appendix presents the thermal and physical properties measurements made on the ADL Cryogenic Urethane Foam Insulation. Emphasis was placed on temperature stabilized specimens to assess the influence of the heat treatment on properties. The properties include thermal conductivity, compressive strength, tensile strength, bending strength, flexural modulus of elasticity and permeability. The material for test samples was prepared from a sample which had a density of about 51.3 kg/m^3 (3.2 pounds per cubic foot). Each of the samples of material (approximately 97 cm in diameter and 1.5 cm thick) was temperature stabilized in an oven for 6 hours at 400 K (260°F) and for 6 hours at 450 K (350°F).

Thermal Conductivity

The thermal conductivity of temperature-stabilized ADL Cryogenic Foam Insulation was measured by one of two techniques, depending upon the temperature range. For measurements at a mean temperature of 177 K (-140°F), the guarded hot plate method was used in accordance with ASTM Standard C-177. In this technique, two 20.3 cm (8 inch) diameter samples of material were placed on either side of a 20.3 cm (8 inch) diameter heater element, which contained both a central heater 10.1 cm (4 inch) in diameter and a ring guard-heater. On the external surface of each of the two samples, temperature controlled cold plates were placed to absorb the heat that was transferred through the samples. The thermal conductivity was calculated from one-half of the heat generated in the central heater (it is assumed that half of the heat flows out through each sample), the temperature of the central heater, the temperature of the two cooling plates (both maintained at the same temperature level), and the thickness of the sample in accordance with the following formula:

$$k = \frac{q \cdot t}{A(T_h - T_c)}$$

Thermal conductivity was measured also at temperatures of 266, 297, 362, and 442 K (19.4, 75.2, 192, and 336°F) by the heat-flow meter method in accordance with ASTM Standard C-518. This technique called for placement of the insulation sample in a stack of elements consisting of a hot plate, a heat-flow meter, the sample, and a cold plate. Heat flowed from the hot plate, through the heat-flow meter (which has a guard around its outer perimeter), through the sample, and then to a cold plate. Temperatures are measured on the hot plate, on the side of the heat-flow meter facing the sample, and on the cold plate. The heat-flow meter consisted of a multi-junction thermopile placed on the surfaces of the core of the heat-flow meter. The heat-flow meter is calibrated by the comparative method with the use of a pair of thermally matched rigid specimens for which the average thermal conductivity has been determined in accordance with ASTM Standard C-177. Because the heat flowmeters are temperature-sensitive and change with the mean temperature, calibrations are carried out at various mean temperatures. The thermal conductivity of each sample tested was calculated from a measurement of the heat flux through the sample (determined from the calibration of the heat-flow meter), the temperature of the cold plate, the temperature of the face of the heat-flow meter in contact with the sample, and the thickness of the sample.

Results of all thermal conductivity tests are summarized in Table XIII. The thermal conductivity of temperature-stabilized ADL Cryogenic Foam Insulation is summarized in Figure 35.

Mechanical Properties

The mechanical properties of ADL polyurethane foam insulation were measured at three nominal test temperatures, 77.4, 294, and 442 K (-320, 70, and 300°F). Attempts to measure properties at 450 K (350°F) were unsuccessful because the material softened and reliable data could not be obtained. Compressive strength at a 10% deflection was measured in accordance with ASTM Standard D-1621, "Compressive Strength of Rigid Cellular Plastics." In this procedure, square samples 5.08 x 5.08 cm (2 x 2 inch) were placed between flat platens in an Instron tester. For tests at 77.4 K (-320°F), a stainless steel box was constructed to contain the sample and was filled with liquid nitrogen before and during testing of the sample. A thermocouple placed in the sample was used to determine the sample temperature prior to compressive testing. For tests at 422 K (300°F), a cylindrical oven was used for heating the samples and the two platens and a thermocouple in the oven wall determined the temperature.

Flexural strength and flexural modulus of elasticity of the sample materials were measured at temperatures of 77.4 and 294 K (-320°F and 70°F) in accordance with ASTM Standard D-90, "Flexural Properties of Plastics." A bar of rectangular cross section 5.08 x 1.52 x 20.3 cm (2 x 0.6 x 8 inches) was tested in flexure as a simple beam, with the bar resting on two supports and the load applied by means of a loading nose midway between the supports. Each specimen was deflected until rupture occurred. In all tests, samples failed when the tension side of the beam ruptured. The bending strength at failure was calculated for each sample, and the flexural modulus of the elasticity was calculated from the stress-strain relationship.

As a result of softening of the material, measurements of the bending strength of the foam insulation was impossible at temperatures above 422 K (300°F). A tensile test was performed instead in accordance with ASTM Standard D-638, "Tensile Properties of Plastics."

In Table XIV, all mechanical properties tests are summarized as well as the number of test samples in each determination. The results of tests of compressive strength, the flexural yield strength, the flexural modulus elasticity, and the tensile strength are given with calculated standard deviations for each series.

TABLE XIII
SUMMARY OF THERMAL CONDUCTIVITY MEASUREMENTS
TEMPERATURE-STABILIZED URETHANE FOAM INSULATION

Test Technique	Density		Mean Temperature		Temperature Difference		Thermal Conductivity	
	kg/m^3	lb/cu. ft	K	°F	K	°F	kW/m^2 -K	BTU-in/ ft^2 -hr -°F
Heat Flow Meter (ASTM C-518)	51.8	3.23	266	19.4	36.5	65.8	0.127	0.246
	51.8	3.23	297	75.2	48.3	87.1	0.145	0.280
	51.8	3.23	362	192	49.2	88.7	0.189	0.365
	51.8	3.23	442	336	51.4	92.5	0.249	0.480
Guarded Hot Plate (ASTM C-177)	51.1	3.19	297	75.2	12.2	22.0	0.149	0.288
	51.1	3.19	177	-141	74.4	134	0.084	0.163

TABLE XIV
MECHANICAL PROPERTIES OF TEMPERATURE-STABILIZED
ADL CRYOGENIC POLYURETHANE FOAM INSULATION

	Test Temperature		Property		Standard Deviation	Number of Test Samples
	K	°F	kN/m^2	psi		
Compressive Strength at 10% deflection (ASTM D-1621)	77	-320	176.	25.6	3.6	10
	294	70	266.	38.6	2.4	8
	422	300	12.9	1.76	0.41	10
Flexural Yield Strength (ASTM D-790)	77	-320	611.	88.7	7.7	10
	294	70	365.	52.9	2.1	
Flexural Modulus of Elasticity (ASTM D-790)	77	-320	2980.	432	541	10
	294	70	990.	144	130	10
Tensile Strength (ASTM D-638)	422	300	50.5	7.33	2.1	
Tensile Modulus of Elasticity	422	300	2100.	310	0.096	10

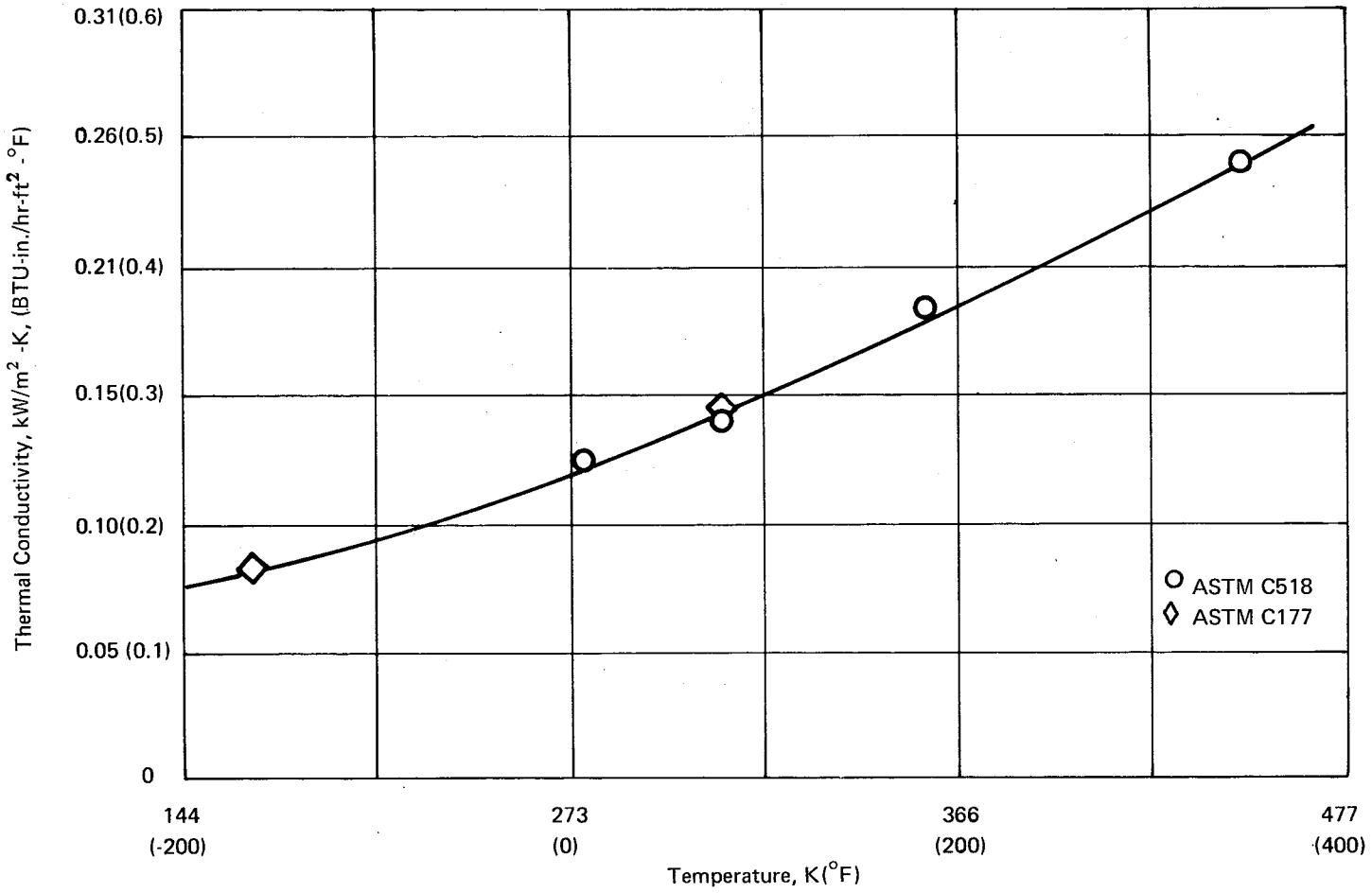

Figure 35. Thermal Conductivity of Temperature Stabilized ADL Cryogenic Polyurethane Foam Insulation

APPENDIX F
CALORIMETER DESIGN

During the early phases of the contract, specimen tests were used to eliminate materials that had an unacceptable permeability or did not prevent the flow of liquid nitrogen. However, the overall thermal performance of the more promising insulations in an environment similar to those experienced by hydrogen fueled aircraft could not be evaluated with specimen tests. Therefore, during the contract it was necessary to design a test apparatus which would simulate the pressure/temperature/purge gas characteristics of a hydrogen fuel tank while simultaneously acting as a calorimeter. Such an apparatus would be capable of evaluating the overall performance of any hydrogen tankage TPS in environmental conditions associated with present day aircraft as well as future high-speed aircraft. In the appendix, the design details of a 76 cm (30 inch) flat plate test apparatus designed to satisfy these requirements are presented. A flat plate apparatus was selected over a scaled-down hydrogen tank for two reasons. First, it was considered to be more cost-effective, and second it was considered to lend itself to calorimetric measurements more readily than a cylindrical tank.

Design Requirements

To effectively evaluate the overall performance of a thermal protection system for a hydrogen fuel tank, the test apparatus must be capable of representing both the external environmental conditions as well as the internal condition. Since hydrogen fuel tanks are being considered for both subsonic and hypersonic aircraft, the test system had to be designed such that the temperature of the outer surface of the insulation system could be varied from 219K to 1366K (-65°F to 2000°F). In addition, the external pressure had a vary between 3.44 kN/m^2 (0.5 psia) to 104. kN/m^2 (15.2 psia). To investigate conditions representative of top, bottom, or side of the tank (dry, wet, or liquid-gas interface) the equipment was mounted on a trunion.

In addition to simulating the internal heat transfer characteristics, the flat plate test area had to be designed to have thermal characteristics nearly identical to the fuel tank shell. In order to satisfy this requirement, the heat capacity of the flat plate must be equal to the heat capacity of the tank wall. Since the fuel tanks were to be capable of withstanding 811K (1000°F), stainless steel was selected as the tank material. Therefore, the inner vessel of the calorimeter was fabricated from stainless steel with a thickness equal to the equivalent thickness of the fuel tank.

System Description

A schematic flow diagram of the flat plate calorimeter system which satisfies the requirements of simulating the pressure/temperature environment of a hydrogen fuel tank is shown in Figure 36. The system consists of 4 separate flow networks, i.e., the hydrogen system, the liquid nitrogen system, the purge gas system, and the cooling water system. In addition, vacuum and compressed gas connections are provided to both the liquid hydrogen vessel and the seal side. These connections facilitate initial purge before filling with liquid hydrogen and also provide individual control of the absolute pressure levels within these two vessels. The latter characteristic allows one to follow a pressure history representative of any trajectory. Liquid hydrogen is supplied to the calorimeter from the hydrogen source by means of a vacuum insulated transfer line. For safety purposes relief valves are provided between each shutoff valve. A solenoid operated throttle valve (FCV) is provided to permit

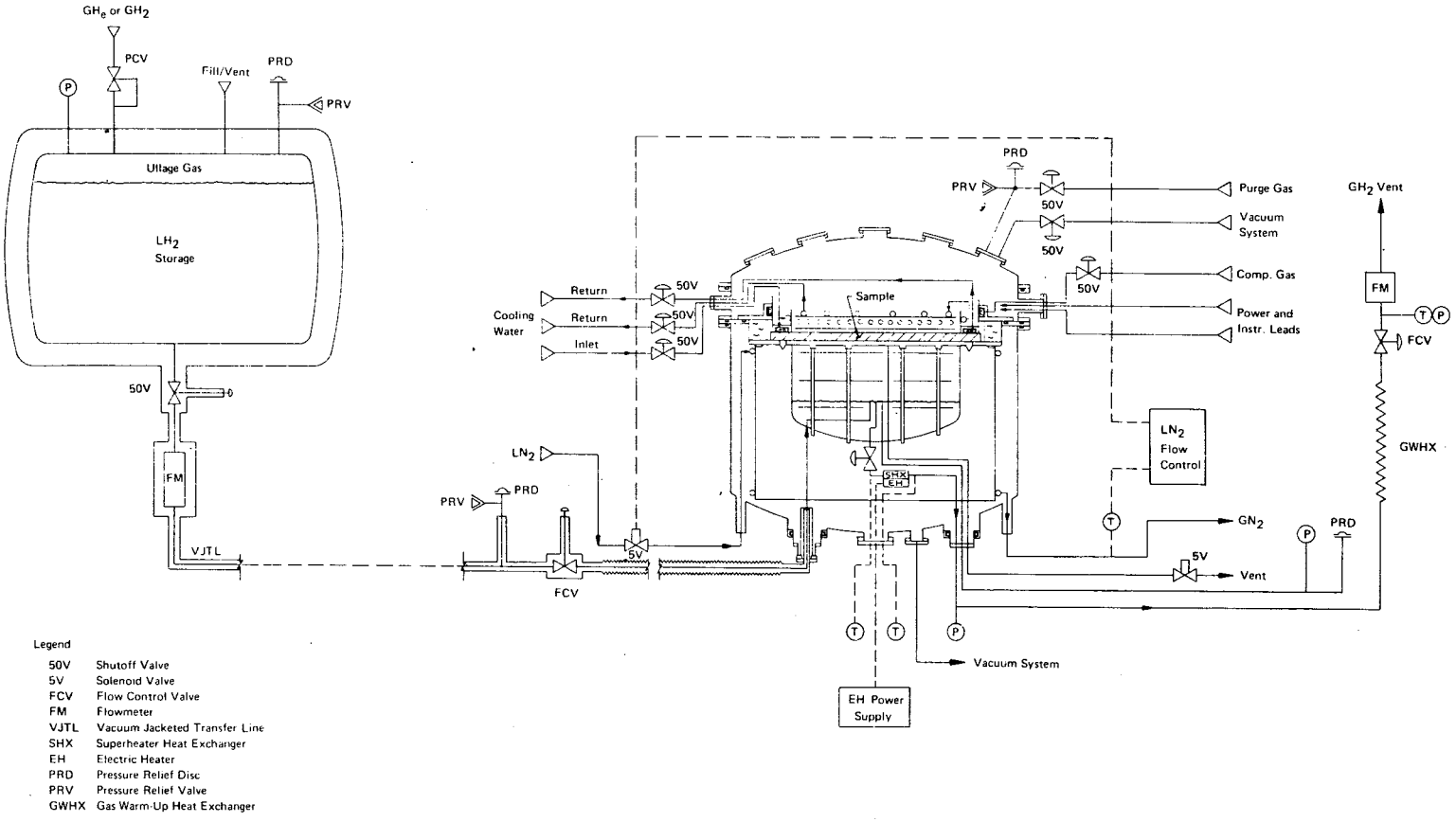

Figure 36. Schematic Flow Diagram of the Flat Plate Calorimeter System

remote control of the liquid hydrogen flowrate and subsequently the pressure on the inner vessel. The hydrogen boiloff, resulting from heat inputs through the test sample, flows through a superheat heat exchanger and then through a gas warmup heat exchanger. The superheat heat exchanger vaporizes any liquid possibly remaining in the boiloff whereas the warmup heat exchanger heats the gas to near ambient temperatures so that a more accurate measurement of the boiloff rate can be determined. The superheat heat exchanger is located between the liquid nitrogen cooled radiation shield and the inner vessel so that heat input from the surroundings into the heat exchanger is minimized. This permits an accurate heat balance of the overall system. Several vent lines are provided so that the liquid level can be controlled in any possible flat plate orientation. Shutoff valves are provided in the vent lines to permit purging of the vacuum transfer lines to the hydrogen source and also for controlling the liquid level. Relief valves and burst discs are included in the vent lines for safety purposes during system warmup.

Liquid nitrogen is employed as a means for minimizing the heat flow to the inner vessel from any other area other than the test sample. It flows through a solenoid valve to the liquid cooled radiation shield at which point it vaporizes and then vents to the surroundings. A thermocouple in the gaseous nitrogen line is used as the means for automatically controlling the liquid nitrogen flowrate. An increase in sensor temperature above a preset level demands an increase in flowrate. The purge gas enters the outer shell and maintains an inert environment on the sample side of the calorimeter. Even though not shown in the schematic, a means for measuring the total purge gas consumption during a test would be provided. The cooling water circuit is required to cool the shields for the quartz lamp heaters and to seal the edge of the insulation sample to a mounting surface.

The main assembly of the calorimeter, shown in Figure 37, consists of the following major subassemblies:

1. The liquid hydrogen vessel including its support and sample insulation system,
2. The heater and its cooling system,
3. The internal thermal protection system, and
4. The outer shell and its mounting arrangement.

The flat plate liquid hydrogen vessel is connected to a mounting flange through a thermal isolation ring support arrangement. This flange is connected to a second outer flange by a thin wall stainless steel cylinder which also acts as a thermal isolation system. This outer flange is then bolted between two flanges on the outer vessel. O-Rings between the mating surfaces of all flanges are the outer seal mechanism.

Internally, pneumatic and hydraulic seals are used to isolate the test sample. An aluminum ring which encircles the heater system defines the sample area. In order to prevent edge leakage of purge gas, a hydraulically pressurized seal is employed at the flat surface of the insulation sample. This seal is located near the outer perimeter of the sample. Flowing water is used to pressurize the seal, thus providing cooling and also reducing the edge heat leakage. An edge seal assembly is formed by welding an aluminum cylinder to the outer perimeter of the ring. This assembly is mounted to another ring flange assembly by means of threaded rods. A pneumatically inflated seal in this assembly seats against the aluminum cylinder of the edge seal assembly, thus isolating the edge of the insulation sample from the purge gas. With the pneumatic seal deflated, the edge seal member can be moved with respect to the flat plate by adjustment of the threaded rods.

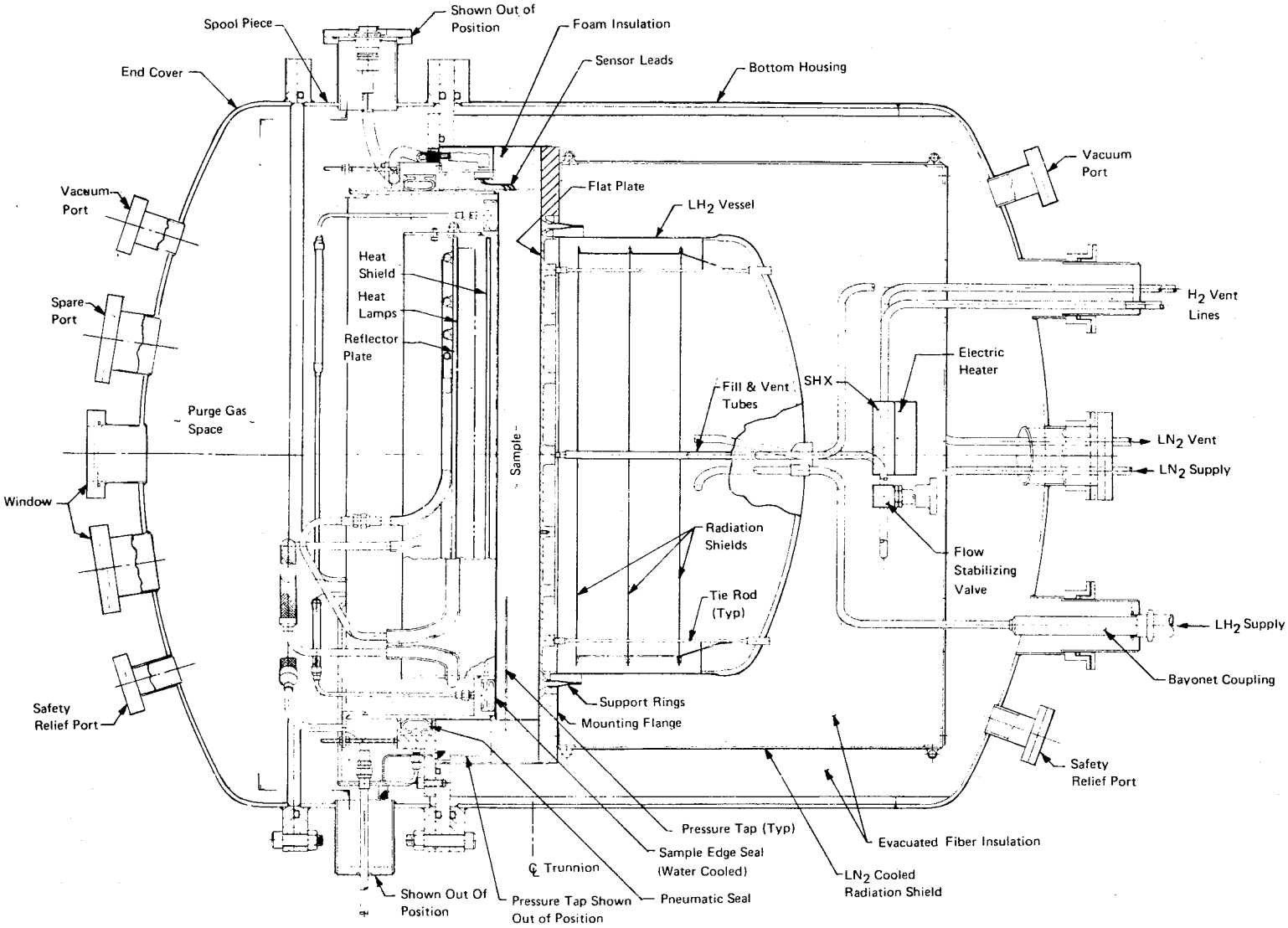

Figure 37. Main Assembly of the Flat Plate Calorimeter

The heater circuit subassembly consists of tungsten-halogen quartz heat lamps mounted on a highly polished aluminum reflecting plate. A high temperature alloy heat shield, between the lamps and outer surface of the sample, simulates the heat shield on a fuel tank and insures a uniform heat flux over the sample surface. The reflector plate is cooled by water flowing through tubing bonded to its back side. This system utilizes a combination of 40, 25, and 12.5 cm (16, 10, and 5 inch) lamps closely spaced to provide approximately 100 kW of power. With this amount of heat input, the system is capable of maintaining the outside of the insulation at any temperature between room temperature and 1366K (2000°F) and of reproducing the temperature histories for either the hypersonic airplane trajectory or the space shuttle boost and re-entry conditions.

In order to evaluate the performance of the insulation sample, it is necessary to perform an accurate heat balance of the complete calorimeter. Major causes of error in the heat balance are usually due to heat inputs from the surroundings to the liquid hydrogen hence a concerted effort was directed at minimizing these losses. The thermal protection system consists of a radiation shield, water cooled hydraulic seals, and evacuated fibrous insulation. In addition, the structural support of the hydrogen vessel is limited to a thin convoluted stainless steel ring, and the piping connected to the vessel is designed to have a long path length by forming coils in a low temperature region, thus, conduction via the supports and piping is nearly negligible. Because of the weight of the calorimeter and the relatively large differences in thermal expansion between the calorimeter and its support, a detailed thermal/structural analysis of the convoluted stainless steel ring was required. This analysis is described in Appendix G.

Radiation is nearly eliminated by using a highly polished aluminum shield cooled by liquid nitrogen between the outer shell and the liquid hydrogen vessel. This shield is thermally coupled to the mounting flange of the hydrogen vessel so the flange is also cooled to near liquid nitrogen temperature. This reduces the temperature difference between the supporting flange and the liquid hydrogen vessel,hence,minimizing the heat leak through the convoluted isolation ring. Evacuated fibrous insulation, employed between the outer shell and heat shield and also between the heat shield and the liquid hydrogen vessel, serve to minimize conduction and convection between these areas.

The outer shell is comprised of a bottom housing, a spool piece, and an end cover. O-rings in the spool piece are required to make sure that the outer vessel is vacuum/pressure tight so that during test the internal pressure can be varied to simulate either the pressure history of the hypersonic transport or the space shuttle. The outer shell has been designed for ease of assembly and for easy access to the sample during test setup. During initial assembly, the pre-assembled components consisting of the:

1. Liquid hydrogen vessel, its mounting flanges and the sample isolation system,
2. Heater system,
3. Liquid nitrogen cooled radiation shield, and
4. Necessary piping

are lowered into the bottom housing of the outer shell. The ring flange assembly, spool piece, test sample, and edge seal assembly are then installed in that order. The necessary electrical and instrumentation lines, in addition to all required piping, feed through compression sealed outlets in the bottom housing and spool piece. The end cover can now be added and test operation commenced. Changing of the sample requires removing the end cover and edge seal assembly only.

In order to simulate different regions on hydrogen tank, it was previously mentioned that the liquid hydrogen vessel must be capable of being rotated 180°. This is accomplished through rotation of the outer shell on trunions as shown in Figure 38. Enough flexible line must be provided to permit the complete rotation.

Since the test surface had to be flat rather than cylindrical as is the case in a typical tank and also since the thermal characteristics of the flat surface must be representative of a typical tank, the design of the test surface was complicated. This latter criteria fixes the wall thickness and internal heat transfer conditions. After many iterations, a compromise between satisfying both the structural thickness requirements and the thermal constraint was reached and it consisted of adding tie rods between the flat surface and the bottom of the hydrogen vessel as shown in Figure 39. This solution adequately represents the condition when liquid hydrogen is in contact with the tank wall; however, it provides an additional heat flow path to the liquid when gaseous hydrogen is in contact. Since the size of the rods was kept at a minimum, the amount of heat flow increases by less than 10% above the anticipated value without supports.

Other design details of the liquid hydrogen vessel are shown in Figures 39 and 40. Figure 39 shows that tapped holes are provided in the surface of the flat plate for attachment of the insulation sample, whereas Figure 40 shows the vent line locations. Because of the many orientations with respect to the vertical of the inner vessel, the vent line must be capable of venting in all of the positions. This is accomplished by using two separate vent lines. By being offset from the vessel centerline, the normal vent satisfies the upward facing flat plate and sideward facing vent requirements, whereas the auxiliary vent satisfies the downward facing vent requirements. The third vent line is provided for safety and as such is referred to as the emergency vent line.

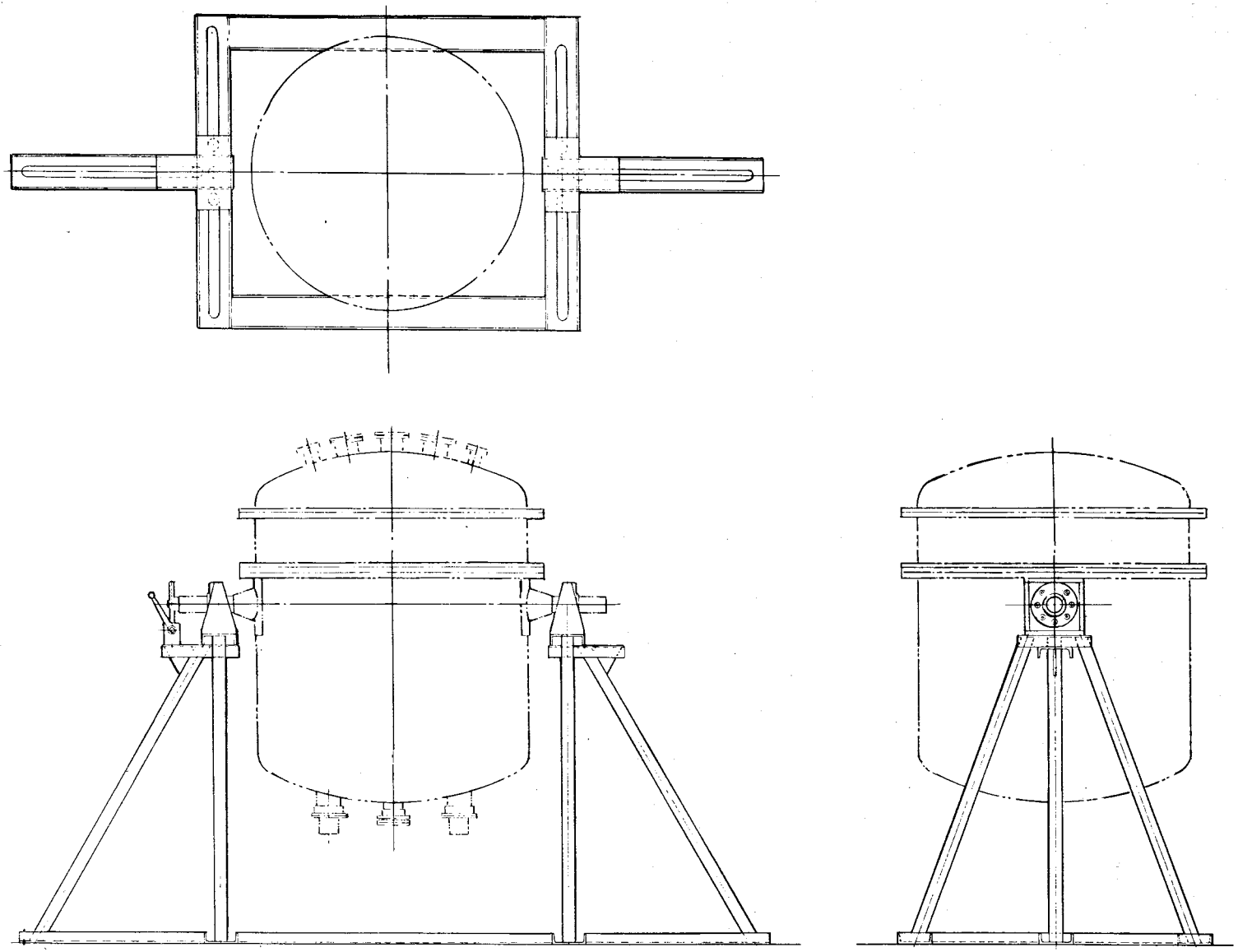

Figure 38. Structural Support of the Flat Plate Calorimeter

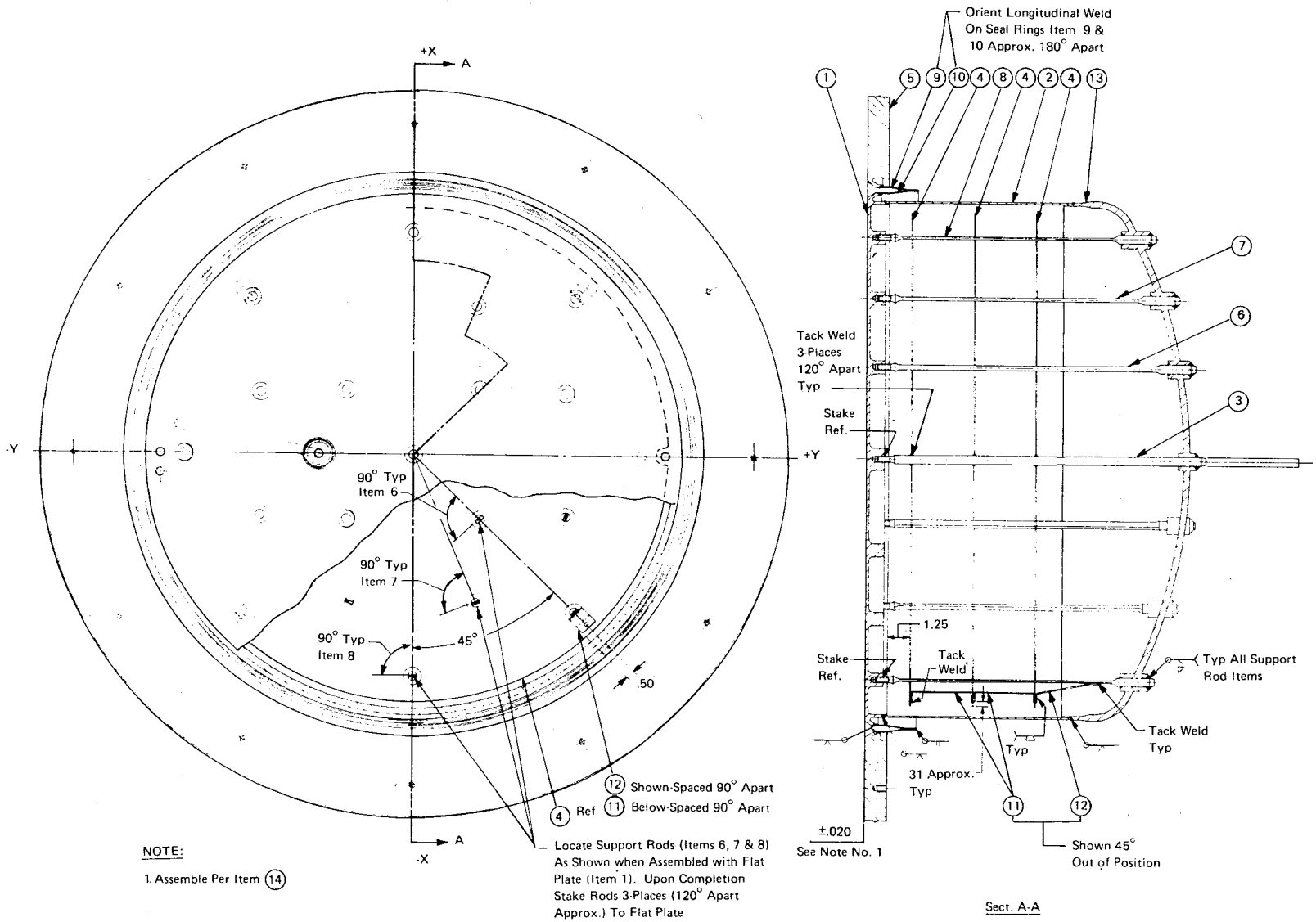

Figure 39. LH_2 Vessel Assembly of the Flat Plate Calorimeter

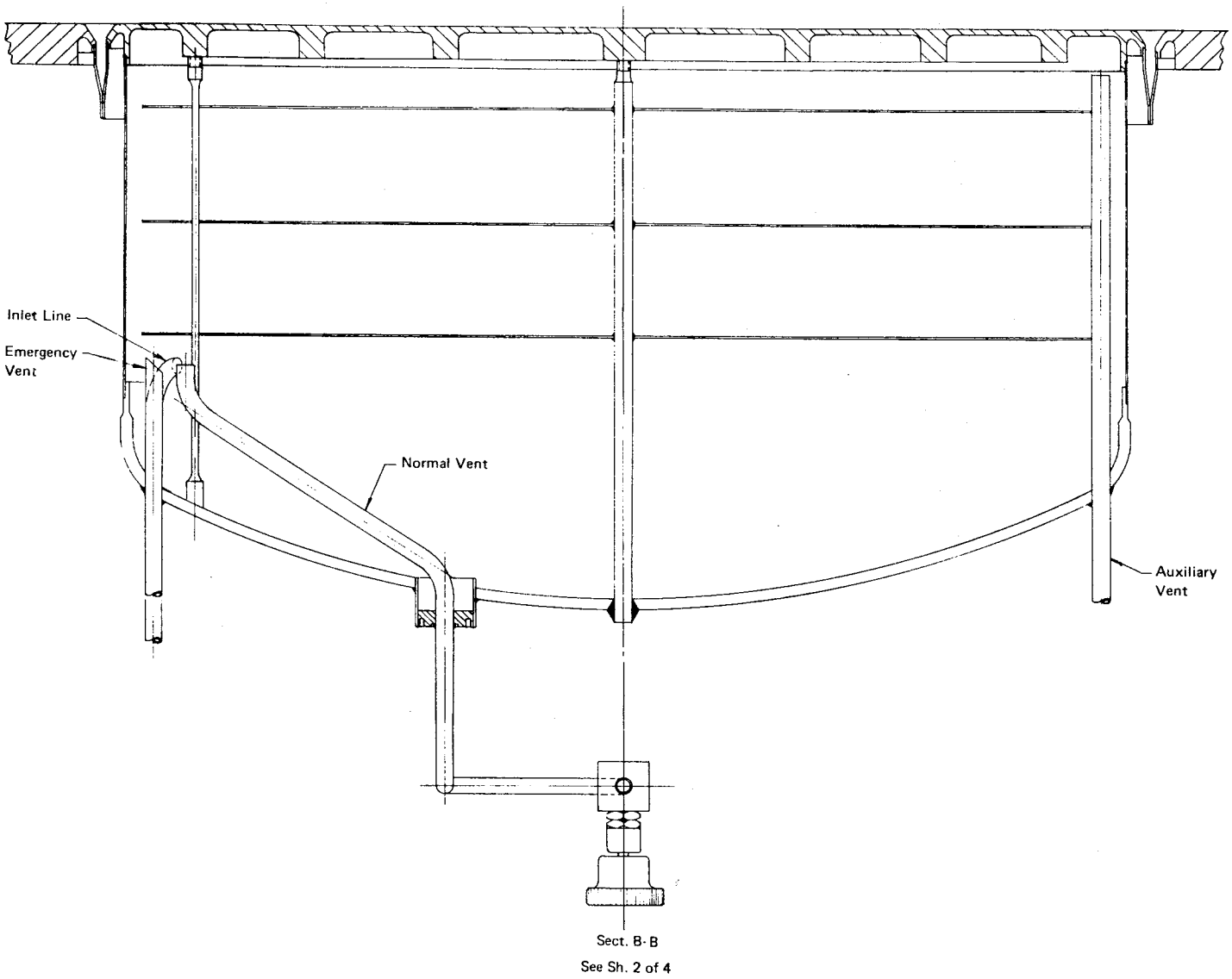

Figure 40. Main Assembly Section B-B of the Flat Plate Calorimeter

APPENDIX G

STRESS ANALYSIS OF CALORIMETER SEAL

Thermal Stress Analysis

The calorimeter seal was analyzed utilizing the Toroidal Ring Element in the MAGIC III computational system of structural analysis. As shown in Figure 41, twelve elements were used in the idealization of the seal. Prescribed radial displacements were specified at Node Points 1 and 13 corresponding to the thermal deformations of the calorimeter and supporting structure, respectively.

Thermal Analysis

To perform the thermal analysis, the calorimeter was subdivided into two regions, one in which the heat flow is nearly one-dimensional and the other in which the heat flow is two-dimensional. At the center of the calorimeter plate, most of the heat flow is into the liquid hydrogen with only a small fraction flowing in the plane of the plate, hence it is a one-dimensional problem. At the edge/seal of the calorimeter the heat flows in both the in-plane and through-plane direction due to thermal conduction paths along the seal to the nitrogen cooled support structure, and also down the wall of the hydrogen vessel. In order to account for any radial heat flow from the center of the calorimeter to the edge in the two-dimensional model, the one-dimensional results were used as boundary control temperatures for the two-dimensional problem.

In order to initiate the transient analysis, the steady-state temperature distribution of the calorimeter and insulation layer was evaluated for the calorimeter completely filled with liquid hydrogen and the support at the edge of the seal, at 77K (-320° F). The hydrogen was then assumed to be completely drained and the calorimeter was allowed to increase in temperature due to the external temperature of 1366K (2000° F). The temperature history of the calorimeter plate is shown in Figure 42 for the one-dimensional case.

The temperature distribution through the calorimeter plate and calorimeter seal is shown as a function of time in Figure 43. Because of the heat capacity of the seal, the shape of the temperature gradient through the seal varies significantly for the first 2000 seconds. After that time it becomes nearly linear.

Temperatures and Displacements

The temperatures and displacements imposed on the seal were taken for the condition of 20,000 seconds after emptying the calorimeter of hydrogen. The radial temperature distribution in the calorimeter and seal for this condition is given in Figure 44.

The displacement at the rim (38.1 cm (15 in) radius) of the calorimeter is completely determined by the temperature distribution in the calorimeter plate. An analysis based on a disc with an axisymmetric temperature gradient gave an expansion at the rim of 1.73 mm (0.068 inch) and an elastic circumferential stress of 301 MN/m^2 (43,700 psi) tension.

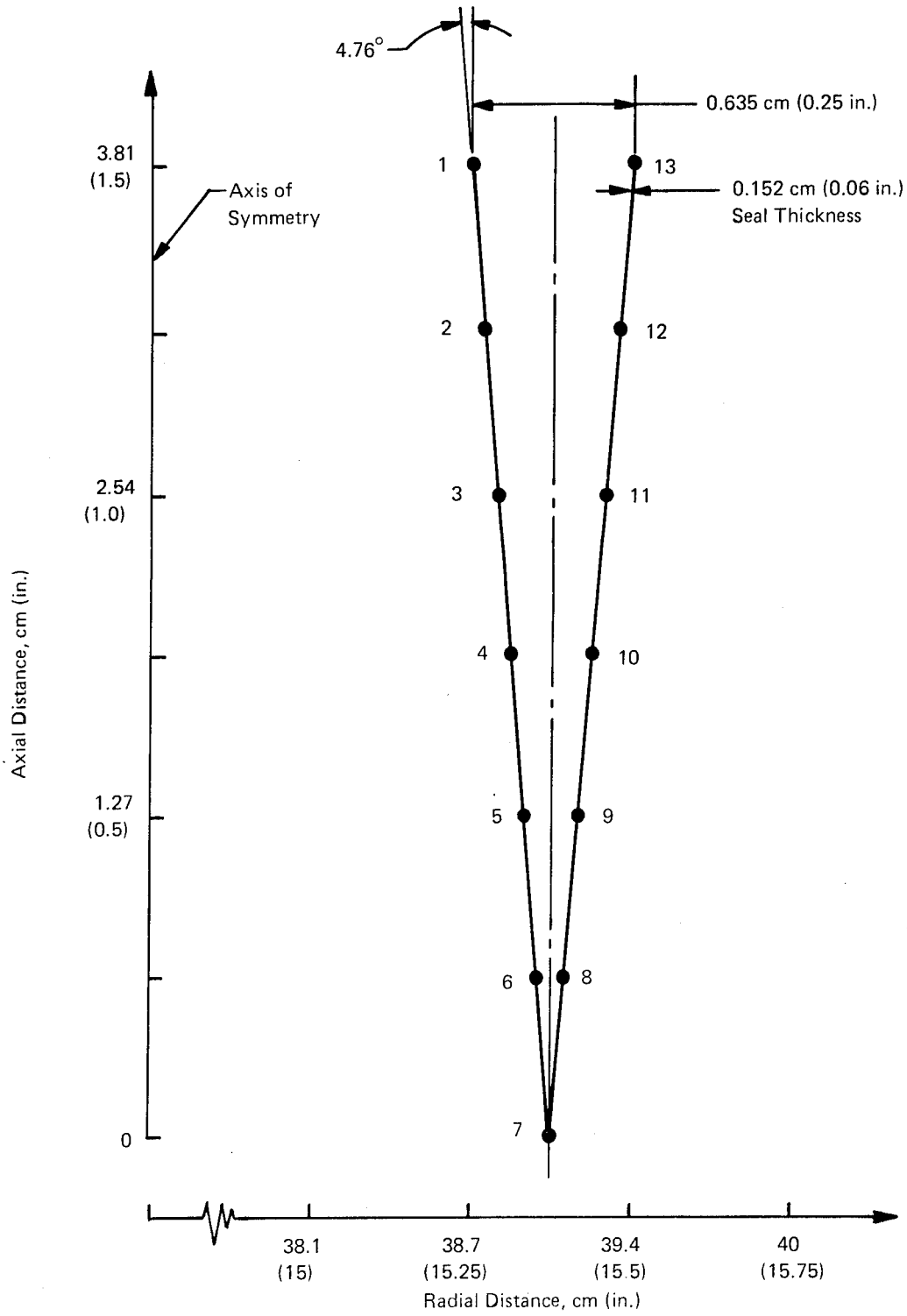

Figure 41. Idealization of Seal

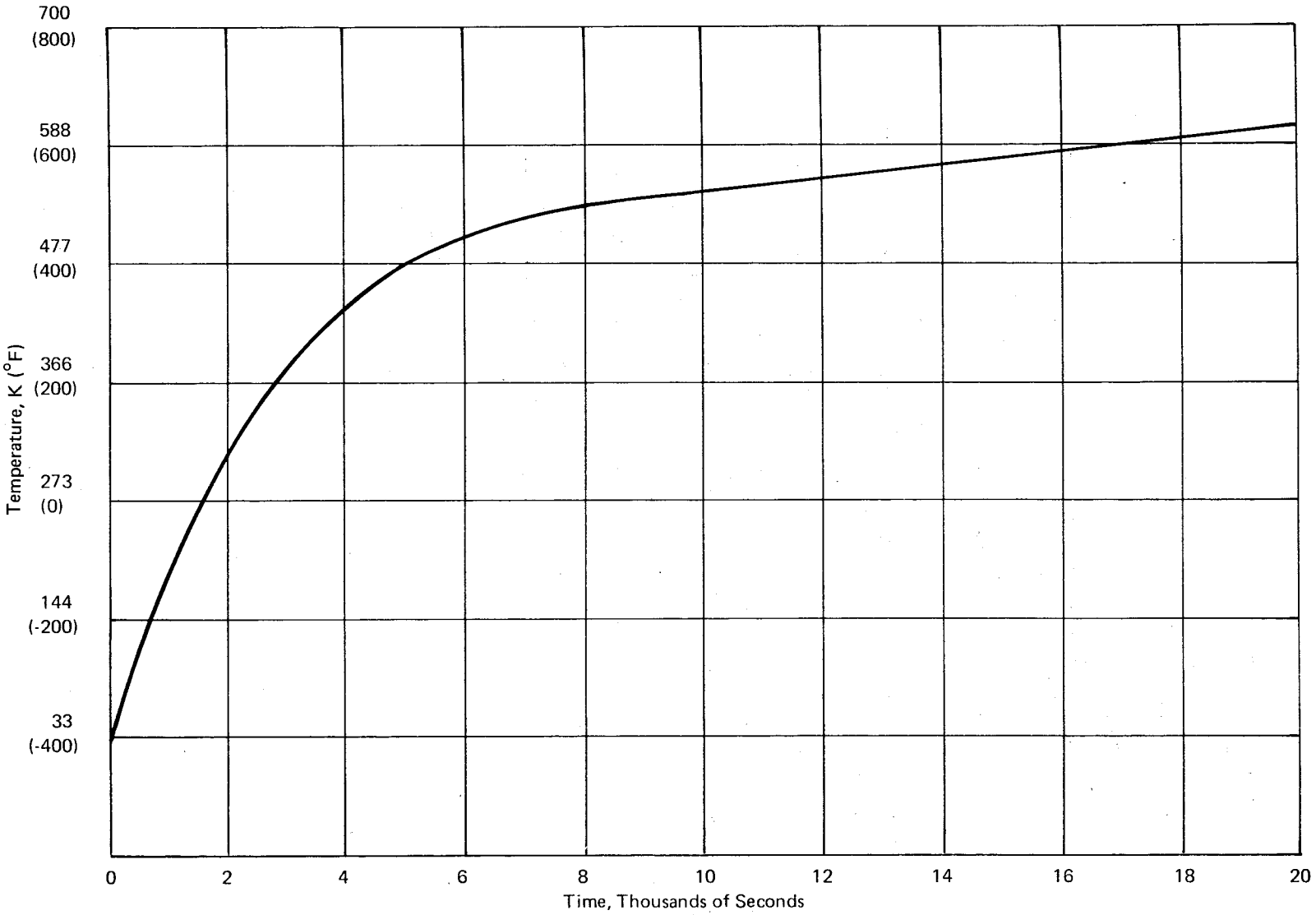

Figure 42. Calorimeter Plate Temperature History after Empyting, External Temperature = 1644K (2000° F)

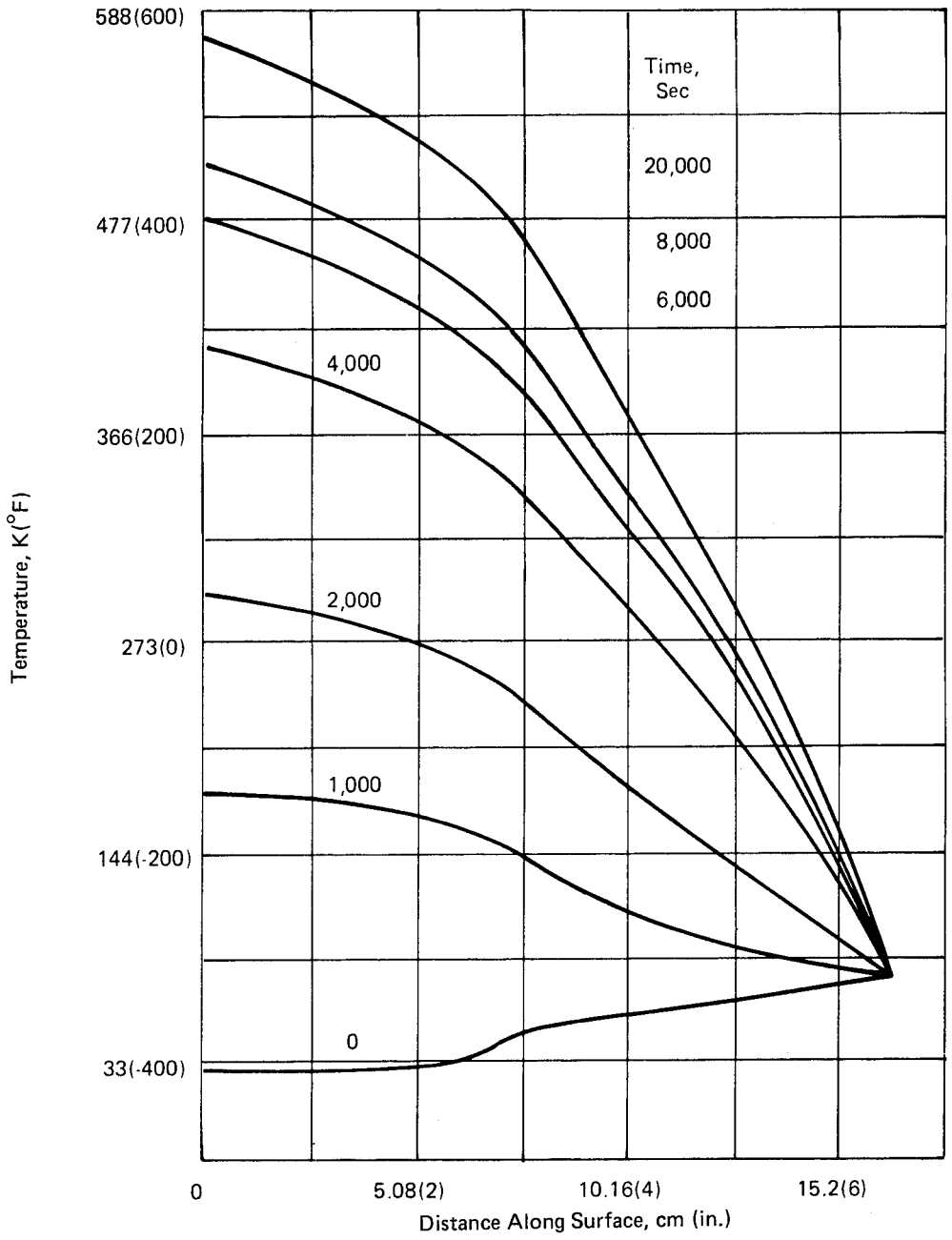

Figure 43. Temperature Distribution of Seal at Various Times After Emptying Calorimeter

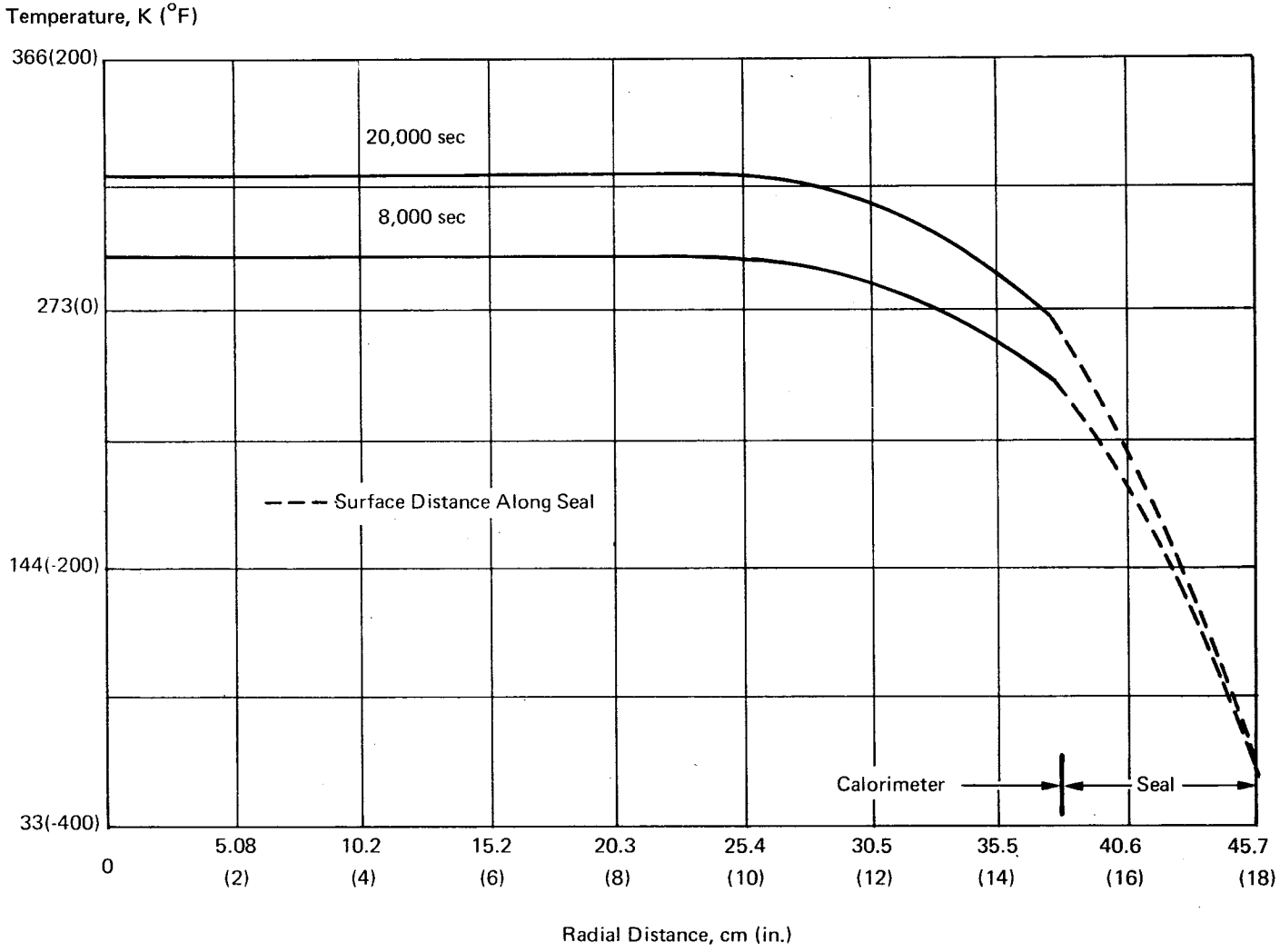

Figure 44. Radial Temperature Distribution of Calorimeter and Seal

The temperature of the supporting structure at the end of the seal opposite the calorimeter is taken as 77K (-320° F) which results in a 1.16 mm (0.0455 inch) contraction of the radius.

Results

Membrane Thermal Stresses - The axial and circumferential thermal membrane stresses computed by the MAGIC computational system are plotted in Figure 45. The axial stresses are within 68 MN/m^2 (± 10,000 psi), while the circumferential stresses vary from 310 MN/m^2 (45,000 psi) tension at the calorimeter end to 48 MN/m^2 (7000 psi) compression at the opposite end. It is readily apparent that there is no problem from buckling due to large circumferential compressive stresses.

Since plasticity was not considered in the analysis, the 324 MN/m^2 (47,000 psi) tensile stress at the calorimeter end is an elastic strain resulting from the thermal expansion of the calorimeter. To correct this stress for plasticity, it is necessary to use the stress-strain curves in Figure 46. From the 477K (400° F) curve the elastic strain at 324 MN/m^2 (47,000 psi) is 0.00205 cm/cm which corresponds to an actual (elastic-plastic) stress 172 MN/m^2 (25,000 psi) Point "A" on Figure 46.

Upon cooling to room temperature 295K (70F), the thermal expansion at the rim of the calorimeter will disappear and there will exist a residual compressive stress of 193 MN/m^2 (28,000 psi) in the seal shown by Point "B" in Figure 46. This stress is below the yield stress of 241 MN/m^2 (35,000 psi) and it is concluded that an "elastic shakedown" condition is reached after the first cycle. No further membrane plastic flow will take place upon additional testing cycles of the calorimeter.

Bending Thermal Stresses - The maximum bending stresses of 1030 MN/m^2 (± 150,000 lb/in^2) occur at the calorimeter end of the seal. Performing a plastic correction, similar to the procedure outlined for the membrane stresses in the preceding discussion, gives outer fiber elastic-plastic stresses of 189 MN/m^2 (± 27,500 lb/in^2) on the 477K (400° F) stress-strain curve. Upon cooling to room temperature these bending stresses result in residual outer surface stresses of 248 MN/m^2 (36,000 lb/in^2) which are just at the yield stress.

Combination of membrane and bending strains gives a value at the outer surfaces of the seal, at node point 1, of 0.0075 cm/cm. This value is large although very localized; with a large number of thermal cycles fatigue cracking could occur. However, since the material is very ductile and the number of full thermal cycles will be small, (< 25), no fatigue failure is expected.

Calorimeter Differential Pressure Load Analysis

The calorimeter end of the seal is loaded axially by the differential pressure across the LH_2 pressure vessel. This load is carried through the seal to the supporting structure at the opposite side. This condition was analyzed by the same idealization of the seal as the thermal stress and analysis.

A load of 39.4 kN/m (225 lb/in) corresponding to a 206 kN/m^2 (30 psi) differential pressure. (atmospheric pressure x 2.0), was imposed at Node Point 1 in the Z-direction of Figure 41. The opposite end, Node Point 13, was considered to be completely fixed.

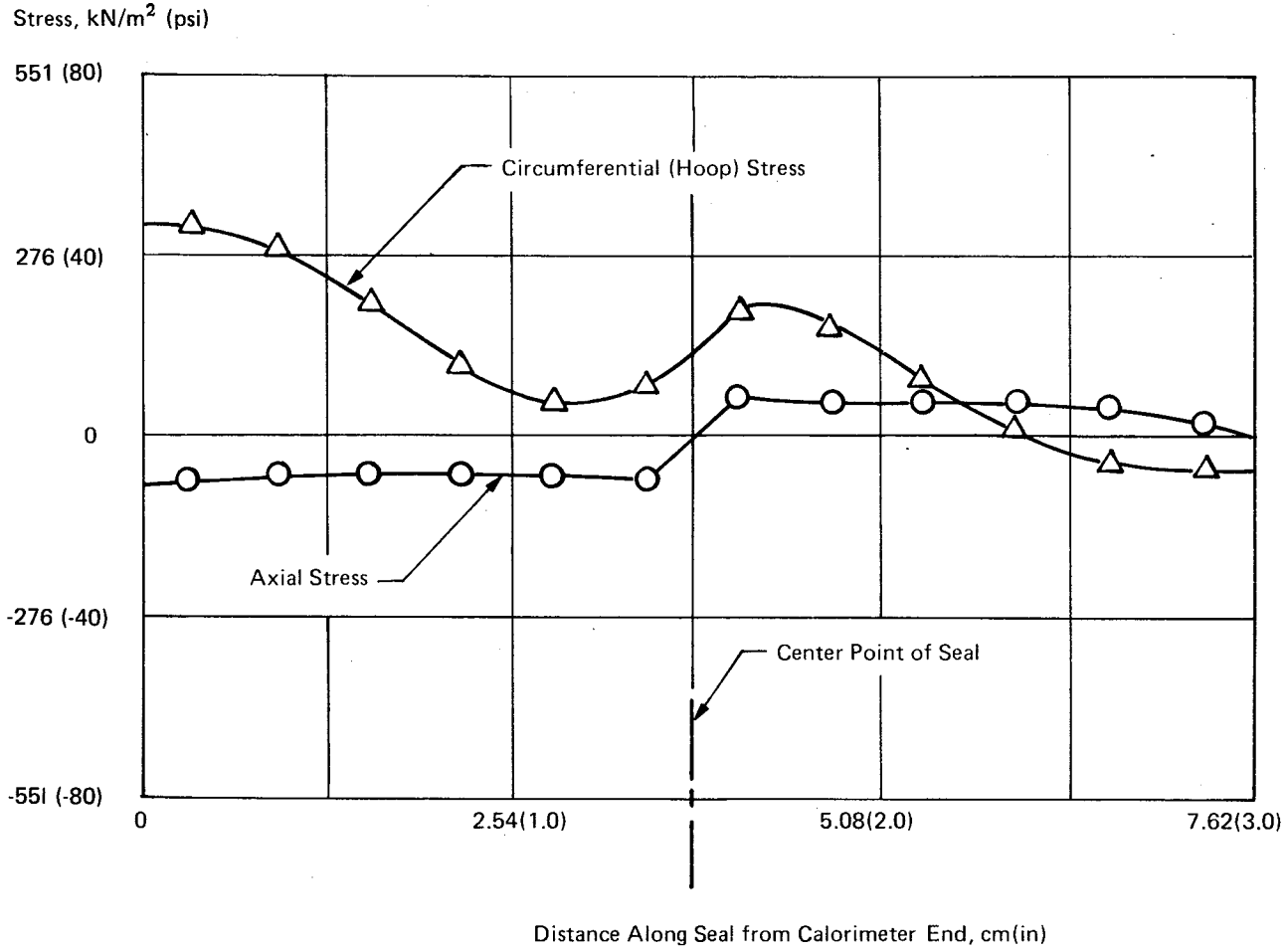

Figure 45. Thermal Membrane Stress Distribution in Calorimeter Seal at 20,000 Seconds after Emptying

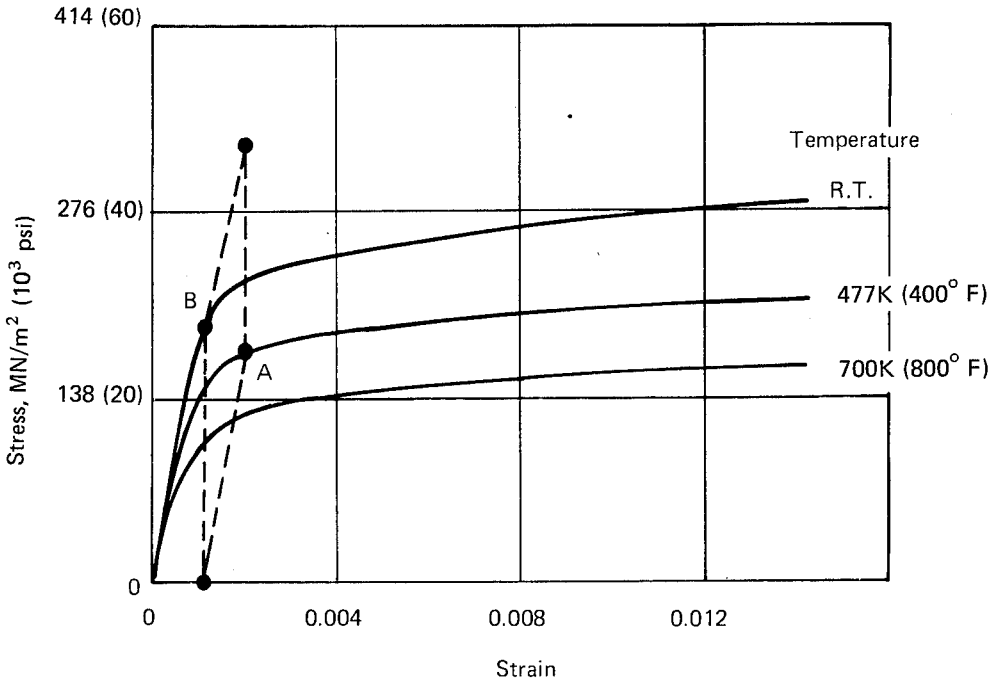

Figure 46. Stress/Strain Relationships for 304 Stainless Steel at Various Temperatures

Results

The membrane stresses resulting from the 207 kN/m^2 (30 psi) differential pressure are shown in Figure 47. The axial stresses are approximately 27 MN/m^2 (4000 lb/in^2) with tension on the calorimeter side of the seal and compression on the opposite side. The circumferential stresses are primarily compression increasing to approximately 96 MN/m^2 (14000 lb/in^2) at the center point of the "V."

The circumferential stresses tend to produce buckling. Using the critical buckling stress formula for a plate

$$s' = K \frac{E}{1 - \nu^2} \left(\frac{t}{b}\right)^2$$

and assuming a loaded plate width, b, of 3.81 cm (1.5 inches) and a buckling coefficient, k, of 3.29 for simply supported edges; the critical buckling stress 1110 MN/m^2 (162,000 lb/in^2). Thus the possibility of buckling is not a problem.

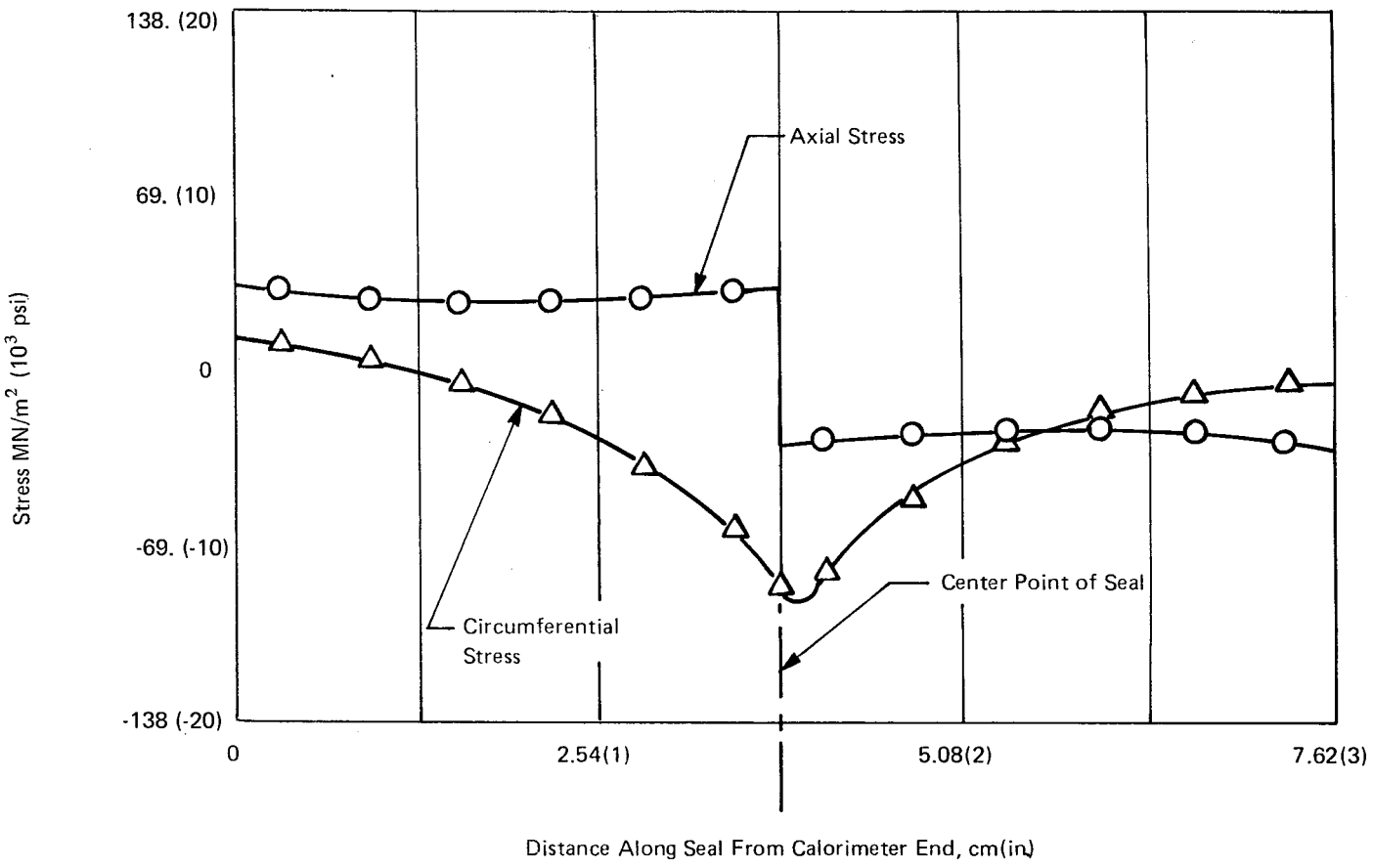

Figure 47. Differential Pressure Load Stress Distribution for 207 kN/m² (30 psi)

APPENDIX H
LARGE SCALE TESTS

Early in the program the calorimeter described in Appendices F and G was designed. The design objective was to closely simulate hypersonic aircraft mission duty cycles. As all its capabilities were not required for the preliminary evaluation of candidate insulations, only a major subassembly of the calorimeter was built during the present program. When more detailed data for insulation systems are required, the present simple apparatus can be readily incorporated into the calorimeter as it is designed. This appendix describes the life cycle apparatus and presents the results of large scale insulation tests.

Apparatus Description

The life cycle test apparatus consists of an insulated liquid hydrogen vessel of approximately .17 m^3 (45 gallon) capacity, a heater-blanket and a lower shell, as shown in Figure 48. The basic material of construction is stainless steel. Since hydrogen fuel tanks will be of large diameter a flat test specimen was determined to be adequately representative of the actual insulation contour and the test apparatus was designed for flat specimens. Figures 49 through 56 pictorially show the components of the test apparatus during the fabrication process. The apparatus was designed to accommodate an insulation specimen with a 76 cm (30 inch) LH_2 contact area diameter which provided it with an outer diameter of 99 cm (39 inches) to provide for specimen mounting.

Figure 49 shows the inside of the liquid hydrogen vessel's flat plate with its concentric rings for stiffening and tapped holes for the head support rods. This component simulates the liquid hydrogen tank wall. The containing cylinder is welded to the flat plate at one end. A weld lip is also provided for the thermal isolation support convolute. The flexible convolute is then weld attached to a mounting ring (refer to Figure 39) to complete this subassembly. The mounting ring has a bolt circle used for bolting the outer periphery of the insulation specimen which is not in contact with the hydrogen cooled simulated tank wall. Figures 50 and 51 show the support rods and upper radiation baffle installed in the vessel.

Eleven chromal-constantan thermocouples were spaced vertically at 2.54 cm (1.0 inch) intervals in the cylindrical section of the vessel to provide a means for determining the liquid cryogen level. In addition, four other thermocouples were mounted on the fill and vent lines.

Figures 52 to 54 show the hydrogen vessel closure. Four inlet lines are provided for venting, emptying and cryogen loading. The support rod holes are countersunk to provide leak-tight welds. Assembly of the cryogen tank is affected by welding the lower tank support rods to the countersunk bores of the closure and girth welding the two subassemblies. The top and sides of the assembly are then foamed with ADL polyurethane with a density approximately 80 kg/m^3 (5 lb/cu. ft) to a depth of approximately 15.2 cm (6 inch) or more.

The insulation specimen is mounted to the flat plate tank wall of the cryogen vessel and enclosed with the purge vessel shown in Figure 55. This purge vessel provides two sight ports for viewing the insulation specimen and provides 16 ports for instrumentation and electrical lines. Two ports were used for evacuating the vessel and supplying purge gas to the insulation. To simulate high

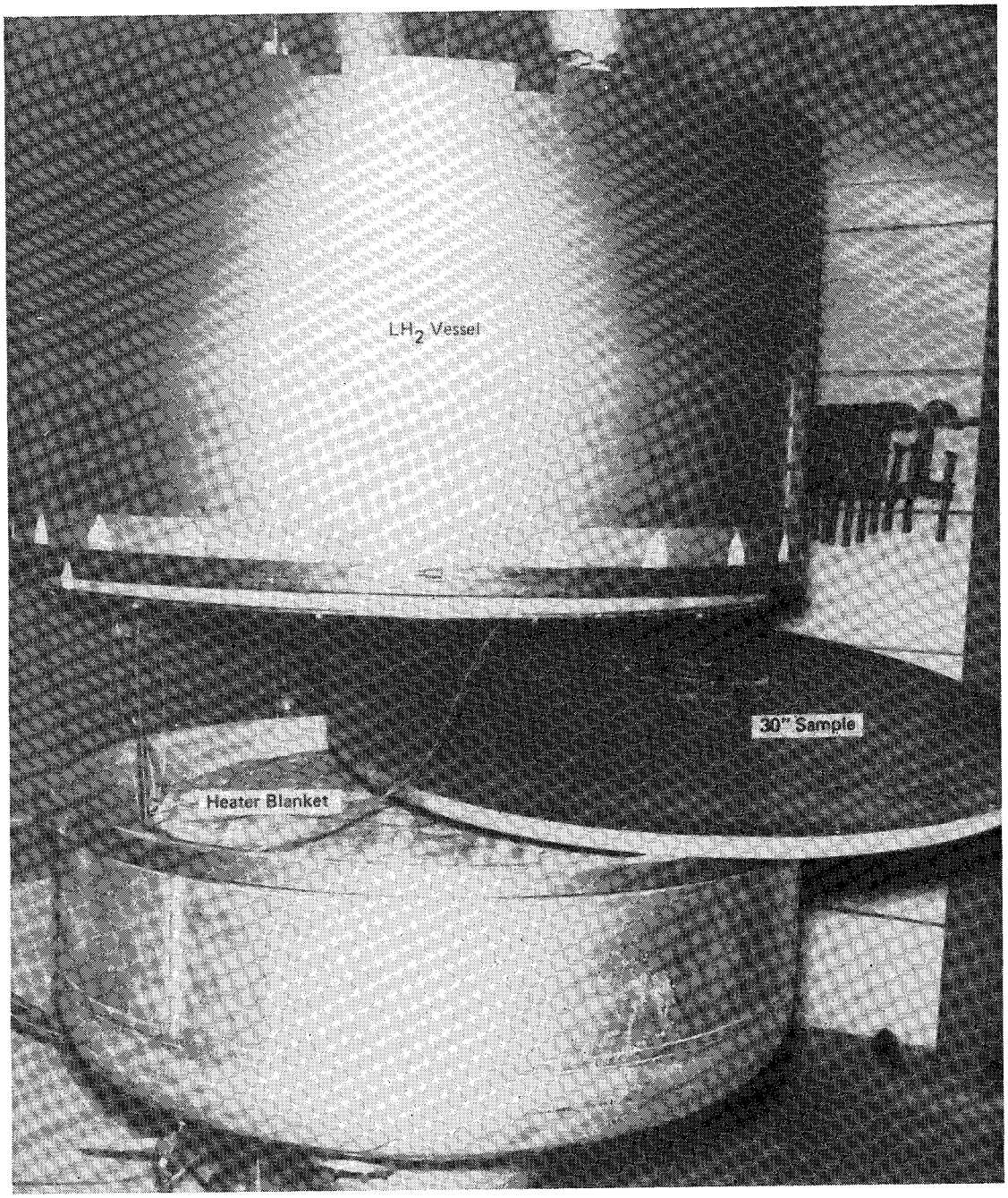

Figure 48.- Life Cycle Test Apparatus and Sample

Figure 49.- Underside of Test Surface of Life Cycle Test Apparatus

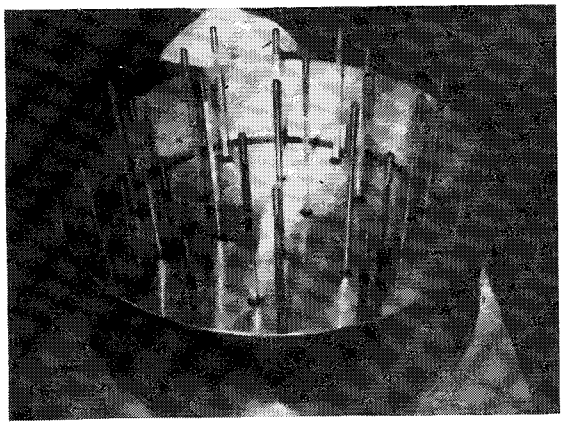

Figure 50.- Support Rods of Life Cycle Test Apparatus

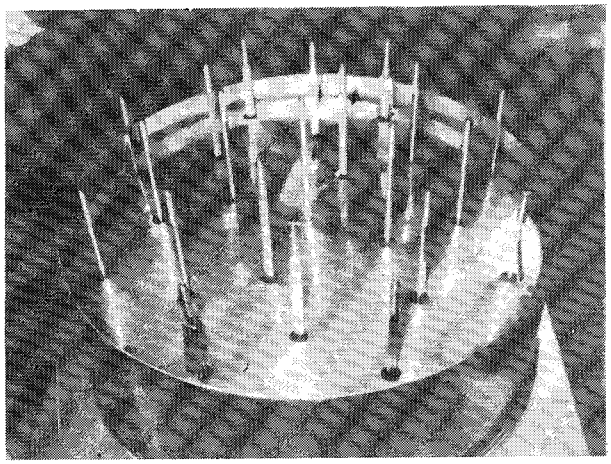

Figure 51.- Baffle Plate Installed in LH_2 Vessel of Life Cycle Test Apparatus

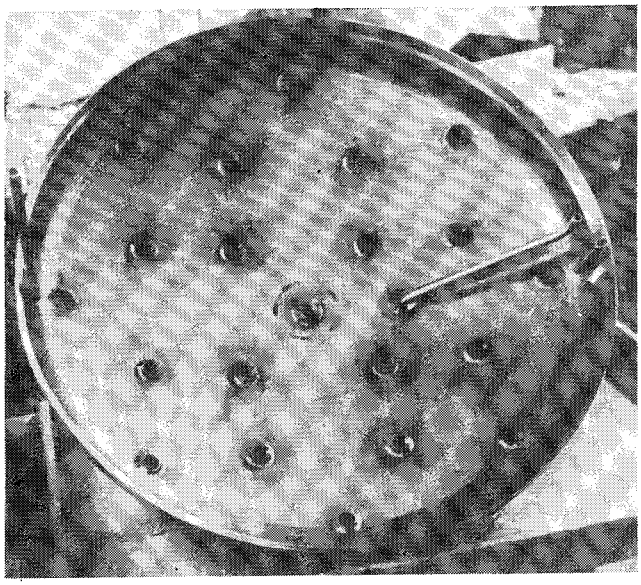

Figure 52.- Vent Line Locations in LH_2 Vessel of Life Cycle Test Apparatus

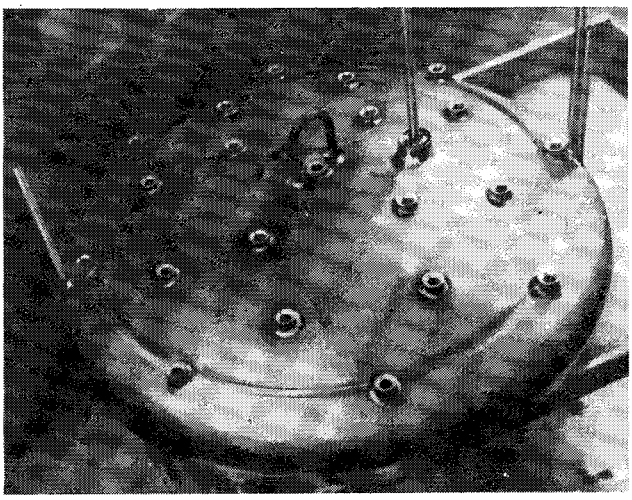

Figure 53.- LH_2 Vessel Head Assembly of Life Cycle Test Apparatus

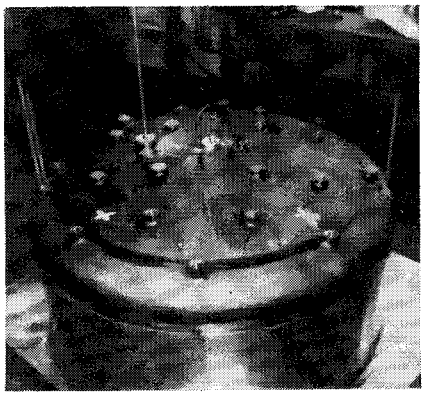

Figure 54.- LH_2 Vessel of Life Cycle Test Apparatus

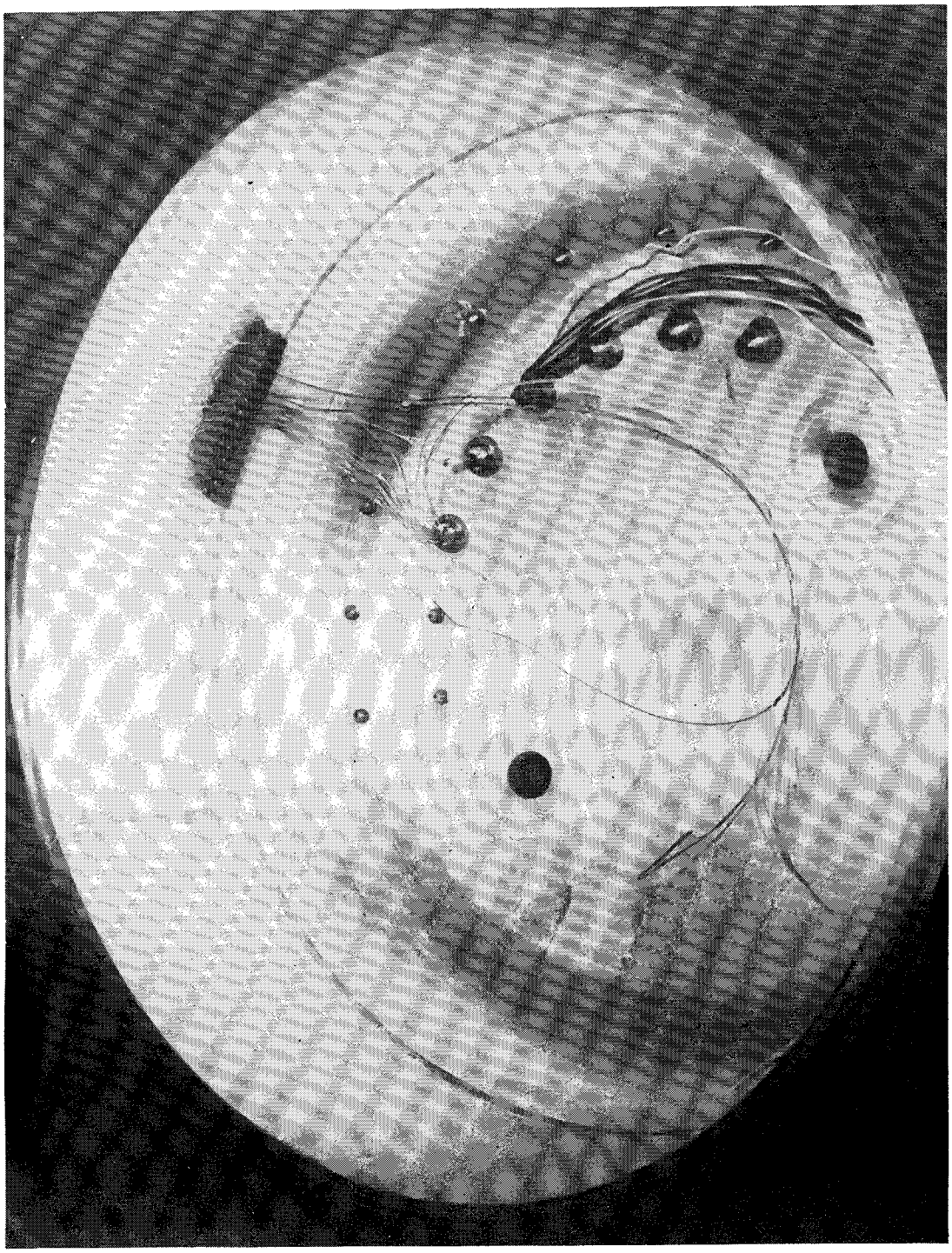

Figure 55.- Purge Vessel of Life Cycle Test Apparatus

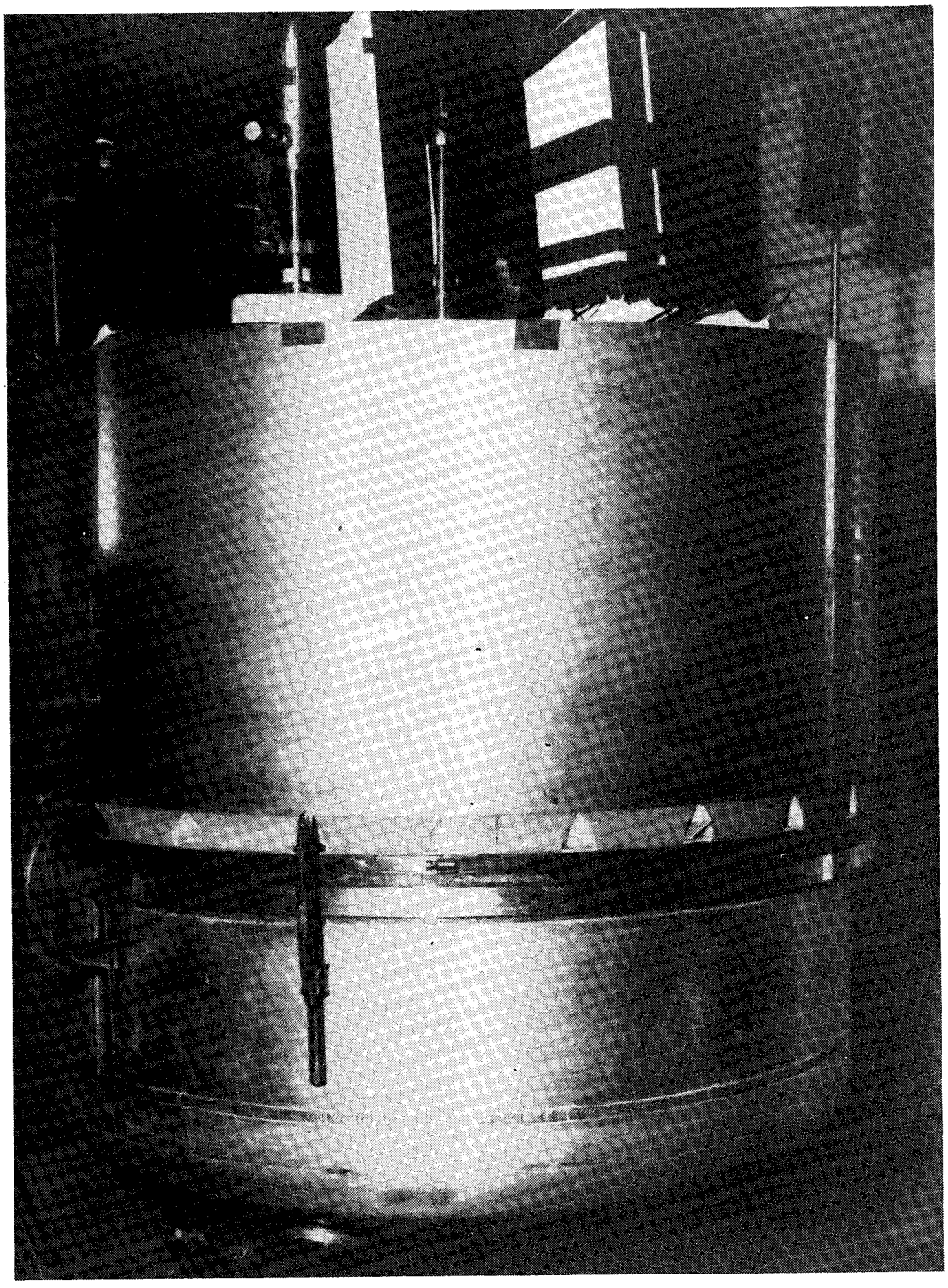

Figure 56.- Life Cycle Test Apparatus Sealed for Test

altitude pressures the vessel had to be designed to support an external differential pressure 103 kN/m^2 (15 psi). Prior to attachment of the purge vessel to the LH_2 vessel an electric heater blanket is fixtured with an adjustable aluminum rack in the purge vessel to provide the means of heating the external side of the insulation. The 76.2 cm (30 inch) diameter fiberglass insulating blanket (220 volts - 5500 watts) has sufficient power output to heat the insulation surface to 810 K (1000° F). To insure contact between the blanket and the insulation specimen the aluminum rack is set so that clearance between it and the insulation is 0.63 cm (¼ inch) less than the thickness of the heater blanket. Attachment to the cryogen vessel is accomplished by C-clamping its flange to the mounting flange of the former. (Refer to Figure 56). Sealing between the two flanges is provided by a 105 cm (41.3 inch) silicone O-ring.

Environment Simulation

Once the cryogen vessel had been filled, repetitive simulation of the thermal/pressure environment commenced. The electric heater blanket was used to heat the outer surface of the insulation. Cooling of the insulation was solely by conduction through the insulation to the liquid hydrogen. The temperature schedule of the outer surface of the closed cell foam insulation was determined analytically using a finite difference thermal analysis computer program. The solid line of Figure 12 shows the predicted temperature history of the interface between the closed cell foam and the Dynaflex insulation for the mission profile of Figure 1. However, since an evaluation of the thermal stresses showed that maximum stresses were adequately represented by a much simpler history, the temperature history shown by the broken line of Figure 12 was used for the cyclic tests of the insulation.

In the event of a hydrogen leak on the actual vehicle, accumulation of hydrogen within the purge space must be prevented. This is accomplished by requiring that a positive 3.4 kN/m^2 (0.5) psi pressure differential be maintained between the purge space and the free stream pressure. This requirement results in the absolute pressure history shown in Figure 13. Similar to the temperature history, the pressure profile used for test was simplified so that manual control could be used. The broken line in Figure 13 shows the profile used during the cyclic test.

Tests and Results

Closed cell plastic foams of two different compositions, polyurethane and polymethacrylimide, were evaluated. The polyurethane specimens which were formulated by Arthur D. Little, Inc. and contained reinforcing glass fibers included unaged specimens with integral plastic skins formed at the interface of the mold when the material was foamed and aged specimens with the skins intact and with the skins removed. (The aging process, which was to increase the maximum allowable temperature of the foam and thereby reduce the system weight, consisted of curing the specimen at 400K (260°F) for six hours and 450K (350°F) for six hours while the material was completely constrained against thermal expansion.) Details of the specimens tested in the large scale apparatus are presented in Table XV. Results of the test are discussed in the sections that follow.

Polyurethane Specimens. – The test of the three unaged polyurethane samples with integral skins served to check out the test apparatus and verify the operating procedures. For the first test the specimen was held against the test apparatus by the clamped mounting ring around the perimeter (see Figure 12). Silicone grease was used to minimize restraint of differential expansion between the test apparatus and the sample and to seal the expansion slot between the thermal isolation support convolute from the purge environment. During initial evacuation of the purge gas compartment a loud noise was heard; subsequent inspection indicated the disk material had cracked in three places near the center. The checkout with liquid nitrogen/carbon dioxide as the cryogen and purge

TABLE XV
LARGE SCALE TEST SPECIMENS

Test Number	Description	Thickness		Density	
		cm	in	kg/m^3	lb/ft^3
1	ADL reinforced polyurethane foam unaged with skins; not bonded to tank	2.7	1.06	94.2	5.88
2	ADL reinforced polyurethane foam unaged with skins; not bonded to tank	2.7	1.06	91.0	5.68
3	ADL reinforced polyurethane foam unaged with skins; bonded to tank	2.5	1.0	94.3	6.20
4	ADL reinforced polyurethane foam aged without skins; bonded to tank	1.6	0.62	49.7	3.10
5	ADL reinforced polyurethane foam aged with skins; bonded to tank	2.5	1.0	105	6.55
6	Rohacell 31 aged; bonded to tank	1.6	0.62	30	1.87
7	Rohacell 51 aged; bonded to tank	1.6	0.62	50	3.2

gas combination was continued despite the cracks. An average purge gas deposition rate of 0.64 kg/m^2 hr (0.131 lb/ft^2) was measured during the 70-minute checkout run. Post test inspection clearly indicated the extensive cracks and the buildup of solid carbon dioxide between the simulated tank wall and the insulation. Apparently, 82 kN/m^2 (12 psi) pressure differential outward across the insulation during evacuation of the purge gas chamber, stressed the edge supported foam excessively and the cracks that formed permitted easy flow of the purge gas to the tank wall where cryopumping occurred.

For the second test the specimen was installed in the same manner as the previous sample, but provisions were made to evacuate the expansion slot and the space between the simulated tank wall and the insulation. In this way the differential pressure always held the insulation against the surface of the test apparatus. Minor cracking occurred during the carbon dioxide/liquid nitrogen test. A number of deficiencies in the test apparatus (such as leaks) were corrected before proceeding with tests of a third sample.

The third sample was attached to the apparatus with a polyurethane adhesive (Crest 7343) cured at room temperature. A 2.5 hour test was conducted with the insulation going from ambient to liquid nitrogen temperature on the cold side and to the carbon dioxide freezing point on the warm side. The cryogen tank took approximately 20 minutes for cooldown while deposition of purge gas was not noted until nearly two hours after the start of liquid nitrogen fill. There was no apparent damage to the insulation after the test (see Figure 15).

In order to provide the low density, 1.5 cm (0.6 inch) thick foam indicated desirable by the analytical results the first aged specimen of ADL polyurethane foam was cut from a thicker disk (prior to aging). Consequently, it was devoid of integral skins. The sample was bonded to the apparatus with Crest 7343 adhesive. During checkout of the evacuation system for the expansion slot region, leakage through the insulation was observed and several local regions were sealed with PVC patches bonded with Crest adhesive. Following a 71 minute liquid nitrogen/carbon dioxide cooldown, there was an indicatin of a ridge about 10 cm (4 inches) long and about 13 cm (5 inches) in from one edge of the insulation; a frost line was noted at the ridge. Tapping of the insulation surface suggested a void in the adhesive almost diametrically opposite to the cracked location. An attempt was made to repair the crack by injecting Crest adhesive into the region with a hyperdermic needle. Inspection after a second 75 minute liquid nitrogen/carbon dioxide run suggested the possibility of an additional 15 cm (6 inch) long crescent shape crack near the edge of the void region identified previously by tapping. Because of the apparent crack in the sample, it was removed and replaced with a thermally aged specimen with skins.

The aged specimen with skins was bonded to the apparatus with Crest 7343 adhesive. During a liquid nitrogen/carbon dioxide test of 2.8 hours approximately 0.9 kg (2 lb) of carbon dioxide were deposited; however, no frost or solid carbon dioxide was observed on the surface of the specimen at the end of the test. As the surface of insulation began to heat to room temperature, the skin began to crack and ripple with approximately 80% of the outer skin separated from the core. In addition, a plug if insulation some 25 cm (10 inches) in diameter was loose as shown in Figure 16. This damage, which was apparently the result of outgassing of ingested purge gas, indicated that the aged specimen was permeable. Post test checks of the permeability of the aged polyurethane foam confirmed this finding.

Polymethacrylimide Specimens. – The rather disappointing results experienced for aged ADL polyurethane foam led to the selection of the polymethacrylimide for evaluation. Rohacell 31 was chosen from the series of candidates of different densities because of its low density and because of its performance during the screening tests. It was bonded to the apparatus with Crest adhesive and subjected to a liquid nitrogen/carbon dioxide exposure. A high flow rate of carbon dioxide was noted during the test. Post test examination indicated the heater blanket was stuck to the insulation at several spots due to a frosting of carbon dioxide. There appeared to be several long cracks in which carbon dioxide was deposited. Tapping indicated a very large void area. Insulation removal operations determined that approximately 80% of the area was not bonded. Thus, bending stresses were induced due to the 96 kN/m^2 (14 psi) outward pressure differential during evacuation of the purge gas chamber.

Rohacell 51 was used for the next series of tests summarized in Table V and discussed below. Although its density of 50 kg/m^3 (3.2 pcf) is not as low as that of Rohacell 31, its mechanical properties are higher. During the liquid nitrogen check with this sample, several loud noises were heard and inspection indicated fracture of the test specimen with a circular ring separating from the central disk, see Figure 17. A portion of the central disk that was not properly bonded to the test apparatus stayed with the circular ring. It was postulated that the cause was differential expansion between the cryogenic inner vessel and the outer, warmer periphery of the specimen. Stresses in the insulation should have been avoided by the slip fit between the insulation and the clamping ring in that region. Apparently, binding had occurred so that differential expansion could not be accommodated. Careful examination of the center of the disk revealed no cracks. The high structural integrity of the central disk portion of this material was encouraging. Rather than replace the insulation sample, it was decided to try to seal the crack with annular segments of aluminum foil cemented to the surface of the insulation with Crest adhesive. This repair, Figure 18, appeared satisfactory and testing continued. (This concept provides a potential solution to the problem of sealing joints between adjacent pieces of insulation in an actual application.)

During the next liquid nitrogen test that lasted for 2 hours and 50 minutes, the heater blanket was operated successfully. Warm side temperatures ranged from 422 K (300° F) down to 166 K (-160° F). This very low warm side temperature caused some carbon dioxide frost between the insulation and the heater blanket as noted during the post test inspection. A small blemish was incurred in the center of the specimen when the blanket, which was stuck to the specimen by the frost, was removed.

The next liquid nitrogen/carbon dioxide run was aborted after 20 minutes when a relief valve froze and a burst disk ruptured on the nitrogen supply cart. After equipment repairs, three simulated thermal cycles were conducted without damage to the insulation. Minimum warm side temperatures ranged from 183 to 194 K (-130 to -110° F) while maximum values ranged from 372 to 422 K (210 to 300° F).

The good performance with the liquid nitrogen/carbon dioxide combination of cryogen and purge gas provided sufficient confidence to initiate testing with liquid hydrogen and the nitrogen purge. During the first LH_2 test, which lasted 48 minutes, the external surface was not heated. During the first day of actual cycle testing with liquid hydrogen as the cryogen and nitrogen as the purge gas, two cycles were completed. The minimum warm side temperature of the insulation ranged from 77 to 83 K (-320 to 310° F) while maximum values ranged from 425 to 433 K (307 to 320° F) Visual examination of the external surface of the insulation indicated no change as the result of the two thermal cycles. The minimum warm side temperatures during the next six cycles were 77 K

(-320° F) while maximum values ranged from 412 to 422 K (283 to 300° F). Examination of the insulation after the eighth cycle with LH_2/N_2 revealed no apparent damage. However, when the specimen was re-examined after a weekend shutdown, there was evidence of damage over a small area which extended from the edge to a position near to the center of the specimen. It was postulated that the damage was the result of moisture freezing in an area near the edge of the specimen where the bond was defective. The moisture had entered the slot which was vented to atmosphere after the test and diffused into the defective bond while the tank and specimen were still cold. The damage included the loss of a 3.8 cm (1.5 inch) by 5 cm (2 inch) portion of foam at the edge of the specimen, and indications of two possible surface flaws in the center of the sample.

Since only a relatively small area of the total specimen was damaged positively, it was decided to replace this region with sections of Rohacell insulations R-31, R-51, and R-61S. A small amount of moisture was applied behind the R-51 section to see if this would promote bond failure and subsequent cracking of the insulation. All but one edge around these specimens were sealed with aluminum foil cemented to the insulation with Crest adhesive. No attempt was made to cement the sides of the insulation materials together. In this way additional information was gained regarding the sealing of butt joints between sections of insulation.

After completion of the ninth thermal cycle a short was noted in the heater blanket wiring. Inspection of the insulation revealed no apparent change. Therefore, after some electrical modifications and repairs, and the sealing of the one joint with aluminum foil, an additional four cycles were conducted bringing the total to 13. Minimum temperatures on the warm side were 77K (-320° F) while maximum values ranged from 422 to 428 K (300 to 312° F). Current and voltage readings in the heater blanket circuit were quite erratic during all four thermal cycles. At the end of the 13th cycle, the surface of the insulation was inspected and had a slight surface waviness that had not been observed previously and was thought to be indicative of excessive heating. In addition, a relatively large crack was noted in the R-61S section. A separate test conducted later indicated a temperature of 477 K (400° F) was required to cause waviness on the surface of R-51 material.

Because of the apparent overtemperature condition during cycles, 11, 12 and 13, a thermocouple was placed between the heater blanket and the cryogenic insulation but was not attached to either. This would provide data in addition to that obtained from the control thermocouple taped to the cryogenic insulation and the other thermocouple adhesively bonded pressed into the surface of the insulation. During the next four thermal cycles significant differences were observed between the three thermocouples. Maximum temperatures indicated by the new thermocouple ranged from 437 to 446 K (326 to 343° F) and were as much as 33 K (60° F) higher than temperatures indicated by the control thermocouple. After completion of the 17th thermal cycle, inspection of the insulation surface revealed more pronounced distortion, shrinkage lines, on 2.5 cm (1 inch) spacing (approximately that of the heater blanket wires), irregular crisscrossing frost lines, and a region about 5 cm (2 inches) in diameter that appeared to be lifted slightly near the center of the original large disk of Rohacell 51.

To improve the uniformity of heating a 0.8 mm (0.032 inch) aluminum alloy sheet was placed against the surface of the cryogenic insulation and three layers of fiberglass cloth were place between the aluminum sheet and the heater blanket. Three additional thermal cycles were conducted during which minimum warm side temperatures ranged from 81 to 89 K (-296 to -300° F) while maximum temperatures varied by as much as 70 K (125° F) between the three thermocouples at a particular

time with a maximum value of 483 K (410° F) being measured by the unattached thermocouple. This was 39 K (70° F) higher than the control. Despite these high temperature indications there was no observable difference in the appearance of the insulation surface after 20 cycles as compared to its appearance after 17 cycles.

Before the next series of tests the thermocouple that had been unattached between the aluminum sheet and the insulation was taped to the surface of the insulation in its prior location as evidenced by a slight depression thought to have been caused by the 483 K (410° F) temperature experienced during the 18th thermal cycle. During the next four thermal cycles, the control thermocouple continued to read about 44 K (80° F) higher than the other two thermocouples. (A later calculation indicated that such a difference could be attributed to the fact that the other two thermocouples were below the surface of the insulation and the temperature difference corresponded to the temperature at a depth of about 1.5 mm below the surface.) The other two thermocouples just below the surface of the insulation agreed within about 15 K (26° F). This would correspond to a difference in installed depth of about .5 mm.

During cycles 21, 22, 23, and 24 the maximum warm side temperature of the insulation ranged from 397 to 400 K (255 to 261° F) rather than the 422 K (300° F) as used in prior tests. With this reduction in measured value, it was expected that the maximum surface temperature of the insulation would be about 422 K (300° F). After completing the 24th cycle, a section of the insulation surface revealed a relatively large crescent shaped crack in the original R-51 disk and the loss of the 5 cm (2 inches) raised portion of insulation noted previously. This piece simply fell out of the insulation leaving only a very thin layer attached to the simulated tank wall by the Crest adhesive. In addition, the irregular crisscross frost line pattern appeared to be more noticeable after the frost had evaporated than had been the case previously, and was considered to be caused by cracks in the insulation. The crack in the R-61S seemed to be unchanged.

Even though the insulation material appeared to have sustained damage at the end of the 24th cycle, it was not considered a detrimental failure and it was decided to conduct another 4 cycles to see what additional degradation would occur. No repairs were made; the 5 cm piece of insulation that fell out of the Rohacell 51 disk was not replaced. During the last four cycles minimum warm side temperatures ranged from 77 to 89 K (-320 to -301° F) while maximum temperatures ranged from 391 to 398 K (244 to 256° F). Visual inspection of the insulation surface following the 28th cycle showed no major change as compared to its appearance following the 24th cycle although nitrogen frost was observed in the region where the 5 cm disk of insulation had been lost. The warm side of the insulation is shown in Figure 20. The cracking and the shrinkage near the heater wires are apparent. However, the insulation stayed in place on the LH_2 vessel, the rate of purge gas usage was not prohibitive and no change was observed in the boiloff rate of the LH_2.

NATIONAL AERONAUTICS AND SPACE ADMINISTRATION
WASHINGTON, D.C. 20546

OFFICIAL BUSINESS
PENALTY FOR PRIVATE USE $300

SPECIAL FOURTH-CLASS RATE
BOOK

POSTAGE AND FEES PAID
NATIONAL AERONAUTICS AND
SPACE ADMINISTRATION
451

U.S.MAIL

3[illegible] 001 C1 U D 770527 S00[illegible]42DS
DEPT OF THE ARMY
PICATINNY ARSENAL, BLDG 176
PLASTEC DRDAR-LCA-[illegible] BLDG 3401
ATTN: [illegible] M ANZALONE
DOVER NJ 07801

POSTMASTER : If Undeliverable (Section 158 Postal Manual) Do Not Return

"The aeronautical and space activities of the United States shall be conducted so as to contribute . . . to the expansion of human knowledge of phenomena in the atmosphere and space. The Administration shall provide for the widest practicable and appropriate dissemination of information concerning its activities and the results thereof."

—NATIONAL AERONAUTICS AND SPACE ACT OF 1958

NASA SCIENTIFIC AND TECHNICAL PUBLICATIONS

TECHNICAL REPORTS: Scientific and technical information considered important, complete, and a lasting contribution to existing knowledge.

TECHNICAL NOTES: Information less broad in scope but nevertheless of importance as a contribution to existing knowledge.

TECHNICAL MEMORANDUMS: Information receiving limited distribution because of preliminary data, security classification, or other reasons. Also includes conference proceedings with either limited or unlimited distribution.

CONTRACTOR REPORTS: Scientific and technical information generated under a NASA contract or grant and considered an important contribution to existing knowledge.

TECHNICAL TRANSLATIONS: Information published in a foreign language considered to merit NASA distribution in English.

SPECIAL PUBLICATIONS: Information derived from or of value to NASA activities. Publications include final reports of major projects, monographs, data compilations, handbooks, sourcebooks, and special bibliographies.

TECHNOLOGY UTILIZATION PUBLICATIONS: Information on technology used by NASA that may be of particular interest in commercial and other non-aerospace applications. Publications include Tech Briefs, Technology Utilization Reports and Technology Surveys.

Details on the availability of these publications may be obtained from:

SCIENTIFIC AND TECHNICAL INFORMATION OFFICE

NATIONAL AERONAUTICS AND SPACE ADMINISTRATION

Washington, D.C. 20546